Electroanalytical measurements of neurotransmitter release and uptake in zebrafish

By

University of Kansas 2016

Mimi Shin

Submitted to the graduate degree program in Chemistry and the Graduate Faculty of the University of Kansas in partial fulfillment of the requirements for the degree of Doctor of Philosophy.

_____
Chairperson Michael A. Johnson Ph.D.

_____
Cindy L. Berrie Ph.D.

_____
Carey K. Johnson Ph.D.

_____
Susan M. Lunte Ph.D.

_____
Blake R. Peterson Ph.D.

Date Defended: August 19th, 2016

The Dissertation Committee for Mimi Shin
certifies that this is the approved version of the following dissertation:

Electroanalytical measurements of neurotransmitter release and uptake in zebrafish

_____

Chairperson Michael A. Johnson Ph.D.

Date approved: August 19, 2016

Abstract

Fast-scan cyclic voltammetry at carbon-fiber microelectrodes (FSCV) is a commonly used electrochemical technique to measure sub-second concentration changes in electroactive neurotransmitters, including dopamine, and neuromodulators both in *vivo* and in *vitro*. FSCV provides several advantages, including good chemical selectivity and temporal resolution. Our research group is currently interested in studying rapid interactions between neurotransmitters in the context of neurodegenerative disease and toxic neurological events. Many research groups including ours use rat or mouse animal models to study neurotransmission; however, these animal models have some drawbacks, including low throughput analysis and the need to use invasive treatment methods, such as intravenous tail injections. In addition, developing transgenic rodent models for neurodegenerative disease is expensive and time consuming. Therefore, we seek to develop the use of an alternative animal model that has potential for high-throughput analyses and easy genetic manipulation.

Zebrafish (*Danio rerio*) have recently been established as popular animal model for the study of neuronal functions due to their fast-life cycle, ease of genetic manipulation and drug treatment, and central nervous system similarities with humans. Unfortunately, real time measurement methods to study sub-second neurotransmitter release and uptake events in zebrafish have not yet been well developed, representing a serious roadblock to the use of this organism for elucidating brain function. In this study, FSCV was used to measure locally-evoked dopamine release and uptake in zebrafish whole brain preparations as well as brain slices. Our results indicate that dopamine release is easily measured in the whole brain. Moreover, peak dopamine concentration ($[DA]_{release}$) was similar to that of sagittal brain slice preparations (0.49 ± 0.13 µM in whole brain and 0.59 ± 0.28 µM in brain slices, $p = 0.41$, t-test). Several

pharmacological studies using α-methyl-p-tyrosine methyl ester (αMPT), an inhibitor of tyrosine hydroxylase, sulpiride, a D2 dopamine autoreceptor antagonist, and nomifensisne, a dopamine reuptake inhibitor, were conducted to confirm the presence of dopamine and to determine if zebrafish dopamine receptor and transporter are similar to that of rodents.

In addition to quantifying dopamine release and stimulation optimization, we established zebrafish as a chemobrain animal model. We investigated the changes in dopamine release and uptake in zebrafish that were treated with chemotherapy drugs, carboplatin and 5-fluorouracil using either habitat water treatment or food treatment. The data here suggest that the chemotherapy drugs have an effect on dopamine release and uptake in zebrafish similar to that observed in the rodent animal models. Moreover, zebrafish treated orally with chemotherapy drugs shown greater effect on evoked dopamine release compared to zebrafish exposed to the treated habitat water system.

Last, our group has been interested in studying the relationship between glutamate and dopamine. However, glutamate is neurotoxic and cannot be applied to a harvested brain as was the other pharmacological agents. To overcome this challenge, we employed *p*-hydroxyphenylacyl (pHP) based caged compounds to deliver glutamate to the target location while not interfering with glutamate's known biological response. However, direct electrochemical quantification of how much glutamate is photo-released is impossible since glutamate is not electroactive. Therefore, instead of measuring the amount of glutamate photoreleased, we decided to measure 4-hydroxyphenylacetic acid (4HPAA) instead. 4HPAA is an electroactive by-product generated from the photostimulation of pHP based caged glutamate. Due to the electroactivity of 4HPAA, the amount of photoreleased glutamate can be quantified using FSCV. In addition, our group has successfully demonstrated using both FSCV and high

performance liquid chromatograpy (HPLC) that the quantification of 4HPAA indirectly allow for the quantification of glutamate generated due to the photoactivation. Therefore, we studied 4HPAA's electrochemistry in order to optimize a waveform for the simultaneous detection of dopamine and 4HPAA in a single voltammetry measurement.

Acknowledgments

I would like to thank the Department of Chemistry and the University of Kansas for giving me an opportunity to become an affiliate of the Ralph N. Adams Institute of Bioanalytical Chemistry. I sincerely thank Dr. Michael A. Johnson, my research advisor, for his continued guidance and support throughout my graduate career. I would also like to extend my gratitude to the members of my dissertation committee, Dr. Cindy Berries, Dr. Susan Lunte, Dr. Carey Johnson, and Dr. Blake Peterson for their support. In addition, I would like to acknowledge Dr. Chamani Perera and University of Kansas Molecular Probes Core for the support and providing zebrafish required to conduct my research. I would also like to express my appreciation to my current research group members, Rachel Ginther for support and friendship and Thomas Field for his assistance with the zebrafish project, especially in modeling of dopamine uptake rates.

Lastly, I would like to thank my family and friends who have provided unconditional support throughout my graduate career. Especially, I want to thank to my mom, Choung Ran Park, and my sister, Ashley Breen, for continued support and unlimited love. Without the persistent encouragement of my mom and my sister, I wouldn't be able to achieve the accomplishment in Ph.D. program.

Table of Contents

Chapter 1. Introduction

1.1 Dopamine

Dopamine is an abundant central nervous system (CNS) neurotransmitter that plays an essential role in a wide variety of neurological functions including reward, emotion, locomotion, and cognition. The chemical structure is shown in Fig. 1. In the mammalian brain, shown in Fig. 2, the dopaminergic system consists of four main pathways; the mesolimbic, nigrostriatal, mesocortical, and tuberoinfundibular pathways. The mesolimbic pathway sends dopaminergic projection from the ventral tegmental area of the midbrain to the nucleus accumbens. [1] The nigrostriatal pathway sends dopaminergic projection from the substantia nigra to the striatum. [2] the mesocortical pathway sends dopaminergic projections from ventral tegmental area to the cortical structure. [3] Lastly, the tuberoinfundibular pathway sends dopaminergic projection from the hypothalamus to the hypophysis. [4-6]

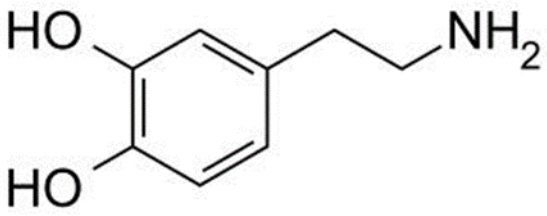

Figure 1: Chemical structure of dopamine

The mesolimbic pathway is predominantly associated with cognitive function, memory, and emotion whereas the nigrostriatal is involved with motor function. [7] The mesocortical pathway is mainly involved with motivation and reward.[8] Lastly, the tuberoinfundibular pathway regulates the secretion of prolactin [4].

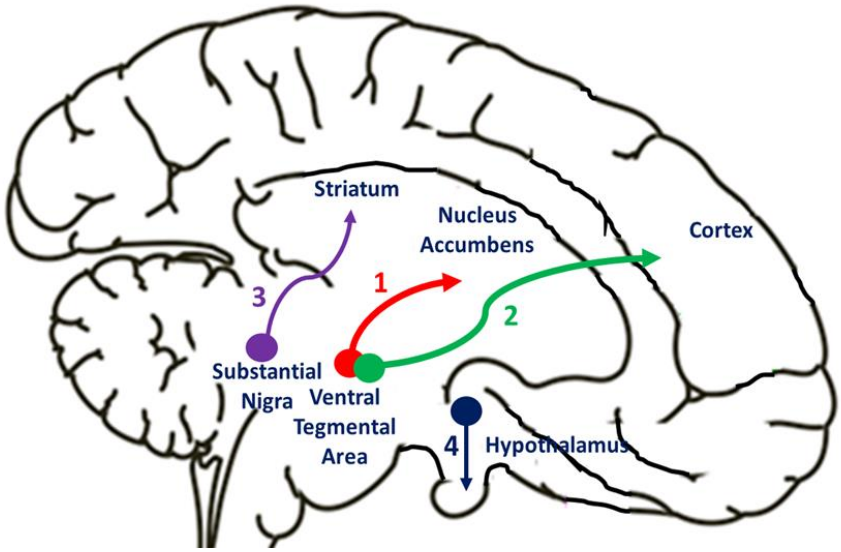

Figure 2. The main four dopaminergic pathways in mammalian brain. Pathway 1 represents the mesolimbolic pathway, pathway 2 represents the mesocortical pathway, pathway 3 represents the nigrostiriatal pathway, and pathway 4 represent the tuberoinfundibular pathway.

Dysfunction of the dopaminergic system is known to be related to neurodegenerative diseases or neurological disorders. Therefore, understanding the mechanisms and kinetics of dopamine neurotransmission is important to gaining an understanding of dopamine's role in these neurological diseases and disorders. However, the study of dopamine system in the brain provides many challenges. The brain contains a complex environment that can interfere with the measurement of dopamine, which is present at low concentration (the basal concentration of

dopamine in the caudate-putamen is reported to be around 5 nM). [9] To understand these challenges and possible solutions, one must understand how dopamine functions in the brain.

1.1.1 Neurotransmission

A typical neuron, as shown in Fig. 3, contains a cell body with two types of projections, dendrites and axons. Dendrites surround the cell body, receiving signals, whereas axons, connected to the cell body, output signals. In the brain, neurotransmitters act as a small chemical messenger to process signals between neurons. When the neuron receives input signals, various ion channels open allowing a rapid influx of Na^+ into the neuronal cells. [10] This influx causes a depolarization of the cell membrane that leads to a rapid voltage change along the membrane, called an action potential. As depolarization continues, the action potential propagates along the axon down to the terminals, at the rate of 0.5m/s, resulting in the release of neurotransmitters into the extracellular space. [11]

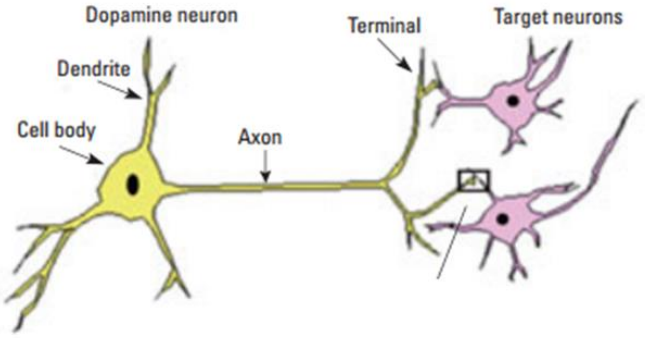

Figure 3. Simple schematic diagram of a neuron. This adapted figure is permitted to use from Ref.12

1.1.2 **Dopamine release and uptake.**

Once dopamine is synthesized inside the dopaminergic neurons from tyrosine, dopamine is packaged into membrane-bound synaptic vesicles by vesicular monoamine transporter 2 (VMAT2) as shown in Fig. 4.[12] Each vesicle contains approximately 0.1 M of dopamine, which is 10 – 1000 times higher than dopamine concentration in the cytosol. [13] When the action potential reaches the end of axonal terminals, voltage dependent ion channels open causing an influx of Ca^{+2}.[2, 14] This Ca^{2+} influx causes the dopamine containing vesicles to fuse to the cell membrane within the synapse. Dopamine stored in the vesicles then releases into the extracellular fluid. This process is called exocytosis, which is related to the external concentration of $Ca^{2+,}$ and occurs on the millisecond timescale [15].

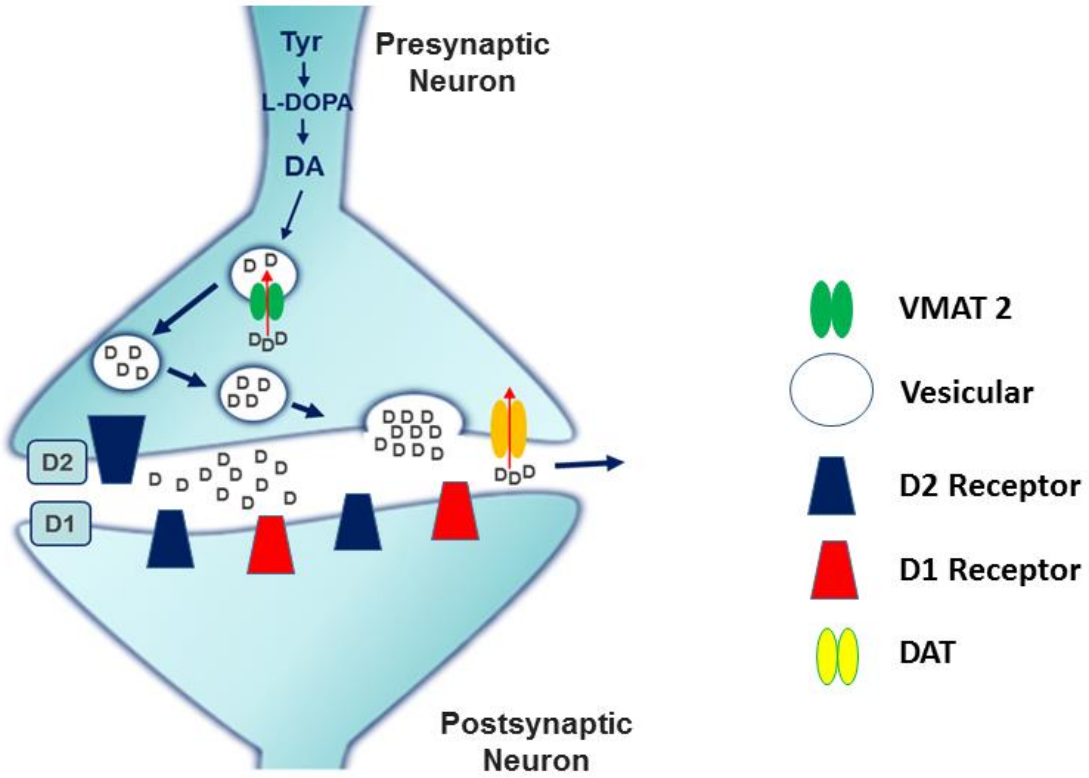

Figure 4. The process of dopamine storage, release, and uptake.

Once dopamine is released into extracellular fluid by exocytosis, it diffuses across the synapse and interacts with dopaminergic receptors located on either postsynaptic or presynaptic terminals (Fig. 4).[10 16] Most dopamine released is uptaken into the presynaptic terminals by dopamine transporter (DAT), a membrane bound protein that regulates the rate of dopamine uptake.[17] The process of uptake depends on the density of DAT available around the release site, and the uptake generally occurs on millisecond time scale. For example, dopamine is transferred back at a maximum rate of 3 µM per second in the rat striatum. [18] After dopamine is transported into the presynaptic neurons, dopamine can either be recycled back into the vesicles or

metabolized. The concentration of dopamine in the extracellular fluid is controlled by the release, uptake and diffusion [19-21].

1.1.3 Dopamine Receptors

Dopaminergic receptors, G-protein coupled receptors, are divided into two families, D1 like receptors and D2 like receptors, based on their ability to regulate adenylyl cyclase (AC) activity. These two different families are divided into five subclasses, the D1 like family includes D1 and D5 receptors, and D2 like family includes D2, D3, and D4 receptors. When dopamine activates D1 like family receptors, AC activity is stimulated whereas activation of D2 like family receptors inhibits AC activity[14 13]. D1 like family receptors are located postsynaptically, and D2 like family receptors are found to be located both postsynaptically and presynaptically [2, 8].

Generally, D2 like family receptors are known to function as autoreceptors, regulating the dopamine release mechanism. When autoreceptors are activated, the inhibition of AC activity leads to decreased dopamine release by either reducing neuronal action potential rate or by inhibiting dopamine synthesis or release [22-25]. Receptor antagonists and agonists can be used to probe the mechanism by which of dopamine release is controlled by these receptors. Receptor antagonists bind to the receptors and block the activation site. Receptor agonist also binds to the receptor to activate the receptors. For example, D2 receptor agonist, such as quinpirole, can decrease the amount of dopamine released into the extracellular space in the brain [26].

1.2 Electrochemical Methods in Neuroscience

As discussed in previous sections, dopamine release and uptake on millisecond time scale; therefore, the dopamine concentration in the extracellular fluid rapidly changes. Dopamine is not the only electroactive neurotransmitter available in the brain but also there are many others, such as norepinephrine and serotonin. In addition, there are other electroactive species available including ascorbic acid and dopamine metabolites, such as homovanillic acid. [27, 28] Therefore, to measure and distinguish dopamine release and uptake, the method requires a good selectivity, sufficient sensitivity, and sub-second temporal resolution.

1.2.1 Voltammetry

Voltammetry, the most widely used electrochemical technique for acquiring information about electrochemical reactions, was first discovered by a Czech chemist, Jaroslav Heyrovsky, who received the Novel Prize in 1959 for inventing polarographic analysis methods. [29] He discovered that organic molecules can be reduced at a dropping mercury electrode upon the application of a proper voltage [30]. Additionally, he found that the electric current information obtained from the electrode is related to the concentration of the reduced molecules. This current information can be plotted as a function of potential to generate a polarogram which can be used to identify analytes being reduced both in aqueous and non-aqueous solutions. [30]

Voltammetry, an electrochemical method that measures current as a function of applied potential in an electrochemical cell, provides qualitative and quantitative information about electroactive species in solutions. [31] There are various voltammetric techniques available based on the relationship between the measured current and applied potential, for instance, cyclic voltammetry, pulse voltammetry, square wave voltammetry, and so on. A voltammogram, a plot

of current measured as a function of applied potential, is used to determine peak potentials at which different electrochemical processes occur. Therefore, the voltammogram can be used to identify the target analyte in solution by observing the shape and the position of the peak potential in the plot. [32, 33]

An electrochemical cell consists of either two electrodes or three electrodes system. Two electrodes system, as shown in Fig. 5A, consists of a working electrode and a reference electrode. A working electrode provides an electroactive surface where electrochemical reactions of the target analytes occur. The potential applied to the working electrode is measured and controlled with respect to a nonpolarizable reference electrode [34]. As the current flows in the electrochemical cell, potential drop is observed. This potential drop is known as IR drop which is governed by Ohm's Law, E= IR, where I is current and R is the solution resistance [31]. The IR drop occurs when the differences in the resistance in solution and the potential required to move ions in solution is large. The IR drop can affect electrochemical methods by shifting the peak potential causing the distortion of voltammetry responses; therefore, the two electrodes system is typically used in low resistive solutions. [29, 31] In order to minimize the error caused by IR drop, a three electrode system, shown in Fig. 5B, can be used. The three electrode system consists of a counter electrode, in addition to the working electrode and the reference electrode. The counter electrode, generally fabricated using chemically inert metal, such as platinum, provides the current required to sustain current flow at the working electrode mitigating the electrochemical measurement errors due to the IR drop.

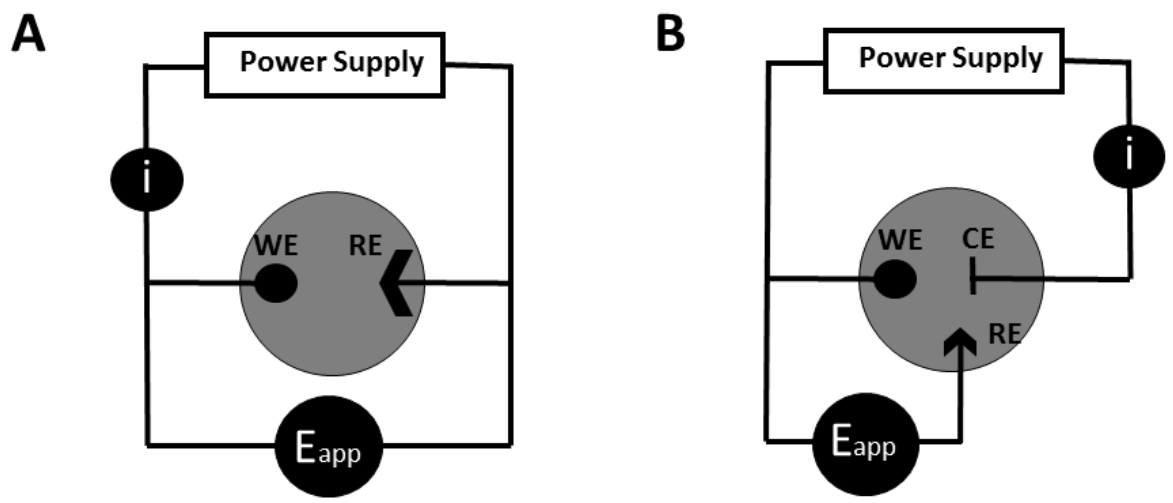

Figure 5. Schematic diagram of two or three electrode system in electrochemical cell. (A). Two electrode system consists of the working electrode (WE) and the reference electrode (RE). i represent an ammeter for measuring the electric current flow. E_{app} represents a voltmeter for controlling potential applied to WE by measuring potential differences between WE and RE. (B) Three electrode system consists of counter electrode (CE), WE, and RE.

.

1.2.2 Cyclic Voltammetry

Cyclic voltammetry is a voltammetric technique that acquires valuable information about redox processes, oxidation and reduction reactions, of electroactive species. Moreover, cyclic voltammetry also provides information on electron transfer reactions, chemical reactions, or adsorption processes. [35] In cyclic voltammetry, potential is applied linearly to the working electrode. As shown in Fig.6, the potential is applied linearly from initial potential to switching potential (forward scan), at which the highest potential is applied. At the switching potential, the

direction of the scan changes back to the initial potential (reverse scan). The direction of initial scan can be either negative, as shown in Fig.6 or positive, depending on the composition of the sample. Typically, one cycle takes less than 100 s and this cycle can be repeated several times. [34]

As the triangular waveform is applied to the electrode, two different faradaic currents can be observed. Anodic current occurs when the analyte in solution is oxidized at the electrode surface as the applied potential is reached to more positive potential, causing electrons to flow from the analyte to the electrode. On the other hand, cathodic current occurs when the analyte in solution is reduced as the applied potential is scanned to more negative potential, causing electrons to flow from the electrode to the analyte in solution. A plot of current responses can be generated as the function of applied potentials resulting a cyclic voltammogram.

Cyclic voltammetry wasn't applied to measure electroactive molecules in the central nervous system *in vivo* until 1970s. [29 36] Ralph Adams, of the Department of Chemistry at The University of Kansas, applied cyclic voltammetry to detect neurotransmitters and their metabolites at a miniaturized carbon paste electrode in the rat brains for the first time. [33, 36, 37] Since then, voltammetry has been used to develop various methods, including constant-potential amperometry and fast-scan cyclic voltammetry, which have been employed in various applications to understand not only fundamental properties of neurotransmitter release and uptake mechanism but also neurochemical basis of neurodegenerative diseases.[38]

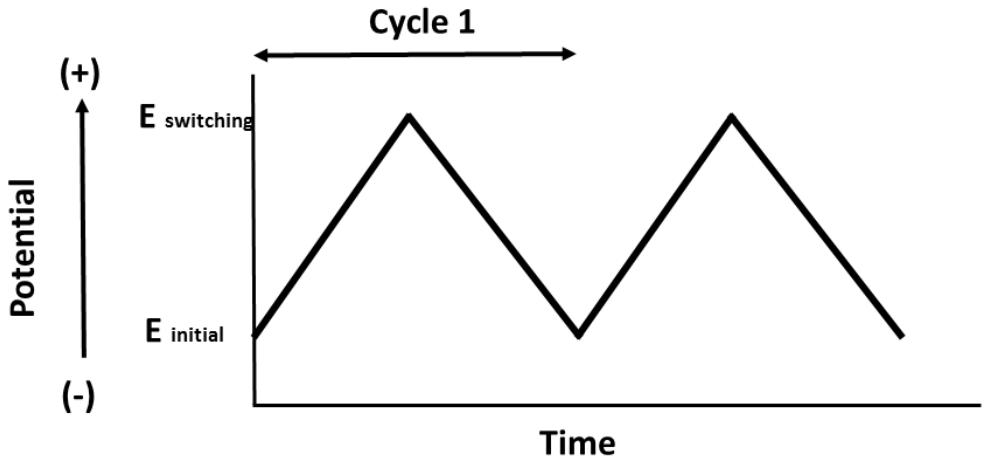

Figure 6. A triangular waveform used in a cyclic voltammetry

1.2.3 Fast-Scan Cyclic Voltammetry

Methodologically, fast-scan cyclic voltammetry is similar to conventional cyclic voltammetry in that a triangular waveform is applied to the working electrode. To perform fast-scan cyclic voltammetry, the potential is increased linearly to the working electrode from holding potential to the switching potential and then scanned back to the holding potential at a fast scan rate, typically higher than 100 V/s. [32, 38] This rapid scanning electrochemical method provides a cyclic voltammogram, which provides valuable information to identify the target analyte by observing the position of oxidation and reduction potential peaks. Moreover, most electroactive species, including neurotransmitters, have distinctive chemical signatures.

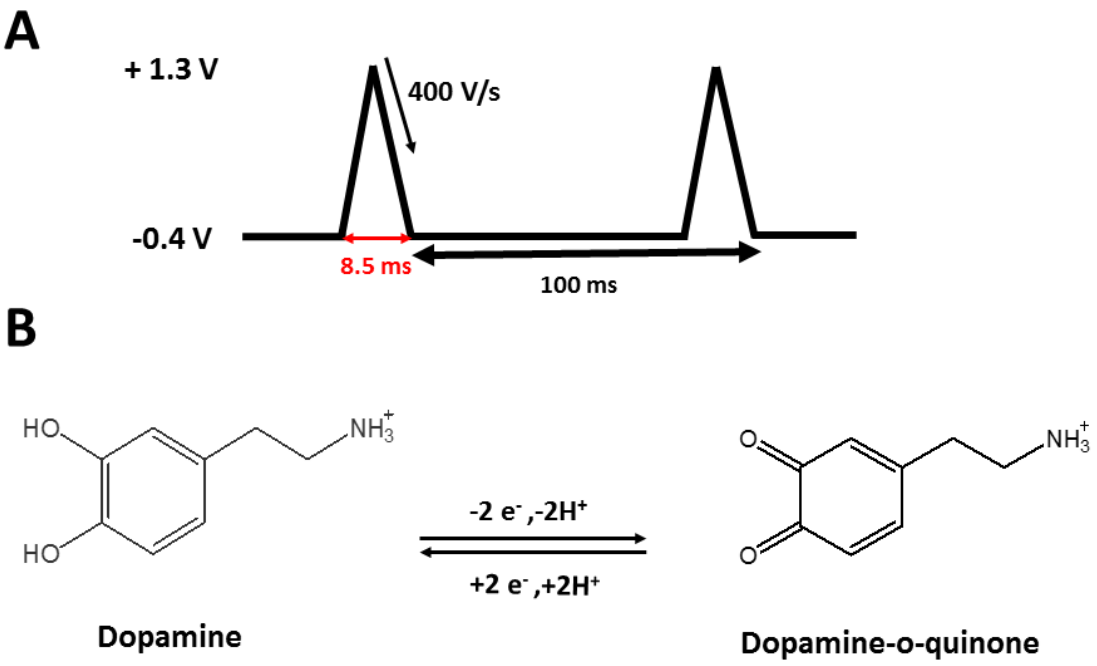

Figure 7. Fast-scan cyclic voltammetry and dopamine oxidation and reduction reaction.

One of challenges of detecting dopamine in the brain is that dopamine is released and taken up rapidly on sub-second time scale [14]. The high scan rate used in fast-scan cyclic voltammetry offers sub-second temporal resolution [39, 40], which allows the measurement of dopamine release and uptake events in the brain. Moreover, the holding potential, the switching potential, and scan rate can be adjusted to improve sensitivity, selectivity, and temporal resolution based on the analyte of interest. For example, Fig. 7 shows the commonly employed waveform to measure dopamine changes in the brain, in which the potential applied to the working electrode is scanned from – 0.4 V to + 1.3 V and back to – 0.4 V at 400 V/s, and this cycle is repeated every 100 ms. As the potential is ramped up linearly, dopamine is oxidized to dopamine-o-quinone on the positive sweep and reduced on the negative sweep.

One of the major disadvantages of employing the fast scan method is large background current generation due to the formation of charging double layers[31, 32]. This large background current exceeds faradaic current, thus making it difficult to observe the current differences. However, the large background current is stable between each scan and can be digitally subtracted providing background subtracted cyclic voltammogram.

1.2.4 Carbon-Fiber Microelectrodes

Fast-scan cyclic voltammetry at carbon-fiber microelectrodes, a popular method used to understand a sub-second fluctuation of neurotransmissions in the brain, was developed largely by the independent work of Martin Fleischmann and R. Mark Wightman around 1980 [41]. Microelectrodes, broadly defined as possessing at least one dimension in micron scale which is typically less than 25 μm [42, 43], provide several advantages over other conventional electrodes. Due to the small feature of the microelectrodes, the tissue damage occurs during the electrode implantation is significantly minimized. [32] Moreover, the diffusional characteristics of microelectrodes allow the fast accomplishment of steady-state currents, permitting sub-second time regime and minimization of IR drop [44]. Additionally, carbon-fiber microelectrodes may be fabricated at low cost and are biologically compatible with the cellular environment. Typically carbon-fiber used to fabricate microelectrodes as range between 5 – 10 μm [45]; however, the carbon-fiber microelectrodes used in this study, shown in Fig. 8, are fabricated in house using 7 μm diameter carbon-fiber and cut to 30 – 50 μm in length from the end of pulled capillary. The fabrication process of the carbon-fiber microelectrode is discussed in detail under *the Material and Method* section of the subsequent chapters.

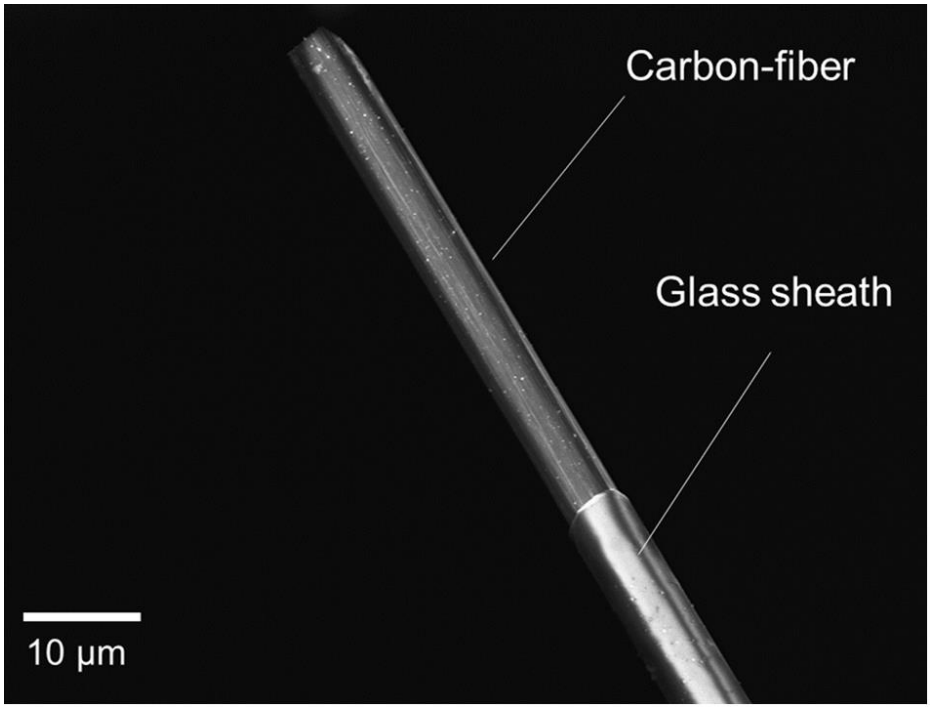

Figure 8. Scanning electron microscopy image of a carbon-fiber microelectrode

1.3 Animal models in neuroscience

Animal models with simple nervous systems have been widely used in neuroscience research to explore monoamine dynamics as well as to gain an understanding of the genetic basis of neurological disease. Rodents, especially rats and mice, have been the most commonly used animal models in the neuroscience community. [46] Fast-scan cyclic voltammetry at carbon-fiber microelectrode have been widely used with rodent models to determine the fast fluctuations of neurotransmitter release, including dopamine and serotonin, in both *vitro* and *vivo* [47 48-51] However, rodent model system have several disadvantages. The life cycle of rats and mice are long, increasing the time needed for the identification of neuronal changes in longitudinal studies

[52]. For example, our group used rats for chemobrain model and a month of intravenous injections (I.V) of carboplatin administered through the tail vein.[53] This I.V tail vein injection is stressful both on the rats and person who performs the treatment. The majority of times, it is hard to restrain the rat causing more than one trial to insert syringe needle into the tail vein. Additionally, genetic manipulation of rodents, especially rats, is costly and time-consuming [54 55].

1.4 Zebrafish

Zebrafish (*Danio rerio*); Fig. 9, has emerged as a popular alternative vertebrate animal model to rodents to investigate human disease, extensively used in neuroscience, toxicology, pharmacology, and developmental biology. [56-58] Zebrafish were established as an animal model in the 1970s by Dr. George Streisinger at the University of Oregon. [57, 59, 60] Zebrafish are small and require a simple natural habitat environment; thus it is relatively easier to house zebrafish under more natural conditions compared to rodent animal models. Zebrafish produce a large number of eggs, generally 100 – 200, compared to 5 – 10 pups per litter produced by rodents, providing the opportunity for high-throughput analyses.[61] Zebrafish embryos are transparent and develop externally thus permitting researchers to understand how certain genetic gene are impacted by either pharmacological treatment or environment changes during the development stages, shown in Fig. 10. Zebrafish also share large number of orthologue genes with humans.[62] [63] For instance, it appears to be that about 71.4% of human genes contain at least one obvious zebrafish orthologue, and 82% of it is related to disease-causing human genes. [63] Additionally, the significant contribution to use of zebrafish as animal model is the availability of human disease models, including neurodegenerative models[54].

Figure 9. Image of adult zebrafish.

Genetic manipulations in zebrafish are less costly and more straightforward to perform by microinjecting of mRNA encoding the target gene into embryo during the single cell stage[64]. Using such methodology, transgenic zebrafish models for neurodegenerative disorders, such as Parkinson's disease [65, 66], Huntington's disease [67], and Alzheimer Disease [68], have been developed. Additionally, there are many genetic similarities between the zebrafish and human central nervous systems. For instance, zebrafish that model Parkinson's disease have the *parkin* gene that encodes proteins sharing 62% identity and 92% similarity in its functional domains [69], and Huntington's disease zebrafish model shares about 70 % identity with human *htt* gene [70].

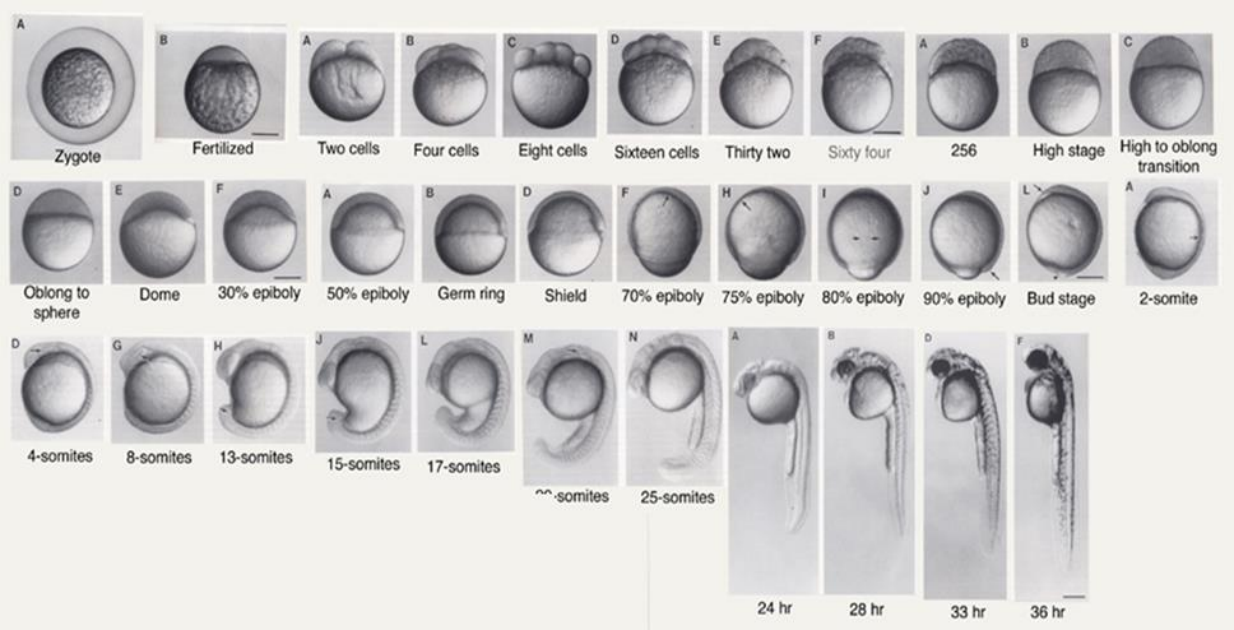

Figure 10. Stages of zebrafish embryonic development. This obtained figure was permitted to use from Ref. 64

1.4.1 Zebrafish Dopamine System

The dopamine system in zebrafish share similarities to that in mammalian systems. Gene expression studies have suggested that zebrafish expressed tyrosine hydroxylase (TH) in dopaminergic neurons and dopamine transporters [71] and identified D1 and D2 like dopamine receptor genes [72]. Immunohistochemistry studies in zebrafish have shown that the dopaminergic neurons can be differentiated as early as 18 hours post fertilization (hpf) and their dopamine system is well advanced by 72 hpf [71]. Moreover, the most of dopamine neuronal cluster was found to be located in diencephalon and no dopamine cluster was observed in the hindbrain.

The ventral telencephalon, shown in Fig. 11, the target region of the brain we are interested to measure dopamine release and uptake, is suggested to be analogous to that of striatum in human. [73, 74] In addition, zebrafish dopaminergic neurons send ascending projection

from ventral diencephalon, known to contain the majority population of dopamine cluster, to the ventral telencephalon [75]. This ascending dopaminergic pathway, shown in Fig. 12, is suggested to be similar to nigrostriatal pathways in mammalian dopamine system [75].

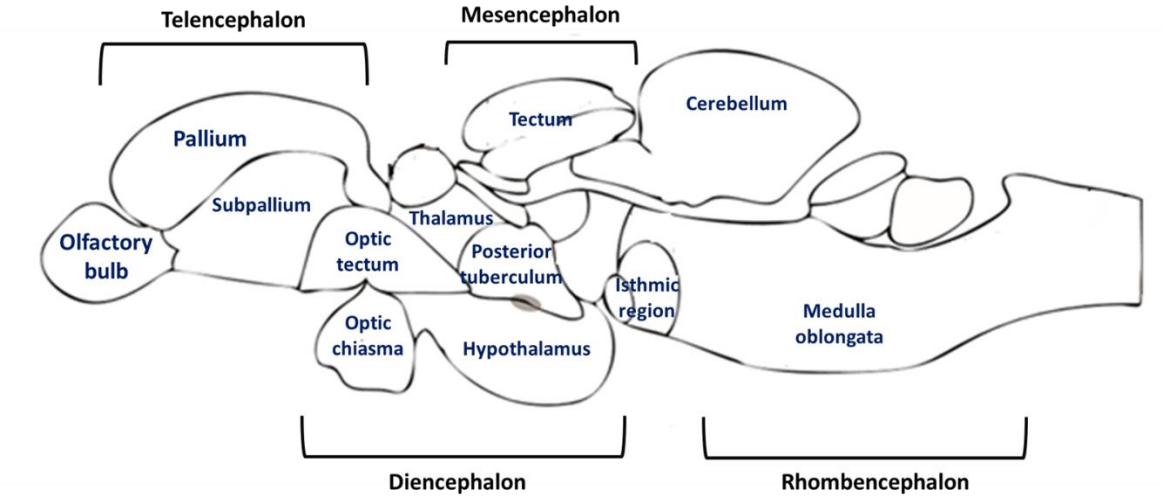

Figure 11. Schematic of simple illustration of zebrafish brain anatomy.

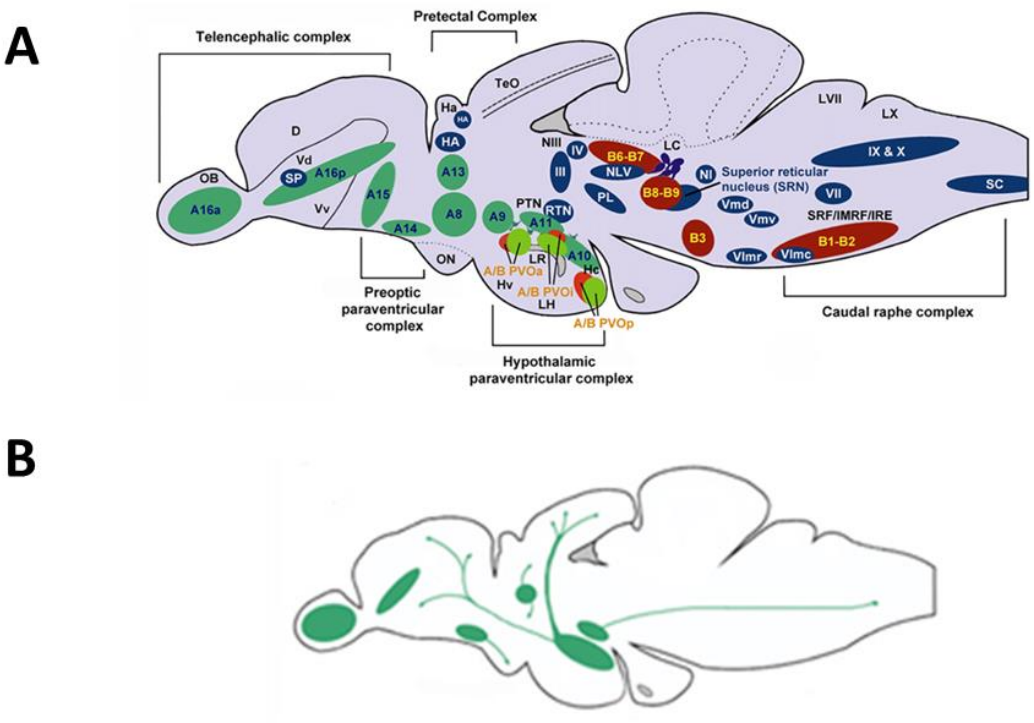

Figure 12. Schematic sagittal view of comparing dopaminergic neuronal population in zebrafish in green dots (A) and schematic view of the location of dopaminergic projection in adult zebrafish (B). These adapted figures are permitted to use from Ref. 75

1.4.2 Measurement of Dopamine in Zebrafish

Immunohistochemistry with high resolution imaging technique have been successfully used in zebrafish to understand the anatomy of neurotransmitters system in the brain. [76-78] These methods have been helpful in understanding how neurotransmitters are distributed in developing in zebrafish; however, these methods do not inform how zebrafish neurotransmitter function differs from that of rodents.

High pressure liquid chromatography (HPLC) has been employed to quantify the amount dopamine and their metabolites in zebrafish and determine changes in dopamine content. Chartterjee *et al*. applied HPLC, for the first time, to analyze alcohol induced dopamine changes in zebrafish [79] Moreover, HPLC was coupled with mass spectrometry to identify and quantify more than 17 neurotransmitters throughout the zebrafish life cycle. [80] Electrophysiology is another technique used in zebrafish to improve understanding of the central nervous system. [81] However, elucidating the neurotransmission in zebrafish compared to that of rodents is critical to extend the use of zebrafish as useful model in neuroscience. Therefore, direct measurement of neurotransmitter release and uptake is necessary.

The real-time measurement of dopamine in zebrafish has not been extensively investigated. Recently, Jones, *et al.* measured dopamine release in sagittal slices of zebrafish brain with fast-scan cyclic voltammetry at carbon-fiber microelectrodes.[82] In this study, they measured neurotransmitter release upon the application of either electrical stimulation or high concentration of K^+ at telencephalon using a saw tooth waveform. This study represent that the direct measurement of neurotransmitter release can be done in zebrafish brain using the electrochemical method. Neurotransmitter release study in brain slices haven been extensively done in rodents yielding much more information related to not only dopamine regulations in

different disease states but also the characterization of dopamine release and uptake kinetics. However, brain slice experiments can provide some drawback, such as disrupting the neuronal pathways [83] and causing tissue damage due to slice preparation.

Another study recently done to monitor real time measurement of dopamine release was conducted in larval zebrafish. In this study, Shang *et al*. developed a real- time method using amperometric detection method with carbon-fiber microelectrode to observe differences in response after introducing food extract to one of nostrils.[84] Moreover, *in vivo* imaging method was employed to understand the circuitry mechanism of dopamine release demonstrating that pretectal dopaminergic neurons are involved in evoked dopamine release in olfactory. This study was innovative since the experiment was done *in vivo* using larva zebrafish; however, it is practically difficult to measure dopamine release in adult zebrafish; limiting to study dopamine release throughout the life cycle.

1.5 The Summary of the Following Chapters

The goal of this introduction chapter was to provide background information about the detection methodology, dopamine, and animal models used in neuroscience research. The following chapters will be focused on developing methods to measure sub-second dopamine release in ex-vivo, harvested whole brain, and brain slices, with FSCV.

The Chapter 2 is focused on developing a robust protocol to position both stimulation and working electrodes in the whole brain to measure dopamine release and provide evidence of dopamine release upon the electrical stimulation by conducting several pharmacological studies. Dopamine release was measured not only in the harvested whole brain and but also different

brain slice preparations, coronal and sagittal slices. Moreover, the amount of dopamine was calculated using calibration factors obtained from measuring current responses against known concentrations and comparing different brain preparations and before and after pharmacological manipulation.

Chapter 3 is focused on developing zebrafish as a possible chemobrain model by treating zebrafish with carboplatin and 5-fluorouracil. In addition, drug was administrated to zebrafish by two different pathways: the habitat water treatment and food treatment. Once zebrafish were treated with each drug by different pathways, electrically evoked dopamine release was measured and compared.

Finally, Chapter 4 discusses about developing a method to quantitatively and simultaneously measure dopamine and 4-hydroxyphenylacetic acid (4HPAA). In addition, the oxidation mechanism of 4HPAA was studied and the waveform was optimized to enhance the sensitivity, selectivity, and temporal resolution of 4HPAA and dopamine detection. The reason we studied 4HPAA was because 4HPAA is the by-product of p-hydroxyphenylglutamage (pHP-Glu), caged glutamate used to improve spatial resolution of drug delivery to the targeted area thorough the simple process of photostimulation. Therefore, by determining the amount of 4HPAA photoreleased, the amount of released glutamate can be also quantified.

1.6 Reference

[1] Alcaro, A., Huber, R., and Panksepp, J. (2007) Behavioral functions of the mesolimbic dopaminergic system: An affective neuroethological perspective, *Brain Res. Rev., 56*, 283-321.

[2] Missale, C., Nash, S. R., Robinson, S. W., Jaber, M., and Caron, M. G. (1998) Dopamine receptors: from structure to function, *Physiol. Rev., 78*, 189-225.

[3] Olijslagers, J. E., Werkman, T. R., McCreary, A. C., Kruse, C. G., and Wadman, W. J. (2006) Modulation of midbrain dopamine neurotransmission by serotonin, a versatile interaction between neurotransmitters and significance for antipsychotic drug action, *Curr. Neuropharmacol., 4*, 59-68.

[4] Weiner, R. I., and Ganong, W. F. (1978) Role of brain monoamines and histamine in regulation of anterior pituitary secretion, *Physiol. Rev. 58*, 905-976.

[5] Volkow, N. D., Wang, G.-J., Fowler, J. S., Logan, J., Jayne, M., Franceschi, D., Wong, C., Gatley, S. J., Gifford, A. N., Ding, Y.-S., and Pappas, N. (2002) "Nonhedonic" food motivation in humans involves dopamine in the dorsal striatum and methylphenidate amplifies this effect, *Synapse, 44*, 175-180.

[6] Barbeau, A. (1962) The pathogenesis of Parkinson's disease: a new hypothesis, *Can. Med. Assoc. J., 87*, 802-807.

[7] Bjorklund, A., and Dunnett, S. B. (2007) Dopamine neuron systems in the brain: an update, *Trends Neurocsi., 30*, 194-202.

[8] Vallone, D., Picetti, R., and Borrelli, E. (2000) Structure and function of dopamine receptors, *Neurosci. Biobehav. Rev., 24*, 125-132.

[9] Justice, J. B., Jr. (1993) Quantitative microdialysis of neurotransmitters, *J. Neurosci. Meth., 48*, 263-276.

[10] Joseph, J. D., and Wightman, R. M. (2002) Mechanisms and kinetics of neurotransmission measured in brain slices with cyclic voltammetry, *Electroanalytical Methods Of Biological Materials*, pp 255-278, Marcel Dekker, Inc.

[11] Grace, A. A., and Bunney, B. S. (1980) Nigral dopamine neurons: intracellular recording and identification with L-dopa injection and histofluorescence, *Science, 210*, 654-656.

[12] Lee, W. Y., Chang, J. W., Nemeth, N. L., and Kang, U. J. (1999) Vesicular monoamine transporter-2 and aromatic L-amino acid decarboxylase enhance dopamine delivery after L-3,4-dihydroxyphenylalanine administration in Parkinsonian rats, *J. Neurosci., 19*, 3266-3274.

[13] Elsworth, J. D., and Roth, R. H. (1997) Dopamine synthesis, uptake, metabolism, and receptors: relevance to gene therapy of Parkinson's disease, *Exp. Neurol., 144*, 4-9.

[14] Venton, B. J., and Wightman, R. M. (2003) Psychoanalytical electrochemistry: dopamine and behavior, *Anal. Chem., 75*, 414 A-421 A.

[15] Cooper, J. R. (1997) Principles of Neuropsychopharmacology by R. S. Feldman, J. S. Meyer and L. F. Quenzer, *Trends Neurosci., 20*, 544.

[16] Neve, K. A. (2010) The introduction to dopamine receptors, *The dopamine receptors*, pp 1-21, *Humana Press*.

[17] Jones, S. R., Gainetdinov, R. R., Jaber, M., Giros, B., Wightman, R. M., and Caron, M. G. (1998) Profound neuronal plasticity in response to inactivation of the dopamine transporter, *Proc. Nat. Aca. Sci., 95*, 4029-4034.

[18] Kraft, J., Osterhaus, G., Ortiz, A., Garris, P., and Johnson, M. (2009) In vivo dopamine release and uptake impairments in rats treated with 3-nitropropionic acid, *Neuroscience, 161*, 940-949.

[19] Pothos, E. N., Davila, V., and Sulzer, D. (1998) Presynaptic recording of quanta from midbrain dopamine neurons and modulation of the quantal size, *J. Neurosci., 18*, 4106-4118.

[20] Hochstetler, S. E., Puopolo, M., Gustincich, S., Raviola, E., and Wightman, R. M. (2000) Real-Time Amperometric Measurements of Zeptomole Quantities of Dopamine Released from Neurons, *Anal. Chem., 72*, 489-496.

[21] Garris, P. A., and Wightman, R. M. (1994) Efflux of dopamine from the synaptic cleft in the nucleus accumbens of the rat brain: evidence for an extrasynaptic mode of dopaminergic transmission, *J. Neurosci.*, 10, 6084-6090.

[22] Gainetdinov, R. R., Grekhova, T. V., Sotnikova, T. D., and Rayevsky, K. S. (1994) Dopamine D2 and D3 receptor preferring antagonists differentially affect striatal dopamine release and metabolism in conscious rats, *Eur. J. Pharmacol., 261*, 327-331.

[23] Gainetdinov, R. R., Sotnikova, T. D., Grekhova, T. V., and Rayevsky, K. S. (1996) In vivo evidence for preferential role of dopamine D3 receptor in the presynaptic regulation of dopamine release but not synthesis, *Eur. J. Pharmacol. 308*, 261-269.

[24] Cass, W. A., and Gerhardt, G. A. (1994) Direct in vivo evidence that D2 dopamine receptors can modulate dopamine uptake, *Neurosci. Lett., 176*, 259-263.

[25] Meiergerd, S. M., Patterson, T. A., and Schenk, J. O. (1993) D2 receptors may modulate the function of the striatal transporter for dopamine: Kinetic evidence from studies in vitro and in vivo, *J. Neurochem., 61*, 764-767.

[26] Rothblat, D. S., and Schneider, J. S. (1997) Regionally specific effects of haloperidol and clozapine on dopamine reuptake in the striatum, *Neurosci. Lett., 228,* 119-122.

[27] Hermans, A., Keithley, R. B., Kita, J. M., Sombers, L. A., and Wightman, R. M. (2008) Dopamine detection with fast-scan cyclic voltammetry used with analog background subtraction, *Anal. Chem., 80,* 4040-4048.

[28] Richard B. Keithley, P. T., † Elizabeth S. Bucher,† Anna M. Belle,† Catarina A. Owesson-White,†, and Jinwoo Park, a. R. M. W. (2011) higher sensitivity dopamine measurement with fast scan cyclic voltammetry, *Anal. Chem., 9,* 3563-*3571.*

[29] Borland, A. C. m. a. L. M. (2007) *Electrochemical methods for neuroscience,* CRC press.

[30] Heyrovsky, J. (1959) Trends of polarography, *Prix Nobel,* 125-145.

[31] Allen J. Bard, L. R. F. (2001) *Electrochemical Methods: Fundermentals and applications,* 2nd ed., John Wiley and Sons, Inc.: New York.

[32] Peter T. Kissinger, W. R. H. (1996) *In Laboratory Techniques in Electroanalytical Chemistry,* 2nd ed., Marcel Dekker, Inc., New York.

[33] Kissinger, P. T., Hart, J. B., and Adams, R. N. (1973) Voltammetry in brain tissue--a new neurophysiological measurement, *Brain Res., 55,* 209-213.

[34] Loffler, U. (1994) Introduction to cyclic voltammetry, impedance spectroscopy, and modern interfacial analysis for systematic characterization of transducers, and (bio)sensors, *Sensorik, 4,* 100-122.

[35] Mabbott, G. A. (1983) An introduction to cyclic voltammetry, *J. Chem. Educ., 60,* 697-702.

[36] Adams, R. N. (1976) Probing brain chemistry with electroanalytical techniques, *Anal. Chem., 48,* 1126-1138.

[37] Wightman, R. M., Strope, E., Plotsky, P. M., and Adams, R. N. (1976) Monitoring of transmitter metabolites by voltammetry in cerebrospinal fluid following neural path stimulation, *Nature, 262*, 145-146.

[38] Bucher, E. S., and Wightman, R. M. (2015) Electrochemical analysis of neurotransmitters, *Annu. Rev. Anal. Chem., 8*, 239-261.

[39] B. E. Kurama Swamy, a. B. J. V. (2007) Subsecon detection of physiological adenosine concentration using fast scan cyclic voltammetry, *Anal.Chem., 79*, 744-750.

[40] Heien, M. L. A. V., Phillips, P. E. M., Stuber, G. D., Seipel, A. T., and Wightman, R. M. (2003) Overoxidation of carbon-fiber microelectrodes enhances dopamine adsorption and increases sensitivity, *Analyst, 128*, 1413-1419.

[41] Howell, J. O., and Wightman, R. M. (1984) Ultrafast voltammetry and voltammetry in highly resistive solutions with microvoltammetric electrodes, *Anal. Chem., 56*, 524-529.

[42] Hart, J. P. (1998) Laboratory Techniques in Electroanalytical Chemistry edited by Peter T. Kissinger and William R. Heineman, *Anal. Chim. Acta., 361*, 292-293.

[43] Fleischmann, M., and Pons, S. (1987) The behavior of microelectrodes, *Anal. Chem., 59*, 1391A.

[44] Takmakov, P., Zachek, M. K., Keithley, R. B., Walsh, P. L., Donley, C., McCarty, G. S., and Wightman, R. M. (2010) Carbon microelectrodes with a renewable surface, *Anal. Chem., 82*, 2020-2028.

[45] Ewing, A. G., Dayton, M. A., and Wightman, R. M. (1981) Pulse voltammetry with microvoltammetric electrodes, *Anal. Chem., 53*, 1842-1847.

[46] Zimmermann, M. (1987) Ethical principles for the maintenance and use of animals in neuroscience research, *Neurosci. Lett., 73*, 1.

[47] Joseph, J. D., Wang, Y. M., Miles, P. R., Budygin, E. A., Picetti, R., Gainetdinov, R. R., Caron, M. G., and Wightman, R. M. (2002) Dopamine autoreceptor regulation of release and uptake in mouse brain slices in the absence of D3 receptors, *Neuroscience. 112*, 39-49.

[48] Apawu, A. K., Mathews, T. A., and Bowen, S. E. (2015) Striatal dopamine dynamics in mice following acute and repeated toluene exposure, *Psychopharmacology, 232*, 173-184.

[49] Burrell, M. H., Atcherley, C. W., Heien, M. L., and Lipski, J. (2015) A novel electrochemical approach for prolonged measurement of absolute levels of extracellular dopamine in brain slices, *ACS Chem. Neurosci., 1948-7193*.

[50] Walker, Q. D., Rooney, M. B., Wightman, R. M., and Kuhn, C. M. (1999) Dopamine release and uptake are greater in female than male rat striatum as measured by fast cyclic voltammetry, *Neuroscience, 95*, 1061-1070.

[51] Ferris, M. J., Calipari, E. S., Yorgason, J. T., and Jones, S. R. (2013) Examining the complex regulation and drug-induced plasticity of dopamine release and uptake using voltammetry in brain slices, *ACS Chem. Neurosci., 4*, 693-703.

[52] Turner, P. V., Brabb, T., Pekow, C., and Vasbinder, M. A. (2011) Administration of substances to laboratory animals: routes of administration and factors to consider, *J. Am. Assoc. Lab. Anim. Sci., 50*, 600-613.

[53] Kaplan, S. V., Limbocker, R. A., Gehringer, R. C., Divis, J. L., Osterhaus, G. L., Newby, M. D., Sofis, M. J., Jarmolowicz, D. P., Newman, B. D., Mathews, T. A., and Johnson, M. A. (2016) Impaired brain dopamine and serotonin release and uptake in wistar rats following treatment with carboplatin, *ACS Chem. Neurosci., 7*, 689-699.

[54] Xi, Y., Noble, S., and Ekker, M. (2011) Modeling neurodegeneration in zebrafish, *Curr. Neurol. Neurosci. Rep., 11*, 274-282.

[55] Zala SM, M. I., Penn DJ. (2012) Different social-learning strategies in wild and domesticated zebrafish, Danio rerio., *Anim. Behav., 83*, 1519-1525.

[56] Fetcho, J. R., and Liu, K. S. (1998) Zebrafish as a Model System for Studying Neuronal Circuits and Behaviora, *Ann. N. Y. Acad. Sci., 860*, 333-345.

[57] Grunwald, D. J., and Eisen, J. S. (2002) Headwaters of the zebrafish -- emergence of a new model vertebrate, *Nat. Rev. Genet., 3*, 717-724.

[58] Ali, S., Champagne, D. L., Spaink, H. P., and Richardson, M. K. (2011) Zebrafish embryos and larvae: a new generation of disease models and drug screens, *Birth Defects Res. C Embryo Today., 93*, 115-133.

[59] Williams, R. (2010) Thanks be to zebrafish, *Circ. Res., 107*, 570-572.

[60] Li, H.-h., Huang, P., Dong, W., Zhu, Z.-y., and Liu, D. (2013) A brief history of zebrafish research-toward biomedicine, *Yichuan, 35*, 410-420.

[61] Babin, P. J., Goizet, C., and Raldua, D. (2014) Zebrafish models of human motor neuron diseases: Advantages and limitations, *Prog. Neurobiol.*,118, 36-58.

[62] Lieschke, G. J., and Currie, P. D. (2007) Animal models of human disease: zebrafish swim into view, *Nat. Rev. Genet., 8*, 353-367.

[63] Howe, K., and Clark, M. D., and Torroja, C. F., and Torrance, J., and Berthelot, C., and Muffato, M., and Collins, J. E., and Humphray, S., and McLaren, K., and Matthews, L., and McLaren, S., and Sealy, I., and Caccamo, M., and Churcher, C., and Scott, C., and Barrett, J. C., and Koch, R., and Rauch, G. J., and White, S., and Chow, W., and Kilian, B., and Quintais, L. T., and Guerra-Assuncao, J. A., and Zhou, Y., and Gu, Y., and Yen,

J., and Vogel, J. H., and Eyre, T., and Redmond, S., and Banerjee, R., and Chi, J., and Fu, B., and Langley, E., and Maguire, S. F., and Laird, G. K., and Lloyd, D., and Kenyon, E., and Donaldson, S., and Sehra, H., and Almeida-King, J., and Loveland, J., and Trevanion, S., and Jones, M., and Quail, M., and Willey, D., and Hunt, A., and Burton, J., and Sims, S., and McLay, K., and Plumb, B., and Davis, J., and Clee, C., and Oliver, K., and Clark, R., and Riddle, C., and Elliot, D., and Threadgold, G., and Harden, G., and Ware, D., and Begum, S., and Mortimore, B., and Kerry, G., and Heath, P., and Phillimore, B., and Tracey, A., and Corby, N., and Dunn, M., and Johnson, C., and Wood, J., and Clark, S., and Pelan, S., and Griffiths, G., and Smith, M., and Glithero, R., and Howden, P., and Barker, N., and Lloyd, C., and Stevens, C., and Harley, J., and Holt, K., and Panagiotidis, G., and Lovell, J., and Beasley, H., and Henderson, C., and Gordon, D., and Auger, K., and Wright, D., and Collins, J., and Raisen, C., and Dyer, L., and Leung, K., and Robertson, L., and Ambridge, K., and Leongamornlert, D., and McGuire, S., and Gilderthorp, R., and Griffiths, C., and Manthravadi, D., and Nichol, S., and Barker, G., and Whitehead, S., and Kay, M., and Brown, J., and Murnane, C., and Gray, E., and Humphries, M., and Sycamore, N., and Barker, D., and Saunders, D., and Wallis, J., and Babbage, A., and Hammond, S., and Mashreghi-Mohammadi, M., and Barr, L., and Martin, S., and Wray, P., and Ellington, A., and Matthews, N., and Ellwood, M., and Woodmansey, R., and Clark, G., and Cooper, J., and Tromans, A., and Grafham, D., and Skuce, C., and Pandian, R., and Andrews, R., and Harrison, E., and Kimberley, A., and Garnett, J., and Fosker, N., and Hall, R., and Garner, P., and Kelly, D., and Bird, C., and Palmer, S., and Gehring, I., and Berger, A., and Dooley, C. M., and Ersan-Urun, Z., and Eser, C., and Geiger, H., and Geisler, M., and Karotki, L., and Kirn, A., and Konantz, J.,

and Konantz, M., and Oberlander, M., and Rudolph-Geiger, S., and Teucke, M., and Lanz, C., and Raddatz, G., and Osoegawa, K., and Zhu, B., and Rapp, A., and Widaa, S., and Langford, C., and Yang, F., and Schuster, S. C., and Carter, N. P., and Harrow, J., and Ning, Z., and Herrero, J., and Searle, S. M., and Enright, A., and Geisler, R., and Plasterk, R. H., and Lee, C., and Westerfield, M., and de Jong, P. J., and Zon, L. I., and Postlethwait, J. H., and Nusslein-Volhard, C., and Hubbard, T. J., and Roest Crollius, H., and Rogers, J., and Stemple, D. L. (2013) The zebrafish reference genome sequence and its relationship to the human genome, *Nature*, *496*, 498-503.

[64] Kimmel, C. B., Ballard, W. W., Kimmel, S. R., Ullmann, B., and Schilling, T. F. (1995) Stages of embryonic development of the zebrafish, *Dev. Dynam.*, *203*, 253-310.

[65] Anichtchik, O., Diekmann, H., Fleming, A., Roach, A., Goldsmith, P., and Rubinsztein, D. C. (2008) Loss of PINK1 function affects development and results in neurodegeneration in zebrafish, *J. Neurosci.*, *28*, 8199-8207.

[66] Bretaud, S., Allen, C., Ingham, P. W., and Bandmann, O. (2007) p53-dependent neuronal cell death in a DJ-1-deficient zebrafish model of Parkinson's disease, *J. Neurochem.*, *100*, 1626-1635.

[67] Henshall, T. L., Tucker, B., Lumsden, A. L., Nornes, S., Lardelli, M. T., and Richards, R. I. (2009) Selective neuronal requirement for huntingtin in the developing zebrafish, *Hum. Mol. Genet.*, *18*, 4830-4842.

[68] Tomasiewicz, H. G., Flaherty, D. B., Soria, J. P., and Wood, J. G. (2002) Transgenic zebra fish model of neurodegeneration, *J. Neurosci. Res.*, *70*, 734-745.

[69] Flinn, L., Mortiboys, H., Volkmann, K., Koster, R. W., Ingham, P. W., and Bandmann, O. (2009) Complex I deficiency and dopaminergic neuronal cell loss in parkin-deficient zebrafish (Danio rerio), *Brain, 132*, 1613-1623.

[70] Karlovich, C. A., John, R. M., Ramirez, L., Stainier, D. Y. R., and Myers, R. M. (1998) Characterization of the Huntington's disease (HD) gene homolog in the zebrafish Danio rerio, *Gene, 217*, 117-125.

[71] Kastenhuber, E., Kratochwil, C. F., Ryu, S., Schweitzer, J., and Driever, W. (2010) Genetic dissection of dopaminergic and noradrenergic contributions to catecholaminergic tracts in early larval zebrafish, *J. Comp. Neurol., 518*, 439-458.

[72] Schweitzer, J., and Driever, W. (2009) Development of the dopamine systems in zebrafish, *Adv. Exp. Med. Biol., 651*, 1-14.

[73] Rink, E., and Wullimann, M. F. (2004) Connections of the ventral telencephalon (subpallium) in the zebrafish (Danio rerio), *Brain Res., 1011*, 206-220.

[74] Rink, E., and Wullimann, M. F. (2001) The teleostean (zebrafish) dopaminergic system ascending to the subpallium (striatum) is located in the basal diencephalon (posterior tuberculum), *Brain Res., 889*, 316-330.

[75] Parker, M. O., Brock, A. J., Walton, R. T., and Brennan, C. H. (2013) The role of zebrafish (Danio rerio) in dissecting the genetics and neural circuits of executive function, *Front. Neural Circuits., 7*, 63.

[76] Delgado, L., and Schmachtenberg, O. (2008) Immunohistochemical localization of GABA, GAD65, and the Receptor Subunits GABAAα1 and GABAB1 in the Zebrafish Cerebellum, *Cerebellum, 7*, 444-450.

[77] Edwards, J. G., Greig, A., Sakata, Y., Elkin, D., and Michel, W. C. (2007) Cholinergic innervation of the zebrafish olfactory bulb, *J. Comp. Neurol., 504*, 631-645.

[78] McLean, D. L., and Fetcho, J. R. (2004) Relationship of tyrosine hydroxylase and serotonin immunoreactivity to sensorimotor circuitry in larval zebrafish, *J. Comp. Neurol., 480*, 57-71.

[79] Chatterjee, D., and Gerlai, R. (2009) High precision liquid chromatography analysis of dopaminergic and serotoninergic responses to acute alcohol exposure in zebrafish, *Behav. Brain Res., 200*, 208-213.

[80] Santos-Fandila, A., Vazquez, E., Barranco, A., Zafra-Gomez, A., Navalon, A., Rueda, R., and Ramirez, M. (2015) Analysis of 17 neurotransmitters, metabolites and precursors in zebrafish through the life cycle using ultrahigh performance liquid chromatography-tandem mass spectrometry, *J. Chromatogr. B: Anal. Technol. Biomed. Life Sci., 1001*, 191-201.

[81] Vargas, R., Johannesdottir, I. T., Sigurgeirsson, B., Thorsteinsson, H., and Karlsson, K. A. E. (2011) The zebrafish brain in research and teaching: a simple in vivo and in vitro model for the study of spontaneous neural activity, *Adv. Physiol. Educ., 35*, 188-196.

[82] Jones, L. J., McCutcheon, J. E., Young, A. M., and Norton, W. H. (2015) Neurochemical measurements in the zebrafish brain, *Front. Behav. Neurosci., 9*.

[83] Ullrich, C., Daschil, N., and Humpel, C. (2011) Organotypic vibrosections: novel whole sagittal brain cultures, *J Neurosci. Meth., 201*, 131-141.

[84] Shang, C.-f., Li, X.-q., Yin, C., Liu, B., Wang, Y.-f., Zhou, Z., and Du, J.-l. (2015) Amperometric monitoring of sensory-evoked dopamine release in awake larval zebrafish, *J. Neurosci. ,35*, 15291-15294.

Chapter 2. Measurement of dopamine release and uptake in zebrafish

Development of a robust protocol to electrically evoke and measure dopamine release and uptake using fast-scan cyclic voltammetry at carbon-fiber microelectrodes in harvested zebrafish whole brain and brain slices is discussed in this chapter. The results presented in this chapter are from "Ex vivo Measurement of Electrically Evoked Dopamine Release in Zebrafish Whole Brain" that has been submitted to *ACS Chemical Neuroscience.*

2.1 Introduction

Zebrafish (*Danio rerio*) are teleosts that were initially established as a model organism in the 1970s by George Streisinger for the study of development [1-3]. Recently, zebrafish have emerged as a desirable model for the study of neuronal function [4, 5] because they approximate the human central nervous system more accurately than invertebrates and are easier to genetically manipulate than rodents [6]. Moreover, the optical transparency of zebrafish larvae make this organism well-suited for in vivo studies in which intracellular calcium changes [7, 8] and action potentials [9]can be imaged in real-time. Also, the zebrafish central nervous system, when studied using cultured cells [10], brain slices [11], and intact brain [12, 13], has proven amenable to electrophysiological measurements of neuronal firing.

In addition to these methods, the use of electrochemistry to measure the release and uptake of neurotransmitters in zebrafish is just now being realized. Fast-scan cyclic voltammetry (FSCV) at carbon-fiber electrodes is an electrochemical technique that provides good chemical selectivity and sub-second temporal resolution, allowing the measurement of release and uptake of electroactive neurotransmitters [14-17]. FSCV has been used extensively in rodents to measure the

release and uptake dynamics of dopamine, an abundant catecholamine neurotransmitter that plays a role in many aspects of neurological function, including the control of intentional movement [18, 19], cognition [20], and reward [21, 22].

Recently, the release of dopamine and other neurotransmitters was measured in brain slices acutely harvested from zebrafish [23]. The analysis of brain slices from various neuronal systems, including rodents, has yielded much information regarding disease state mechanisms [24-28] and fundamental neurotransmitter release properties [29]. However, brain slice preparations have several drawbacks such as cellular damage induced at the surface of the slice [30-32] and difficulty in capturing entire neuronal pathways [33, 34].

The use of intact brains could mitigate these problems by decreasing the amount of tissue damage and leaving the neuronal pathways intact, thereby allowing remote stimulation of the pathway and eliminating the release of interfering neurotransmitters and neuromodulators that would be present upon local stimulation. However, electrochemical neurotransmitter release measurements within the intact brain of zebrafish have not yet been reported in the literature; thus, the measurement of locally-stimulated dopamine release from acutely harvested, intact zebrafish brains, and comparison of these measurements with those from brain slices, represents a critical first step.

Here, we describe measurements of dopamine release and uptake in whole, intact zebrafish brains with FSCV. Furthermore, we compare these measurements to those obtained in sagittal and coronal brain slices. We found that, when the working electrode is properly placed by reference to the external features of the removed brain, electrically evoked dopamine release and uptake is easily measured in zebrafish whole brain ex vivo. The cyclic voltammograms obtained strongly suggest that the neurotransmitter measured is dopamine. Moreover, we confirmed the detection

of dopamine with pharmacological agents that alter dopamine release and uptake. These results support the use of FSCV in ex vivo whole brain preparations as a useful analytical tool for measuring neurotransmitter release and uptake in zebrafish.

2.2 Summary of the Studies Described in This Chapter

This chapter demonstrates the electrochemical measurements of dopamine release and uptake in different zebrafish brain preparations, such as whole brains, sagittal slices, and coronal slices. In these studies, we develop a robust procedure to accurately position stimulating and working electrodes in order to measure evoked dopamine and conduct pharmacological studies, especially in harvested whole brains. The experiments were performed using wild type adult zebrafish.

2.3. Materials and Methods

2.3.1 Zebrafish

All animal procedures were approved by the University of Kansas Institutional Animal Care and Use Committee. Adult zebrafish used for these studies were housed in the Molecular Probes Core of the Center for Molecular Analysis of Disease Pathways at the University of Kansas. Zebrafish were euthanized by rapid chilling, also known as hypothermic shock. To perform euthanasia, the main system water was chilled to 2-4℃. Zebrafish then were transferred by a net from an Aquatic Habitats™ ZF0601 (Pentair, Cary, NC, USA), the main housing system, into the chilled system water.

2.3.1.1 Zebrafish Whole Brain Preparation

The whole brain preparation method was modified from the procedure described previously [35]. To harvest a whole brain from a zebrafish, a euthanized zebrafish was decapitated using a 0.009" single edge blades (VWR Corporates, Radnor, PA, USA). As shown in figure 1A, the decapitated zebrafish head was inserted into pre-prepared dissection pads made with 2% agarose (BioReagent graded agarose, Sigma-Aldrich, St. Louis, MO, USA) in 100mm x 15mm petri dishes (ThermoFisher Scientific, Waltham, MA, USA). The petri dish was filled with oxygenated (95% O_2 / 5% CO_2) zebrafish ice-cold artificial cerebral spinal fluid (ZF aCSF).

The ZF aCSF consisted of 131 mM NaCl, 2 mM KCl, 1.25 mM KH_2PO_4, 20 mM $NaHCO_3$, 2 mM $MgSO_4$, 10 mM glucose, 2.5 mM $CaCl_2 \cdot H_2O$, and 10 mM HEPES, and the pH was adjusted to 7.4. The decapitated zebrafish head was then fixed by pinning it with a syringe needle. The skull of the zebrafish was carefully removed using micro tweezers and forceps, and the brain was accurately removed with a pulled capillary. The brain was then transferred into the recording chamber that was perfused with oxygenated ZF aCSF and the brain was kept at physiological temperature of 28℃. The brain was placed ventral side face up to expose the sub pallium in telencephalon, the region of interest containing dopaminergic innervation [36]. Then the brain was immobilized by placement of a nylon mesh harp on the top. Prior to measurements, the brain was equilibrated for 1 hour.

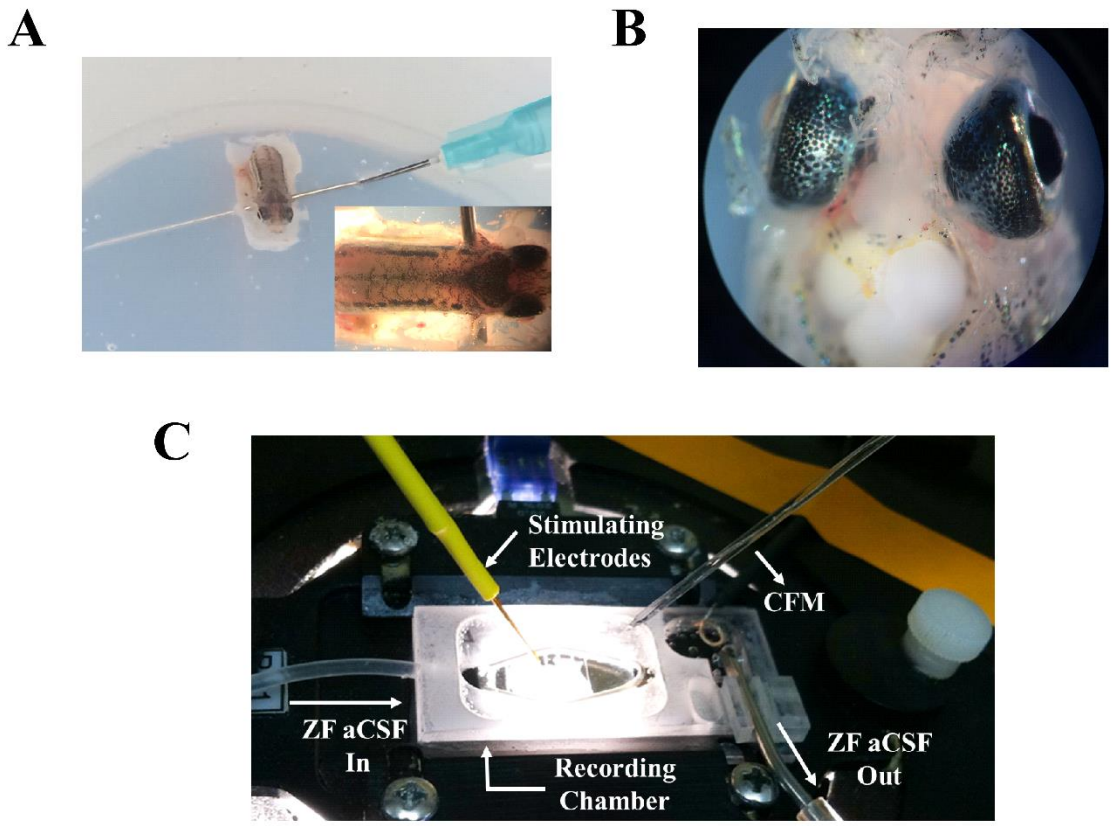

Figure 1. Adult zebrafish whole brain preparation. A. Image of decapitated zebrafish head pinned with a syringe needle in 2% agarose covered petri dish. The petri dish was filled with oxygenated ZF aCSF. B. Image of zebrafish head exposed its brain after the skull was removed using micro-tweezer. C. Image of FSCV recording setup. The harvested zebrafish brain was placed in the recording chamber that was perfused with oxygenated ZF aCSF and the brain was held in the chamber placing a nylon mesh harp on top.

2.3.1.2 Zebrafish Brain Slice Preparation.

Harvested brains were suspended in 2% low gelling point agarose (Agarose type VII-A, Sigma-Aldrich, St Louis, MO, USA) prepared in 50 % distilled water and 50% oxygenated ZF aCSF. After the agarose hardened, a block of agarose containing the brain was cut off and glued

onto a specimen disk and fastened in the buffer tray of a vibratome (Leica microsystem, Bannockburn, IL, USA). The tray was then filled with ice cold oxygenated ZF aCSF and kept at 2 – 4˚C during the slicing process. Sagittal and coronal slices, 350 µm thick, were prepared and transferred to the recording chamber. Prior to the experiments, brain slices were allowed to equilibrate for 1 hour.

2.3.2 Carbon Fiber Microelectrodes Fabrication.

Cylindrical carbon fiber microelectrodes were fabricated as previously described [37]. Briefly, 7 µm diameter carbon fiber (Goodfellow Cambridge LTD, Huntingdon, UK) were aspirated into a glass capillary tubes (1.2 mm D.D and 0.68 mm I.D, 4 in long; A-M System Inc, Carlsborg, WA, USA). Loaded capillaries were then pulled using a PE-22 heated coil puller (Narishige Int. USA, East Meadow, NY, USA). Pulled carbon fibers were trimmed to a length of 30 µm from the pulled glass tip. To seal the carbon fiber, electrodes were dipped into epoxy resin (EPON resin 815C and EPIKURE 3234 curing agent, miller-Stephenson, Danbury, CT, USA) and cured at 100℃ for 1 hour. Prior to the experiments, the electrodes were soaked in isopropanol for 10 minutes, and the electrode surface was electrochemically pretreated by scanning the electrodes with the waveform of – 0.4 V to + 1.3 V back to – 0.4 V at a frequency of 60 Hz for 15 min followed by 10 Hz for 10 min. Electrodes were then backfilled with 0.5 M potassium acetate for electrical connection between working electrode and an electrode holder.

2.3.3 Electrochemical Measurements

2.3.3.1 Data Acquisition and Statistics

Electrochemical measurements were collected and analyzed using an electrochemical workstation consisting of a Dagan Chem-Clamp potentiostat (Dagan, Minneapolis, MN, USA), modified to allow gain settings down to 200 nA/V, a personal computer with TarHeel CV software (provided by R.M. Wightman, University of North Carolina, Chapel Hill, NC, USA), a UEI breakout box (UNC Chemistry Department Electronics Design Facility, Chapel Hills, NC, USA), and two National Instruments computer interface cards, PCI 6052 and PCI 6711 (National Instruments, Austin, TX, USA).

All numerical values were represented as mean ± standard error of the mean (SEM). For all analysis, n is equal to the number of zebrafish brains used. GraphPad Prism 6 (GraphPad Software Inc, La Jolla, CA, USA) was used to conduct statistical calculations and to present data.

2.3.3.2 Dopamine Measurements in Zebrafish Whole Brain and Brain Slices

Carbon-fiber microelectrodes were pre-calibrated against 3 µM dopamine, and the electrode surface was chemically and electrochemically purified as discussed under the electrode fabrication method. The pre-calibrated carbon-fiber microelectrode and the stimulating electrodes (A-M System Inc, Carlsberg, WA, USA) were micromanipulated into the place by referencing the external features of the ventral side of the brain. The carbon-fiber microelectrode was positioned 50 – 100 µm laterally from the medial olfactory tract (MOT) and inserted about 280 – 300 µm deep. Stimulating electrodes were placed at the center of ventral telencephalon and inserted about 100 µm into the brain so that the carbon-fiber microelectrode was positioned between stimulating electrodes.

To evoke dopamine release, 25 electrical pulses (350 µA stimulating current, 4 ms of total duration, and stimulating frequency of 60 Hz) were applied. After the stimulating current was applied, evoked dopamine release was measured at the surface of the carbon-fiber microelectrodes. For dopamine detection, a triangular waveform of – 0.4 V to + 1.3 V to – 0.4 V at a scan rate of 400 V/s was applied to the carbon-fiber microelectrode every 100 ms. After stimulation and dopamine detection, the brain underwent 10 minutes of resting time before the next stimulation was applied.

In experiments, where evoked dopamine release in sagittal or coronal slices was measured, the same stimulating and waveform parameters were used as the harvested whole brain experiment. Stimulating electrodes were positioned at the ventral side of brain slices and inserted about 100 µm into the brain slice. The carbon-fiber microelectrode was inserted about 150 µm and placed between stimulating electrodes. Moreover, the brain slices were allowed to rest for 10 minutes between measurements.

2.3.4 Materials

Dopamine, α-methyl-p-tyrosine methyl ester (αMPT), nomifensine, and (±) sulpride, were purchased from Sigma-Aldrich (St. Louis, MO,USA). All aqueous solutions were made with purified (18.2 MΩ) water. A modified artificial cerebrospinal fluid (aCSF) for zebrafish consisted of 131 mM NaCl, 2mM KCl, 1.25 mM KH_2PO_4, 20 mM $NaHCO_3$, 2mM $MgSO_4$, 10 mM glucose, 2.5 mM $CaCl_2 \cdot H_2O$, and 10mM HEPES, and the pH was adjusted to 7.4. Dopamine stock solutions were prepared in 0.2 M perchloric acid and were diluted with aCSF without glucose to 3 µM for pre/post calibrations. Solutions of 50 µM aMPT, 10 µM of nomifensine, and sulpride, were prepared the day of each experiment.

2.4 Results and Discussion

Zebrafish (Danio rerio) have recently emerged as useful model organism for the study of neuronal functions. Fast-scan cyclic voltammetry at carbon-fiber microelectrodes (FSCV) has been used for the real time measurements of release and uptake of neurotransmitters both *in vivo* and *vitro* in different animal models, such as rodents and fruit flies [38, 39]. However, real time measurements of dopamine release in zebrafish using FSCV has not been studied extensively. Here, for the first time, we measure locally-evoked dopamine release and uptake in zebrafish whole brain preparations, and results were compared with those obtained from brain slices. The peak dopamine concentration ($[DA]_{release}$) was similar in both whole brain and brain slice preparations.

Treatment with α-methyl-p-tyrosine methyl ester (αMPT), an inhibitor of tyrosine hydroxylase, diminished release, and the electrochemical signal reappeared after subsequent washout, confirming the presence of dopamine. Uptake was inhibited in whole brain and slices following treatment with nomifensine. Furthermore, treatment the zebrafish brain with sulpiride, a D2 dopamine autoreceptor antagonist, resulted in increased stimulated dopamine release in whole brain and the results were compared with sagittal and coronal slices.

2.4.1 Evoked Dopamine Releases in Harvested Whole Brain.

We measured the electrically evoked dopamine release and uptake in harvested whole brain preparations from zebrafish (Fig. 2). A photograph of a viable whole brain acutely harvested from an adult zebrafish is shown in Fig. 2A. The brain is situated ventral side up to provide easier access to the subpallium in the telencephalon, a region of the brain that contains dopaminergic innervation

[35-37]. The carbon-fiber microelectrode and the stimulation electrodes were micromanipulated into place by referencing the external features of the ventral side of the brain. The carbon-fiber microelectrode was positioned 50-100 μm laterally from the medial olfactory tract (MOT) and inserted 280–300 μm deep. The region was stimulated locally with a biphasic stimulus pulse regimen of 25 pulses, 2 ms duration and 350 μA current. Application of this regimen resulted in the release of dopamine detected by FSCV at the carbon-fiber microelectrode (Fig. 2B). A stimulated release plot, current versus time profile, sampled from the color plot at the horizontal dotted line, is located above the color plot. A CV, sampled at the vertical dashed line of the color plot, serves as electrochemical evidence that the neurotransmitter released is dopamine.

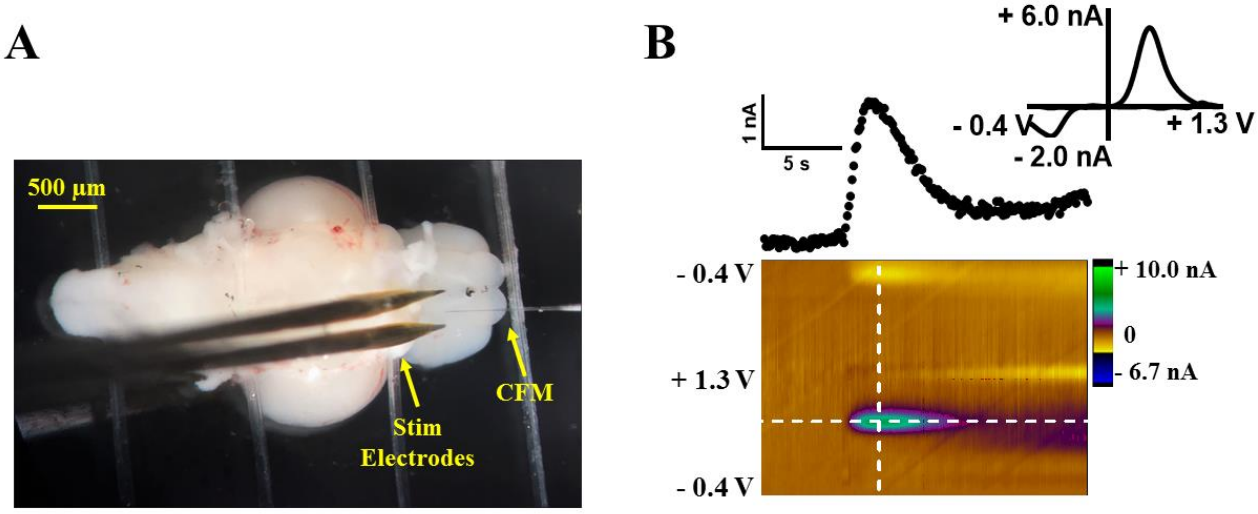

Figure 2. Electrically evoked dopamine release from a harvested whole brain. (A) Image of a harvested zebrafish whole brain indicating the placement of carbon-fiber microelectrode and stimulating electrodes in the ventral telencephalon. (B) Representative data of evoked dopamine release in whole brain. Stimulated dopamine release plot (top), current versus time, was sampled at the horizontal white dashed lines of color plot (bottom). A background subtracted cyclic voltammogram (insert, top) was sampled at the vertical white dashed lines of the color plot.

2.4.2 Evoked Dopamine Release in Brain Slices.

For comparison, dopamine release was also measured in acutely harvested sagittal brain slices (Fig. 3) and coronal slices (Fig. 4). The stimulation and working electrodes were micromanipulated into position at the ventral telencephalon. Dopamine release was evoked locally using the same stimulation parameters used in the whole brain. Both CV and current versus time plots are similar to those obtained in the whole brain preparation. In the representative raw data, $[DA]_{release}$ increased until a peak concentration of about 1 µM was measured ~2 s after stimulus application. $[DA]_{release}$ then decreased as uptake occurred. The color plots suggest that other

electroactive species were not released in substantial quantities. Also, $[DA]_{release}$ throughout the experiment was stable in both preparations.

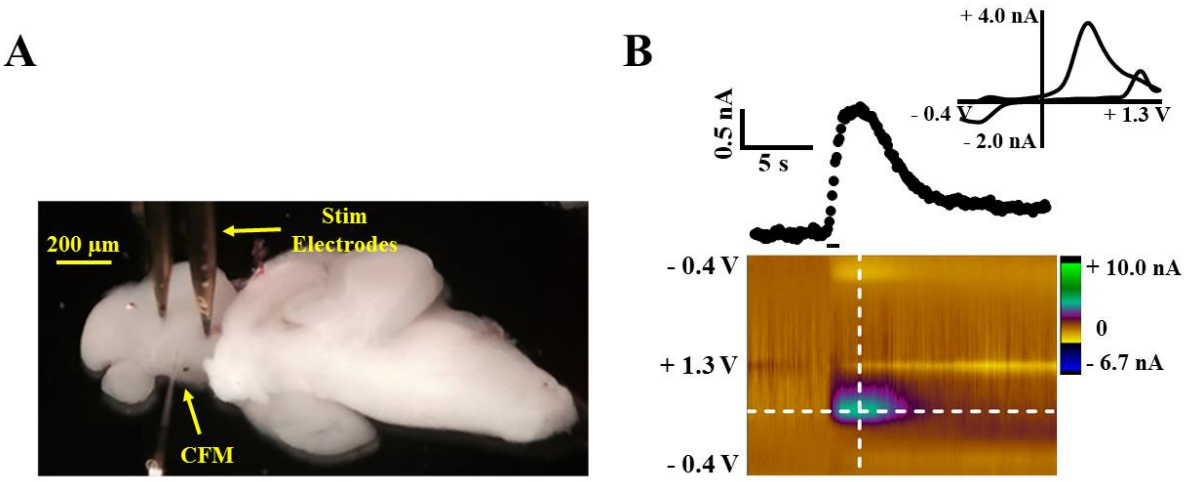

Figure 3. Electrically evoked dopamine release from a sagittal slice. (A) Image of a sagittal slice indicating the placement of carbon-fiber microelectrode and stimulating electrodes in the ventral telencephalon. (B) Representative data of evoked dopamine release in a sagittal slice. Stimulated dopamine release plot (top), current versus time, was sampled at the horizontal white dashed lines of color plot (bottom). A background subtracted cyclic voltammogram (insert, top) was sampled at the vertical white dashed lines of the color plot.

Dopamine release measurements in both preparations were collected for one hour and compared. Data pooled from multiple whole brains and brain slices reveal that, under equivalent stimulation conditions, average $[DA]_{release}$ was not significantly different in whole brain and slices: 0.41 ± 0.07 µM in whole brains, 0.54 ± 0.13 µM in sagittal slices, and 0.44 ± 0.09 µM coronal slices ($p = 0.40$, n=9 sagittal slices, n= 9 coronal slices and 9 brains, t-test). The concentration of

dopamine release evoked by either single or multiple stimulus pulses, both *in vivo* and *in vitro*, has been reported extensively in the literature. For example, application of a single pulse in mouse brain slices resulted in 1.43 ± 0.11 µM (striatum) [40] , 1.42 ± 0.14 µM (nucleus accumbens core), and 1.40 ± 0.19 µM (caudate putamen) [41]. Multiple stimulation pulses were applied in vivo to evoke dopamine release in the rat striatum at a reported peak concentration of 1.04 ± 0.14 µM [42]. Recently, Jones *et al.* [23] found dopamine to be released in zebrafish sagittal slices at a peak concentration of about 100 nM following stimulation with 20, 4-ms duration pulses applied at a current of 500 µA and an application frequency of 60 Hz. In any case, it appears from our results that less dopamine is released in zebrafish whole brain and slices compared to that of rodents.

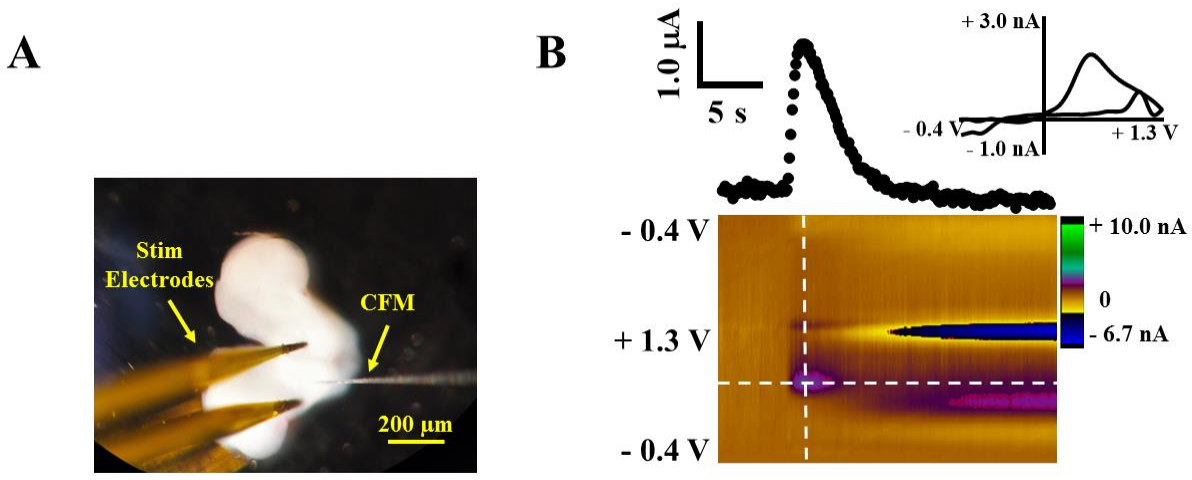

Figure 4. Electrically evoked dopamine release from a coronal slice. (A) Image of a coronal slice indicating the placement of carbon-fiber microelectrode and stimulating electrodes in the ventral telencephalon. (B) Representative data of evoked dopamine release in a coronal slice. Stimulated dopamine release plot (top), current versus time, was sampled at the horizontal white dashed lines of color plot (bottom). A background subtracted cyclic voltammogram (insert, top) was sampled at the vertical white dashed lines of the color plot.

2.4.3. Effect of DAT inhibitors on evoked dopamine release.

Extracellular dopamine levels are tightly regulated by the dopamine transporter (DAT), a membrane-bound protein that transfers dopamine molecules from the extracellular space to the intracellular space within neurons [43]. The stimulated release plot reveals that, similar to the mammalian brain, dopamine is immediately taken up after release. Based on previous measurements in brain slices from mice that lack the DAT [44, 45], it is likely that dopamine is actively taken up and that the decrease in current is not the result of diffusion away from the electrode.

Additional pharmacological studies were conducted in which whole brain and sagittal and coronal slices were perfused with nomifensine (Fig. 5), a well-established dopamine uptake

inhibitor [43]. As a result, the rate of dopamine uptake was sharply diminished, indicated by the decreased slope of the stimulated release curves after peak dopamine release. This treatment resulted in a ~130% increase in $[DA]_{release}$ in the whole brain preparation (Fig. 5A: pre-drug, 0.34 ± 0.14 µM; post-drug, 0.79 ± 0.22 µM, $p < 0.05$, n = 4 brains, t-test). A similar effect was observed when treating sagittal slices with nomifensine, with $[DA]_{release}$ increasing ~100% (Fig. 5B: pre-drug, 0.49 ± 0.13 µM; post-drug, 0.97 ± 0.18 µM, $p < 0.05$, n = 5 slices, t-test). Moreover, evoked dopamine release in coronal slices was altered by ~100% after nomifensine was introduced (Fig. 5C: pre-drug, 0.42 ± 0.11 µM; post-drug, 0.82 ± 0.13 µM, $p < 0.05$, n = 4 slices, t-test). Jones et al. demonstrated the release of dopamine in the ventral telencephalon of zebrafish sagittal slices [23]. Collectively, our result suggests that extracellular dopamine levels are tightly regulated in the telencephalon immediately after release. However, *ex vivo* whole brain preparations can be used to measure locally-stimulated dopamine release and, like sagittal and coronal slices, uptake can be inhibited pharmacologically.

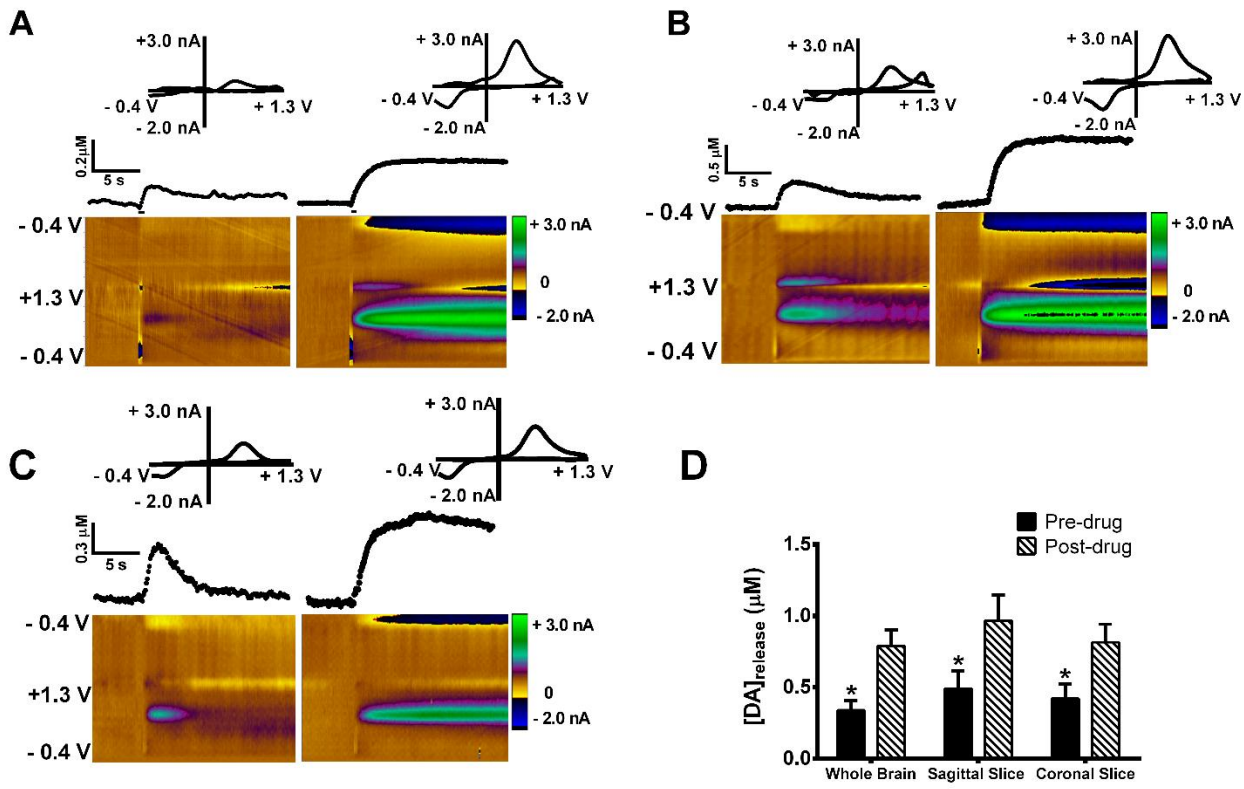

Figure 5. The effect of DAT inhibition on dopamine release in whole brain and sagittal and coronal brain slices. Dopamine release was measured before and after 10 µM nomifensine was administered to whole brains (A) and sagittal (B) and coronal brain slices (C). Color plots (bottom) and current versus time profiles (top) before and after application of nomifensine show that dopamine uptake was diminished in each brain preparation. (D) Evoked dopamine release in whole brain after nomifensine addition was significantly increased (n=4, $P < 0.05$, t-test). Similar to the whole brain results, dopamine release in brain slices significantly increased upon treatment with nomifensine (n=5 coronal slices, n=4 sagittal slices, $P < 0.05$, t-test).

2.4.4. Effect of dopamine synthesis inhibitor on evoked dopamine release.

In order to obtain further confirmation that the neurotransmitter being measured is dopamine, we examined the effect of α-methyl-p-tyrosine methyl ester (αMPT), which inhibits tyrosine hydroxylase and blocks dopamine synthesis, on release (Fig. 6A). Dopamine was electrically-evoked and measured every 10 minutes. Upon stabilization of the dopamine signal, brains were perfused with 50 μM αMPT and, approximately 2 hours later, dopamine release completely disappeared (pre-drug, 0.56 ± 0.08 μM; post-drug, 0.14 ± 0.07 μM, $p < 0.0001$, one-way ANOVA). To ensure that this disappearance of release was not due simply to loss of neuronal viability, the drug was washed out, and release re-appeared approximately 1 hour later (washout, 0.51 ± 0.10 μM, $p = 0.40$, one-way ANOVA), indicating that dopamine release was not significantly different than before the drug was added and providing further confirmation that the neurotransmitter measured is dopamine (Fig. 6B).

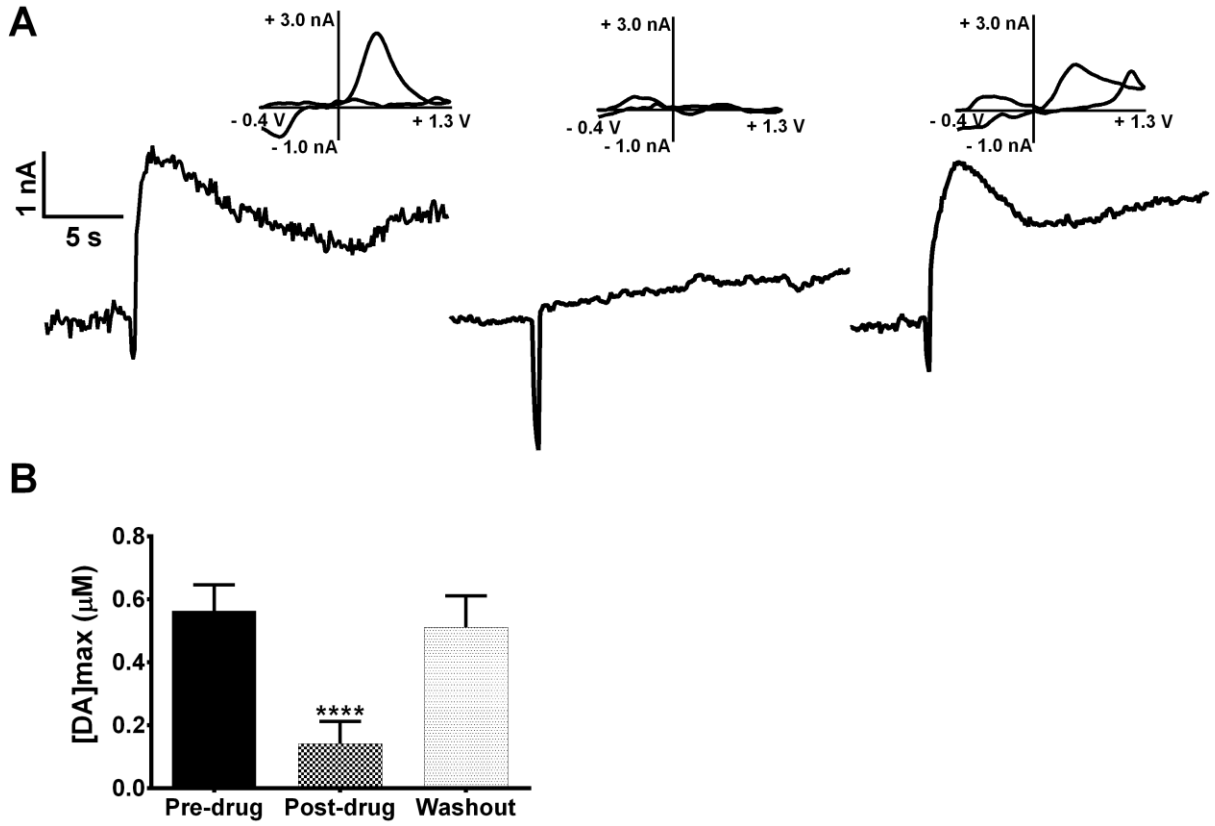

Figure 6. The effect of dopamine synthesis inhibition on dopamine signal. (A) Representative data of stimulated dopamine release before (left) and after (center) administration of 50 μM αMPT. Dopamine release reappeared after a 1-hour washout with drug-free buffer solution in the same recording session (right). Cyclic voltammograms for each step (inserts) confirm the release of dopamine. (B) Evoked dopamine release, measured after 2 hours of treatment with αMPT, significantly decreased (n=5, $P < 0.0001$, one-way AVOVA). Dopamine release after washout was not significantly different from the pre-drug measurement (n=5, $p = 0.40$, one-way ANOVA).

2.4.5. Effect of dopamine receptor antagonist on evoked dopamine release.

Dopaminergic terminals in the mammalian striatum possess D2-family dopamine autoreceptors that serve as a regulatory feedback mechanism for dopamine release [43]. To determine if a similar self-regulatory mechanism is present in dopaminergic terminals of the subpallium, we perfused whole brain ex vivo preparations with 10 µM sulpiride, a D2-family dopamine receptor inhibitor (Fig. 7A). Approximately 1 hour after addition of drug, dopamine release increased by about 80% (pre-drug, 0.41 ± 0.12 µM; post-drug, 0.74 ± 0.13 µM, $p < 0.05$, two-way ANOVA). Thus, D2 receptors are also present in the zebrafish brain and appear to serve a similar regulatory function. However, given that the circuitry is still intact in the whole brain preparation, it is also possible that sulpiride may enhance the release of dopamine by antagonism of dopamine receptors located not only presynaptically, but also at other locations within the brain [46].

To determine if autoregulation by D2 receptors occurs specifically at terminals, electrically-evoked dopamine release was measured in the subpallium of sagittal brain slices before and after sulpiride treatment (Fig. 7B). The slicing process should at least partially disrupt the ascending dopaminergic pathway from the diencephalon to the subpallium, likely leaving only presynaptic terminals without dopaminergic soma [36, 47]. In this case, $[DA]_{release}$ in the sagittal slice preparation increased by about 100% on average within an hour of treatment with 10 µM sulpiride (pre-drug, 0.33 ± 0.12 µM; post-drug, 0.68 ± 0.29 µM, $p < 0.05$, n = 5 slices, two-way ANOVA). However, it is possible that, given the thickness of the slices (350 µm), a substantial portion of the pathway remained. Interestingly, when the brain was sliced coronally, D2 antagonism with sulpiride had no effect on $[DA]_{release}$ (Fig. 7C).

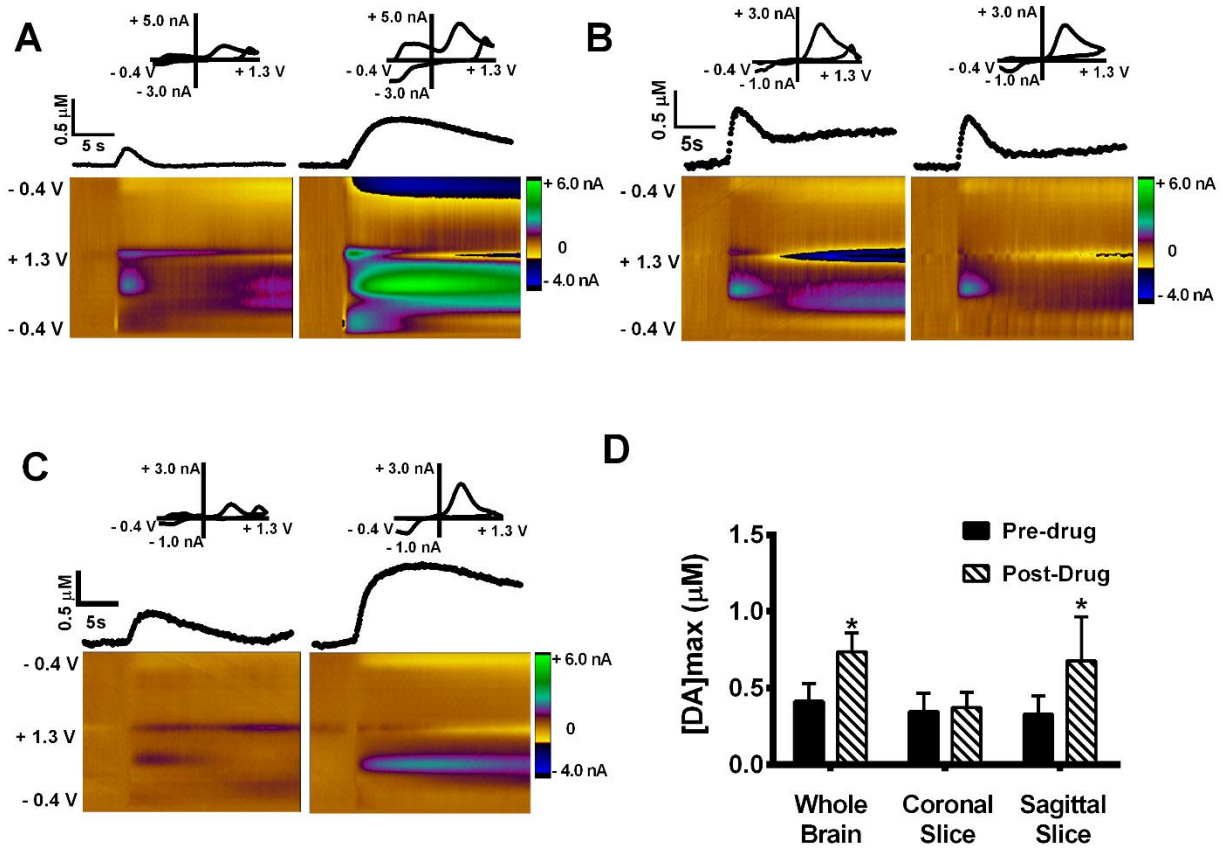

Figure 7. Effect of sulpiride treatment on dopamine release. Evoked dopamine release measured in a whole brain (A), a coronal slice (B), and a sagittal slice (C) before and after treatment with 10 µM sulpiride. (D) Dopamine release significantly increased in whole brains (n=5, $p < 0.05$, two-way ANOVA) and sagittal slices (n=5, $p < 0.05$, two-way ANOVA) after drug treatment. However, dopamine release did not significantly increase in coronal slices after drug treatment (n= 5, $p = 0.99$, two-way ANOVA).

Our results here show that dopamine release did not increase upon exposure to sulpiride (pre-drug, 0.35 ± 0.12 µM; post-drug, 0.38 ± 0.10 µM, $p = 0.47$, n = 5 slices, two-way ANOVA), suggesting that the D2-related mechanism of auto-inhibition in slices is not present in the coronal

preparation. The reason for this lack of effect is not well-understood. However, it is possible that the D2 receptors are not located presynaptically, but rather on the soma. [44] Another possibility is that the coronal slicing process induces more damage to the terminals compared to slicing sagittally. Additional studies will be required to identify the underlying mechanisms of this phenomenon.

2.4.6 Effect of stimulation frequency on evoked dopamine release.

The degree of dopamine release is determined, in part, by the number of stimulus pulses and the frequency (number of biphasic pulses applied per second).[45] Initially, to determine if alteration of stimulation frequency impacts dopamine release similarly in zebrafish, evoked dopamine both in whole brain and sagittal slices was measured and compared at frequencies ranging from 5 Hz to 25 Hz while other stimulus parameters were held constant (120 pulses, 4 ms, and 350 μA; Fig 8A).

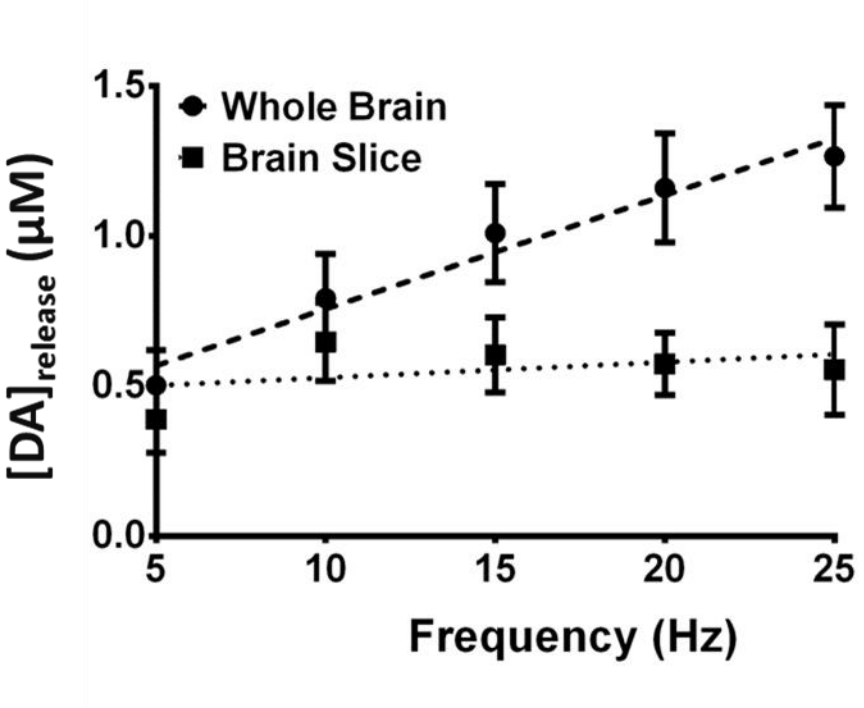

Figure 8. Effect of stimulation frequency on dopamine release. The stimulation frequency was altered while stimulation pulses and width were kept constant (120 pulses, 4 ms pulse duration) and evoked dopamine release was measured both in whole brain and sagittal slices. Linear regression analysis lines are shown for both whole brain (dashed line) and brain slice (dotted line).

We found a trend of increasing dopamine release up to a frequency of 25 Hz in whole brains. Although there appears to be a slight curvature, linear regression analysis revealed a strong correlation coefficient of linearity (R^2=0.96) and also a significantly non-zero slope (p = 0.0030). However, in slices, dopamine release wasn't influenced much by stimulation frequency compared to that in whole brains. The difference in dopamine release may suggest that the preparation impacts the availability of vesicles for release. Indeed, progressively decreasing in dopamine release [28] were observed in rodent brain slices and linear increases were observed in vivo [37] when stimulation frequency was increased. While the causes underlying these differences are not

known, it is possible that higher stimulation frequencies result in mobilization of reserve pool vesicles, as our previous results in striatal mouse brain slices have suggested [28]. In fact, this decrease in release at higher frequencies was exaggerated in transgenic R6/2 mice, which are commonly used to model Huntington's disease (HD). Our previous results have suggested that this decrease is likely due to a diminished reserve pool in R6/2 mice. In the future, it will be interesting to determine if these differences between slices and whole brain arise from a diminished reserve pool or have some other cause.

2.5 Conclusion

In conclusion, we have shown that dopamine release can be easily measured with FSCV in the subpallium of zebrafish whole brain. This preparation offers the advantage of keeping the whole brain intact, thereby preserving the three-dimensional neuronal circuitry and offering the future possibility of measuring release evoked by stimulation of pathways. Similar to slices, extracellular dopamine levels are tightly regulated by uptake through the DAT. Our results also demonstrate that uptake is inhibited by nomifensine in both brain slice and whole brain preparations. Additionally, D2 autoreceptors appear to regulate dopamine release in whole brain and sagittal slice preparations, but not in coronal slice preparations. Moreover, dopamine release properties from the whole brain are similar to those from brain slice preparations under similar conditions of electrical stimulation. These results represent an important step toward more complex studies, such as FSCV experiments that make use of remote stimulation in zebrafish whole brain and measurements of dopamine release in vivo. Furthermore, the expanded use of this model organism will allow researchers to exploit the genetic advantages of zebrafish in the analysis of neurotransmitter release properties.

2.6 Reference

[1] Grunwald, D. J., and Eisen, J. S. (2002) Headwaters of the zebrafish -- emergence of a new model vertebrate, *Nat. Rev. Genet., 3*, 717-724.

[2] Williams, R. (2010) Thanks be to zebrafish, *Circ. Res.*, *107*, 570-572.

[3] Li, H.-h., Huang, P., Dong, W., Zhu, Z.-y., and Liu, D. (2013) A brief history of zebrafish research-toward biomedicine, *Yichuan*, *35*, 410-420.

[4] Friedrich, R. W., Jacobson, G. A., and Zhu, P. (2010) Circuit neuroscience in zebrafish, *Curr. Bio., 20*, R371-R381.

[5] Fetcho, J. R., and Liu, K. S. (1998) Zebrafish as a Model System for Studying Neuronal Circuits and Behaviora, *Annals. NY. Acad. Sci., 860*, 333-345.

[6] Kimmel, C. B., Ballard, W. W., Kimmel, S. R., Ullmann, B., and Schilling, T. F. (1995) Stages of embryonic development of the zebrafish, *Dev. Dynam., 203*, 253-310.

[7] Ahrens, M. B., Li, J. M., Orger, M. B., Robson, D. N., Schier, A. F., Engert, F., and Portugues, R. (2012) Brain-wide neuronal dynamics during motor adaptation in zebrafish, *Nature, 485*, 471-477.

[8] Higashijima, S.-i., Masino, M. A., Mandel, G., and Fetcho, J. R. (2003) Imaging neuronal activity during zebrafish behavior with a genetically encoded calcium indicator, *J. Neurophysiol., 90*, 3986-3997.

[9] Randlett, O., Wee, C. L., Naumann, E. A., Nnaemeka, O., Schoppik, D., Fitzgerald, J. E., Portugues, R., Lacoste, A. M., Riegler, C., and Engert, F. (2015) Whole-brain activity mapping onto a zebrafish brain atlas, *Nat. Metho., 12*, 1039-1046.

[10] Qin, Z., Lewis, J., and Perry, S. (2010) Zebrafish (Danio rerio) gill neuroepithelial cells are sensitive chemoreceptors for environmental CO2, *J. Physiol., 588*, 861-872.

[11] Rothenaigner, I., Krecsmarik, M., Hayes, J. A., Bahn, B., Lepier, A., Fortin, G., Götz, M., Jagasia, R., and Bally-Cuif, L. (2011) Clonal analysis by distinct viral vectors identifies bona fide neural stem cells in the adult zebrafish telencephalon and characterizes their division properties and fate, *Development, 138,* 1459-1469.

[12] Baraban, S., Taylor, M., Castro, P., and Baier, H. (2005) Pentylenetetrazole induced changes in zebrafish behavior, neural activity and c-fos expression, *Neuroscience, 131*, 759-768.

[13] Baraban, S. C. (2013) Forebrain electrophysiological recording in larval zebrafish, *J. Vis. Exp.,71*.

[14] Venton, B. J., and Wightman, R. M. (2003) Psychoanalytical electrochemistry: dopamine and behavior, *Anal. Chem., 75*, 414 A-421 A.

[15] Hermans, A., Keithley, R. B., Kita, J. M., Sombers, L. A., and Wightman, R. M. (2008) Dopamine detection with fast-scan cyclic voltammetry used with analog background subtraction, *Anal. Chem., 80*, 4040-4048.

[16] Wightman, R. M. (2006) Probing cellular chemistry in biological systems with microelectrodes, *Science, 311*, 1570-1574.

[17] Robinson, D. L., Hermans, A., Seipel, A. T., and Wightman, R. M. (2008) Monitoring rapid chemical communication in the brain, *Chem. Rev., 108*, 2554-2584.

[18] Barnéoud, P., Descombris, E., Aubin, N., and Abrous, D. N. (2000) Evaluation of simple and complex sensorimotor behaviours in rats with a partial lesion of the dopaminergic nigrostriatal system, *Euro. J. Neurosci,. 12*, 322-336.

[19] Cousins, M., and Salamone, J. (1996) Involvement of ventrolateral striatal dopamine in movement initiation and execution: a microdialysis and behavioral investigation, *Neuroscience, 70*, 849-859.

[20] Aarts, E., van Holstein, M., and Cools, R. (2011) Striatal dopamine and the interface between motivation and cognition, *Front. Phychol., 2, 163*.

[21] Kelley, A. E., and Berridge, K. C. (2002) The neuroscience of natural rewards: relevance to addictive drugs, *J. Neurosci., 22*, 3306-3311.

[22] Oei, N. Y., Rombouts, S. A., Soeter, R. P., van Gerven, J. M., and Both, S. (2012) Dopamine modulates reward system activity during subconscious processing of sexual stimuli, *Neuropsychopharmacology, 37*, 1729-1737.

[23] Jones, L. J., McCutcheon, J. E., Young, A. M., and Norton, W. H. (2015) Neurochemical measurements in the zebrafish brain, *Front. Behav. Sci., 9*.

[24] Good, C. H., Hoffman, A. F., Hoffer, B. J., Chefer, V. I., Shippenberg, T. S., Bäckman, C. M., Larsson, N.-G., Olson, L., Gellhaar, S., and Galter, D. (2011) Impaired nigrostriatal function precedes behavioral deficits in a genetic mitochondrial model of Parkinson's disease, *FASEB J., 25*, 1333-1344.

[25] Zhang, L., Le, W., Xie, W., and Dani, J. A. (2012) Age-related changes in dopamine signaling in Nurr1 deficient mice as a model of Parkinson's disease, *Neurobiol. Aging, 33*, 1001.e1007-1001.

[26] Robertson, G. S., and Robertson, H. A. (1989) Evidence that L-dopa-induced rotational behavior is dependent on both striatal and nigral mechanisms, *J. Neurosci., 9*, 3326-3331.

[27] Covey, D. P., and Garris, P. A. (2009) Using fast-scan cyclic voltammetry to evaluate striatal dopamine release elicited by subthalamic nucleus stimulation, *Conf. Proc. IEEE. Eng. Med. Biol. Soc., 2009*, 3306-3309.

[28] Ortiz, A. N., Kurth, B. J., Osterhaus, G. L., and Johnson, M. A. (2010) Dysregulation of intracellular dopamine stores revealed in the R6/2 mouse striatum, *J. Neurochem., 112*, 755-761.

[29] Yorgason, J. T., España, R. A., and Jones, S. R. (2011) Demon voltammetry and analysis software: analysis of cocaine-induced alterations in dopamine signaling using multiple kinetic measures, *J. Neurosci. Meth., 202*, 158-164.

[30] Fukuda, A., Czurko, A., Hida, H., Muramatsu, K., Lenard, L., and Nishino, H. (1995) Appearance of deteriorated neurons on regionally different time tables in rat brain thin slices maintained in physiological condition, *Neurosci. Lett., 184*, 13-16.

[31] Buskila, Y., Breen, P. P., Tapson, J., van Schaik, A., Barton, M., and Morley, J. W. (2014) Extending the viability of acute brain slices, *Sci. Rep., 4*, 5309.

[32] Richerson, G. B., and Messer, C. (1995) Effect of composition of experimental solutions on neuronal survival during rat brain slicing, *Exp. Neurol., 131*, 133-143.

[33] Ullrich, C., Daschil, N., and Humpel, C. (2011) Organotypic vibrosections: novel whole sagittal brain cultures, *J, Neurosci, Meth., 201*, 131-141.

[34] Ferris, M. J., Calipari, E. S., Yorgason, J. T., and Jones, S. R. (2013) Examining the complex regulation and drug-induced plasticity of dopamine release and uptake using voltammetry in brain slices, *ACS Chem. Neurosci., 4*, 693-703.

[35] Vargas, R., Johannesdottir, I. T., Sigurgeirsson, B., Thorsteinsson, H., and Karlsson, K. A. E. (2011) The zebrafish brain in research and teaching: a simple in vivo and in vitro model for the study of spontaneous neural activity, *Adv. Physiol. Educ., 35*, 188-196.

[36] Rink, E., and Wullimann, M. F. (2001) The teleostean (zebrafish) dopaminergic system ascending to the subpallium (striatum) is located in the basal diencephalon (posterior tuberculum), *Brain Res., 889*, 316-330.

[37] Kraft, J., Osterhaus, G., Ortiz, A., Garris, P., and Johnson, M. (2009) In vivo dopamine release and uptake impairments in rats treated with 3-nitropropionic acid, *Neuroscience , 161*, 940-949.

[38] Trisha L. Vickery, B. C., and Jill Venton. (2009) Detection of endogeneous dopamine changes in drosophila melanogaster using fast-scan cyclic voltammetry, *Anal. Chem., 81*, 9306-9313.

[39] Cooper, S. E., and Venton, B. J. (2009) Fast-scan cyclic voltammetry for the detection of tyramine and octopamine, *Anal. Bioanal. Chem., 394*, 329-336.

[40] Kile, B. M., Walsh, P. L., McElligott, Z. A., Bucher, E. S., Guillot, T. S., Salahpour, A., Caron, M. G., and Wightman, R. M. (2012) Optimizing the Temporal Resolution of Fast-Scan Cyclic Voltammetry, *ACS Chem. Neurosci., 3*, 285-292.

[41] Cragg, S. J., and Greenfield, S. A. (1997) Differential autoreceptor control of somatodendritic and axon terminal dopamine release in substantia nigra, ventral tegmental area, and striatum, *J. Neurosci., 17*, 5738-5746.

[42] Garris, P. A., Christensen, J. R. C., Rebec, G. V., and Wightman, R. M. (1997) Real-time measurement of electrically evoked extracellular dopamine in the striatum of freely moving rats, *J. Neurochem., 68*, 152-161.

[43] Cooper, J. R., Bloom, F. E., and Roth, R. H. (2003) *The biochemical basis of neuropharmacology,* Oxford University Press.

[44] Jones, S. R., Gainetdinov, R. R., Jaber, M., Giros, B., Wightman, R. M., and Caron, M. G. (1998) Profound neuronal plasticity in response to inactivation of the dopamine transporter, *Proc. Natl. Acad. Sci., 95*, 4029-4034.

[45] Jones, S. R., Joseph, J. D., Barak, L. S., Caron, M. G., and Wightman, R. M. (1999) Dopamine neuronal transport kinetics and effects of amphetamine, *J. Neurochem., 73*, 2406-2414.

[46] Boehmler, W., Obrecht-Pflumio, S., Canfield, V., Thisse, C., Thisse, B., and Levenson, R. (2004) Evolution and expression of D2 and D3 dopamine receptor genes in zebrafish, *Dev. Dynam., 230*, 481-493.

[47] Rink, E., and Wullimann, M. F. (2004) Connections of the ventral telencephalon (subpallium) in the zebrafish (Danio rerio), *Brain Res., 1011*, 206-220.

Chapter 3. Effect of Chemotherapeutic Drugs on Evoked Dopamine Release in Zebrafish

Using zebrafish as a possible chemobrain animal model is discussed in this chapter. To determine whether chemotherapeutic agents have a similar effect on zebrafish as has been observed in rats, zebrafish were treated with carboplatin and 5-fluorouracil by different drug administration pathways, habitat water treatment or food treatment. The data used in this chapter is from "Electrochemical Measurement of Evoked Dopamine Release in Zebrafish Treated with Chemotherapy Drugs", which is in preparation.

3.1 Introduction

Advances in cancer detection and treatment have extended the lifespan of cancer survivors, especially those who have undergone chemotherapy treatment for breast cancer.[1] This increased lifespan brought to light the quality of patients' lives after chemotherapy treatment has concluded. Post-chemotherapy cognitive impairment, also known as chemobrain, is a syndrome characterized by deficits in memory and executive function that occur well after conclusion of treatment [2]. Unfortunately, the actual causes of chemobrain are still uncertain, although several mechanisms have been suggested. These include chemotherapy-induced DNA damage, disruption of vascular blood flow in the brain, and impairment of neurotransmitter signals due to the chronic toxicity of chemotherapy drugs [3-5].

Dopamine is a monoamine neurotransmitter in the central nervous system that is involved in many neurological functions, including cognition[6], reward[7], and locomotor control. [6, 8] In addition, dysfunction of the dopamine system has been shown to be associated with a various clinical problems such as Parkinson's disease [9], Huntington's disease [10-12], and Alzheimer disease

[13]. Our group recently observed that electrically evoked dopamine release and uptake was altered in the striatum of rats treated with carboplatin, a chemotherapeutic agent often used to treat cancers of the head, neck, breast, and lung [14]. Despite the decrease in release, reserve pool dopamine storage and total dopamine content in the brain tissue were unaffected, suggesting that sufficient neurotransmitter levels were available in the neurons, but they could not be effectively released. Importantly, this diminished release also corresponded to an impairment of spatial learning.

Rats and mice have commonly been used as models to understand fundamental mechanisms underlying the onset of neurodegenerative disease states, such as Huntington's disease [15] and Parkinson's disease [9, 16]. However, although they are genetically closer to humans than non-mammalian systems, the use of rodents also poses challenges. First, the relatively long life cycle of rats and mice place limitations on how quickly experiments can be accomplished [17]. For example, in previous experiments accomplished in our laboratory, rats required a month of intravenous injections of carboplatin administered through the tail vein. This treatment procedure was not only stressful on the rats, but it also took a considerable amount of time on the part of the researchers to learn how to carry out the technique and to perform the injections. Additionally, after treatment, the experiments were typically more involved and time-consuming, requiring a great deal of effort to remove the brain and prepare it for analysis. Moreover, genetic manipulation of rodents, especially rats, is costly and time-consuming [18]. With this in mind, we sought an alternative model organism that simulates the complexity of the human central nervous system, but offers higher throughput and easier genetic manipulation.

Zebrafish (*Danio rerio*) is a teleost that has emerged as a popular and versatile animal model in many research areas, such as neuroscience, toxicology, and developmental biology [19]. One major reason for its popularity is that zebrafish is a vertebrate that has a high degree of genetic

and functional homology to human when compared to invertebrate models, such as fruit flies [20]. Additionally, the use of zebrafish mitigates several disadvantages encountered with current rodent models. For example, zebrafish generate a large number of offspring, generally 100 to 200 embryos, which are transparent and develop externally. [21] Additionally, zebrafish are easier to genetically manipulate and easier to take care than rodents. Also, it is easy to treat the zebrafish with drugs or small molecules, which can be simply done by adding to the water environment or to the food source. These factors make zebrafish an exceptional animal model for neurotoxicity studies.

Recently, our group has successfully measured dopamine release and uptake ex vivo in zebrafish whole brains with fast-scan cyclic voltammetry at carbon-fiber microelectrodes. In this work, we treated zebrafish with carboplatin and 5-fluorouracil (5-FU), two commonly used chemotherapeutic agents. We found that electrically-evoked dopamine release, measured with fast-scan cyclic voltammetry at carbon-fiber microelectrodes, was diminished in carboplatin-treated fish, but not 5-FU-treated fish. Moreover, the route of administration appears to be important given that dopamine release decreased more noticeably in fish treated by oral administration compared to water administration.

3.2 Materials and Methods.

3.2.1 Drugs

Pharmaceutical grade carboplatin, 10 mg/mL (CD11650AA, Hospira, Lake Forest, IL, USA), 2.5g/50mL 5-Fluorouracil (LOT 6110679, Fresenius KABI, Bad Homburg, Germany), and 0.9 % sterile saline (Nova-Tech Inc, Grand Island, NE, USA) solutions were used. Dopamine was purchased from Sigma-Aldrich (St. Louis, MO, USA). Aqueous solutions were prepared with

purified (18.2 MΩ) water. A modified artificial cerebrospinal fluid (aCSF) for zebrafish whole brain preparations consisted of 131 mM NaCl, 2mM KCl, 1.25 mM KH_2PO_4, 20 mM $NaHCO_3$, 2mM $MgSO_4$, 10 mM glucose, 2.5 mM $CaCl_2 \cdot H_2O$, and 10mM HEPES, and the pH was adjusted to 7.4. Dopamine stock solutions were prepared in 0.2 M perchloric acid and were diluted with aCSF without glucose to 1 µM for pre/post calibrations.

3.2.2 Zebrafish

All animal procedures were approved by the University of Kansas institutional Animal Care and Use Committee. Zebrafish were housed 20 fish per 2L tank in the University of Kansas Molecular Probes Core (KU-MPC). These animals were originally purchased from Carolina (Burlington, NC, USA) and kept at KU-MPC prior to the experiment. Zebrafish were maintained on a light dark cycle, controlled by a timer with a 16 hour light phase and 8 hour dark phase. The temperature of the recirculating water system was maintained at 26℃. The concentration of nitrates were held at less than 2 ppm and pH of 7-8 was maintained.

3.2.2.1 System Water Treatment with Chemotherapeutic Drugs

To treat the system water with chemotherapeutic drugs, carboplatin or of 5-fluorouracil was added to a single 1L fish tank, making the final concentration 100 µM in chemotherapeutic agent. For this study, there were three treatment groups. Each group (n=5 fish) was treated with either chemotherapeutic drugs or saline (control group) for either 1 day, 4 days, or 7 days. Zebrafish were removed by a net from the main housing system to the tank containing drug treated system water. Every 48 hours, treated system water was replaced with freshly treated system water, so that the zebrafish can be continuously exposed to the chemotherapy treatment.

3.2.2.2. Food Treatment with chemotherapeutic Drugs

For the food delivery method of chemotherapy agents, brine shrimp (San Francisco Bay Brand INC, Newark, CA, USA) was thawed and the excess liquid was removed. A gram of brine shrimp was weighed out and soaked for 30 minutes with either carboplatin, 5-fluorouracil, or saline (n=5 per treatment duration) to give the shrimp an approximate concentration of 20 mg/g shrimp. After 30 minutes, the treated brine shrimp was added to a 1 L tank using tweezers and the fish was allowed to eat the treated food for 3 minutes once a day. After the feeding period, the excess shrimp were removed from the system water. Prior to the electrochemical experiment, the zebrafish were fed with treated food for 1 day, 4 day, and 7 days.

3.2.3 Electrochemistry

3.2.3.1 Zebrafish

All animal procedures were approved by the University of Kansas Institutional Animal Care and Use Committee. Adult zebrafish used for these studies were housed in the Molecular Probes Core of the Center for Molecular Analysis of Disease Pathways at the University of Kansas. Zebrafish were euthanized by rapid chilling, also known as hypothermic shock. To perform euthanasia, a separate beaker of water, taken from the Aquatic Habitats™ ZF0601 (Pentair, Cary, NC, USA) main housing system, was chilled to 2-4℃. Zebrafish then were transferred using a net from the main housing system into the chilled system water.

3.2.3.2 Zebrafish Whole Brain Preparation

The whole brain preparation method was similar to that employed in Chapter 2. Briefly, Zebrafish was euthanized by the rapid chilling procedure which placing zebrafish in pre-chilled (2-4˚C) system water. Once zebrafish heads were decapitated, the heads were placed into pre-prepared dissection pads, made with 2% agarose (BioReagent graded agarose, Sigma-Aldrich, St. Louis, MO, USA) in petri dishes. The petri dish was then filled with oxygenated (95% O2 / 5% CO_2) zebrafish ice-cold artificial cerebral spinal fluid (ZF aCSF). The ZF aCSF consisted of 131 mM NaCl, 2 mM KCl, 1.25 mM KH_2PO_4, 20 mM $NaHCO_3$, 2 mM $MgSO_4$, 10 mM glucose, 2.5 mM $CaCl_2 \cdot H_2O$, and 10 mM HEPES, and the pH was adjusted to 7.4.

The decapitated zebrafish head was then fixed by pinning it with a syringe needle. Using micro tweezer, forceps, and a pulled capillary, the whole brain was carefully removed from the skull of the zebrafish. The harvested brain was then transferred into the recording chamber that was continuously perfused with oxygenated ZF aCSF, and the brain was kept at constant temperature of 28℃. The brain was placed ventral side face up to expose the sub pallium in telencephalon, then the brain was immobilized by placement of a nylon mesh harp on the top. Prior to the experiments, the brains were equilibrated for 1 hour.

3.2.3.3 Carbon Fiber Microelectrodes Fabrication.

Cylindrical carbon fiber microelectrodes were fabricated as previously described[22]. Briefly, a 7 µm diameter carbon fiber (Goodfellow Cambridge LTD, Huntingdon, UK) was aspirated into glass capillary tubes (1.2 mm D.D and 0.68 mm I.D, 4 in long; A-M System Inc, Carlsborg, WA, USA). Loaded capillaries were then pulled using a PE-22 heated coil puller

(Narishige Int. USA, East Meadow, NY, USA). Pulled carbon fibers were trimmed to a length of 50 to 70 µm from the pulled glass tip. To seal the carbon fiber, electrodes were dipped into epoxy resin (EPON resin 815C and EPIKURE 3234 curing agent, miller-Stephenson, Danbury, CT, USA) and cured at 100℃ for 1 hour. Prior to the experiments, the electrodes were soaked in isopropanol for 10 minutes, and the electrode surface was electrochemically pretreated by scanning the electrodes with the waveform of – 0.4 V to + 1.3 V back to – 0.4 V at a frequency of 60 Hz for 15 min followed by 10 Hz for 10 min. Electrodes were then backfilled with 0.5 M potassium acetate for electrical connection between working electrode and an electrode holder.

3.2.3.4 Dopamine Measurements in Zebrafish Whole Brain

Carbon-fiber microelectrodes were pre-calibrated against 1 µM dopamine, and the electrode surface was chemically and electrochemically purified as discussed under the electrode fabrication method. The pre-calibrated carbon-fiber microelectrode and the stimulating electrodes (A-M System Inc, Carlsberg, WA, USA) were micromanipulated into the place by referencing the external features of the ventral side of the brain. The carbon-fiber microelectrode was positioned 50 – 100 µm laterally from the medial olfactory tract (MOT) and inserted about 280 – 300 µm deep. Stimulating electrodes were placed at the center of ventral telencephalon and inserted about 100 µm into the brain so that the carbon-fiber microelectrode was positioned between stimulating electrodes.

To evoke dopamine release, 35 electrical pulses (350 µA stimulating current, 4 ms of total duration, and stimulating frequency of 60 Hz) were applied. After the stimulating current was applied, evoked dopamine release was measured at the surface of carbon-fiber microelectrodes. For dopamine detection, a triangular waveform of – 0.4 V to + 1.3 V to – 0.4 V at a scan rate of

400 V/s was applied to the carbon-fiber microelectrode every 100 ms. After stimulation and dopamine detection, the brain underwent 10 minutes of resting time before the next stimulation was applied. Evoked dopamine released was measured from either treated fish brain or control fish brain for 1 hour after the equilibration.

3.2.3.5 Optimization of Stimulation Parameters

To optimize stimulation parameters, stimulation pulses, width, and frequency were varied. During optimization, the waveform of – 0.4 V to + 1.3 V to – 0.4 V at 400 m/s was applied to the carbon-fiber microelectrodes. The oxidation current response due to dopamine release was converted to concentration by a calibration factor and compared as the stimulation pulses were varied 1, 5, 15, 25, and 35 pulses. The stimulation width and frequency were held constant at 4 ms at 60 Hz. To study how stimulus duration affects dopamine release, durations of 1, 2, 3, and 4 ms were applied while the number of stimulation pulses and frequency were held constant at 25 pulses and 60 Hz. Last, to observe how the stimulation frequency influenced dopamine release, frequency was changed from 10, 20, 30, 40, 50, and 60 Hz while the stimulation pulse and the width were held at 25 pulses and 2 ms.

3.2.4 Data Acquisition and Statistics

Electrochemical measurements were collected and analyzed using an electrochemical workstation consisting of a Dagan Chem-Clamp potentiostat (Dagan, Minneapolis, MN, USA), modified to allow gain settings down to 200 nA/V, a personal computer with TarHeel CV software (provided by R.M. Wightman, University of North Carolina, Chapel Hill, NC, USA), a UEI breakout box (UNC Chemistry Department Electronics Design Facility, Chapel Hills, NC, USA),

and two National Instruments computer interface cards, PCI 6052 and PCI 6711 (National Instruments, Austin, TX, USA).

All numerical values were represented as mean ± standard error of the mean (SEM). For all analyses, n is equal to the number of zebrafish brains used. GraphPad Prism 6 (GraphPad Software Inc, La Jolla, CA, USA) was used to conduct statistical calculations and to present data.

3.2.5 Data Modeling

Modeling was achieved by analyzing the raw data to determine the point of maximum dopamine signal after the application of electrical stimulation and the point where that signal has decayed by 80%. This decay curve was then fit with the 1st order exponential decay equation $A_t = A_{max} e^{-kt}$. A_{max} was held constant at the experimentally determined value and k, the 1st order rate constant, was allowed to float. The accuracy of the fit was determined by using a Pearson coefficient with a cut off of $R \geq 0.8$. Once this k was determined, the half-life of the decay was then calculated using the equation $t_{1/2} = 0.6932/k$. [23, 24] All data analysis and curve fitting were performed using GraphPad Prism 6 (GraphPad Software Inc, La Jolla, CA, USA)

3.3 Results and Discussion

Recently, our lab has developed a method to detect electrically evoked dopamine release in the harvested whole brain of zebrafish. To extend the use of zebrafish as an animal model in neuroscience research, it is important to study dopamine regulation in different neurological systems or neurotoxicity conditions. Our group has studied post-chemotherapy cognitive impairment (Chemobrain) in rat animal models and has found that dopamine release and uptake was impaired in chemotherapy treated rats [14]. Therefore, we have investigated dopamine release

and uptake in zebrafish treated with the chemotherapy drugs carboplatin and 5-FU. In addition, we administrated chemotherapy drugs to zebrafish by either treating the habitat water or by feeding the fish with treated brine shrimp. It was determined that dopamine release was impaired in carboplatin zebrafish that were treated by both habitat water and the food. However, dopamine release was only diminished in the 5-FU treated zebrafish treated by food administration method.

3.3.1 Optimization of Stimulating Parameters

Dopamine in the zebrafish brain can be reproducibly released by electrical stimulation to initiate action potential of neurons. Electrical stimulation has been a valuable method to cause the release neurotransmitters including dopamine both in vivo and vitro. Electrically evoked dopamine release in zebrafish brains needs to be sufficient enough to differentiate the changes. A stimulation parameter study in zebrafish has not been accomplished to the best of our knowledge. Therefore, we compared the amount of dopamine release as the stimulation parameters, pulse number, pulse width, and frequencies, were varied. First, evoked dopamine release was compared as the stimulating pulses were varied 1, 5, 15, 25, and 35 pulses while stimulation pulse width, current, and frequency were held constant at 2 ms , 350 μA, and 60 Hz respectively.

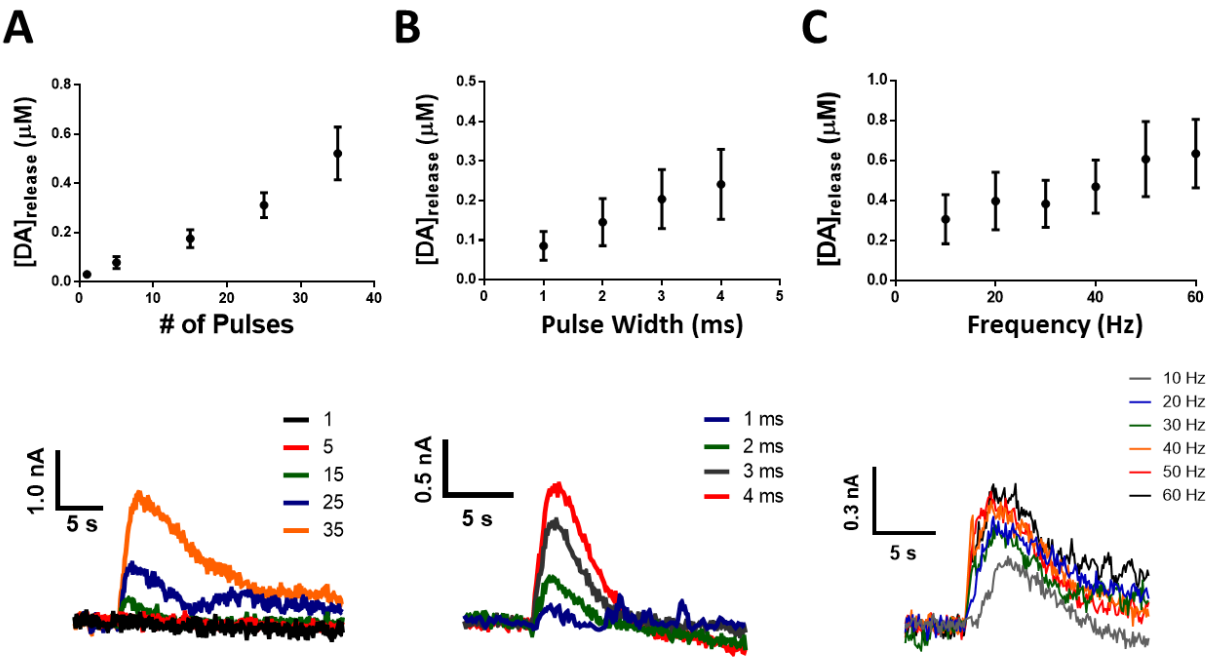

Figure 1. Effect of stimulation parameters on evoked dopamine release. The concentration of dopamine released was compared as the number of pulses were varied from 1, 5, 15, 25, and 35 pulses (A, top), the pulse width changes from 1, 2, 3, and 4 ms (B, top), and the stimulation frequency varied from 10, 20, 30, 40, 50, and 60 Hz (C, top). Current versus time traces was also compared as the number of pulses (A, bottom), pulse width (B, bottom), and frequency (C, bottom) varied.

As the number of stimulation pulses was increased, more dopamine was released into the extracellular space. As shown in Fig. 1A, the amount of evoked dopamine release increased linearly (n=5, R^2 = 0.9749) as the number of stimulation pulses was increased. When 35 pulses were applied to release dopamine, shown in current versus time trace, the duration of signaling after the peak current was reached was longer compared to when lower pulses were applied. This

suggests that the dopamine transporters in zebrafish were not able to clear all the released dopamine fast enough.

Evoked dopamine release was measured at selected pulse widths, varied from 1, 2, 3, 4 ms, while the number of pulses and stimulation frequency and current were held constant at 25 pulses, 60 Hz, and 350 µA. As the pulse width gets longer, the amount of dopamine released per pulse increased (n=6, R^2 = 0.9893). As expected, in Fig.1B, when the stimulation pulse was applied for 4 ms, more dopamine was released compared to when the stimulation pulse was applied for 1 ms. Similar to other stimulation parameters, at higher stimulation frequency, more dopamine was electrically evoked since the number of stimulations per second increased (n=4, R^2 = 0.9283). Therefore, for this study, we evoked dopamine release in zebrafish using 35 stimulation pulses (4 ms per pulse) at 60 Hz.

3.3.2 Evoked Dopamine Release in Chemotherapy Treated Zebrafish

3.3.2.1 Habitat Water Treatment Method

Electrically stimulated dopamine release in the harvested whole brain was measured using FSCV at carbon fiber microelectrode. Dopamine release was measured for one hour at the ventral telencephalon and the peak current responses were averaged and converted to the concentration using the calibration factor. One of many advantages of using zebrafish as an animal model is easy assessment of drug treatment without a complicated procedures[25], such as IV tail vein injection, that are required in such studies using rodents animal models.

In this study, the habitat water is treated with either saline, carboplatin, or 5-FU. The final concentration of carboplatin and 5-FU in the habitat water was 100 µM. Representative data for control, carboplatin treated groups, and 5-FU treated groups are shown in Fig. 2. The color plot

and concentration versus time trace in Fig.2 suggest that there is an electroactive specie released due to the electrical stimulation.

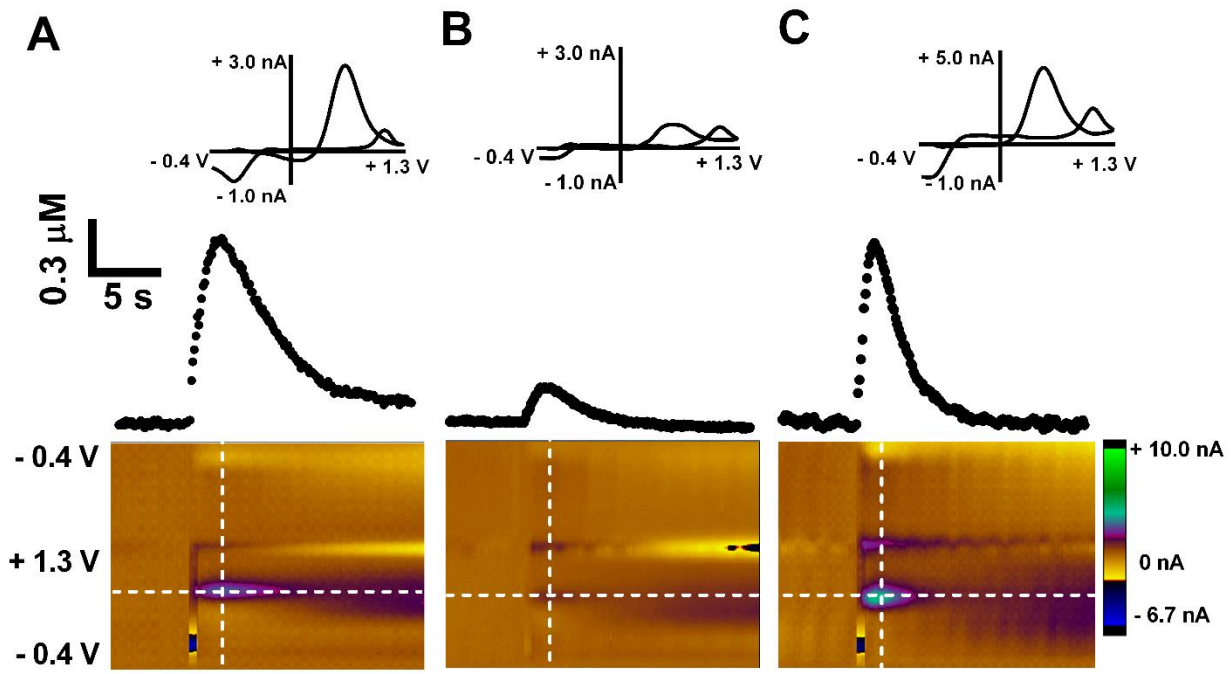

Figure 2. Representative data of evoked dopamine release in chemotherapy treated zebrafish by habitat water treatment. (A) Representative data of dopamine release in water treated control zebrafish. The oxidation current response (top) of dopamine release was sampled at the horizontal trance of color plot (bottom). The background subtracted cyclic voltammogram (top, insert) was extracted from vertical white line of color plot. (B) Representative data of dopamine release in carboplatin treated zebrafish after 7 days of treatment. Oxidation current response of dopamine release, compared to that of control, is reduced after 7 days of carboplatin treatment. (C) Evoked dopamine release in 5-FU treated zebrafish after 7 days of treatment. There is no changes in evoked dopamine release after zebrafish was treated with 5-FU for 7 days.

Background subtracted cyclic voltammograms, which were extracted at the white vertical dashed line of the color plot, suggest that the released specie is dopamine. Dopamine release measured in the carboplatin treated zebrafish after 7 days of treatment decreased as shown in Fig. 2B. However, the amount of dopamine release in the 5-FU treated group did not change when compared to the control group.

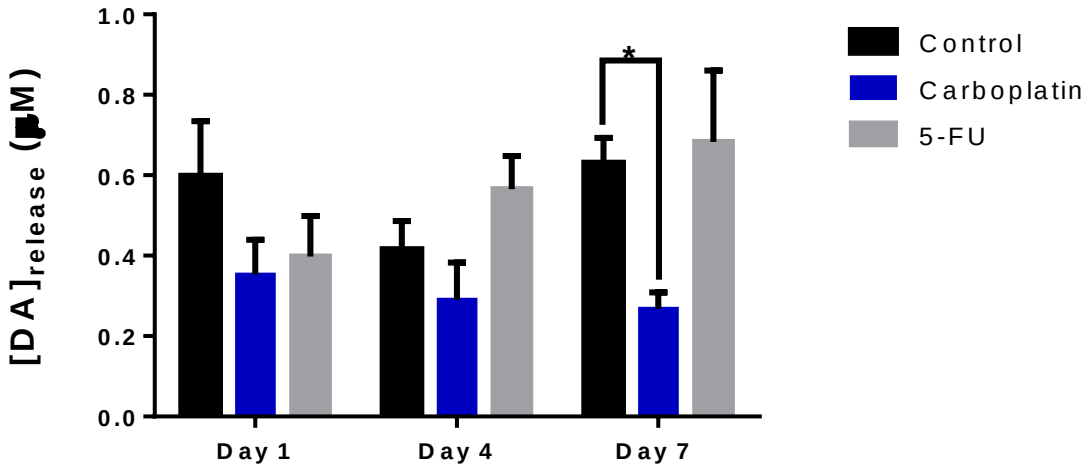

Figure 3. Evoked dopamine release measured in chemotherapy treated zebrafish for different treatment periods. The amount of dopamine release in carboplatin treated fish was significantly reduced after 7 day of treatment (n=5, two-way ANOVA $p < 0.05$).

It has been suggested that diminished dopamine release might play a role in chemobrain. Kaplan *et al.* measured dopamine release in the striatum of carboplatin treated rats and concluded that dopamine release and uptake were attenuated after four weeks of chemotherapy treatment[14].

To understand if zebrafish will show a similar outcome as the rat model of chemobrain, we treated zebrafish not only with carboplatin but also with 5-FU, a widely used anticancer drug for various cancers such as breast cancer and head and neck cancer [26] .

Zebrafish were housed in carboplatin treated habitat water for different periods. The amount of dopamine release after 1, 4, and 7 days of treatment were measured and compared as shown in Fig. 3. At day 7, measured dopamine release was found to be 0.27 ± 0.04 μM, which is significantly reduced compared to the control group ($n=5$, two-way ANOVA, $p < 0.05$). Even though more work needs to be done, the result could suggest that carboplatin might affect zebrafish dopamine regulation similar to that of chemobrain rat models.

To examine the possible impact of other chemotherapy drugs on dopamine regulation in zebrafish, another group of zebrafish was treated with 5-FU. , a thymidylate synthase inhibitor and a known demyelinator[26-28]. Treatment with 5-FU was selected as the second chemotherapeutic in these studies because it was hypothesized that it would degrade the neuron's ability to transmit signals by removing the myelin sheath, leading to diminished dopamine release[27-29]. Like the carboplatin treated group, zebrafish were housed in 5-FU treated habitat water for 1, 4, and 7 days. The result of dopamine release in different treatment duration groups is shown in Fig.3. Unlike carboplatin, dopamine release in 5-FU treated fish was not significantly changed throughout the treatment duration but rather increased. The number of zebrafish used for this study may need to increase to understand if 5-FU have no effect on dopamine release upon the habitat water treatment.

For the control group, the zebrafish were housed in saline treated habitat water for 1, 4, and 7 days, and dopamine release was measured at each treatment duration and compared to the chemotherapy treated groups. The amount of dopamine release throughout the different periods

was not significantly changed: Day 1 (n=5), 0.60 ± 0.14 µM; Day 4 (n=5), 0.41 ± 0.17 µM; Day 7 (n=5), 0.63 ±0.06 µM (two way ANOVA, day 1 versus day 4, p = 0.34; day 1 versus day 7, p = 0.99)

To summarize, it was found that treating zebrafish with carboplatin, added to their system water, resulted in a significant decrease in the maximum dopamine release observed. This matches the results our lab has reported in rats[14]. One possible explanation for this phenomena is general neuronal death caused by carboplatin, a known DNA crosslinker,[30, 31] is limiting the amount of dopamine neurons available for release, thus decreasing the observed dopamine overflow, though to solidify a mechanism more studies need to be done.

Zebrafish treated with 5-FU showed no significant change in dopamine overflow was a surprising result. Moreover, 5-FU is a known demyelinator which would be expected to lower the efficiency of action potential transfer down a neuron thus leading to less neuronal firing and less dopamine release.[32] The fact that this was not observed is interesting and needs to be explored in the future.

3.3.3 Food Treatment

For the study previously discussed, chemotherapy drugs were administered by treating the habitat water. During this treatment the drug is most likely adsorbed through skin or the gills. In order to determine if treatment pathway is important in diminishing dopamine release, a second treatment pathway was explored. It has been reported that platinum based chemotherapeutic drug, such as carboplatin, can be absorbed through the small intestine of rats[33]; therefore, we introduced chemotherapy drug through their food.

Recently, Sterling *et al.* established zebrafish as model for voluntary consumption ethanol. They mixed ethanol with gelatin and allowed the zebrafish to freely feed on it. Additionally, this study examined whether delivering the ethanol to the zebrafish orally had the same effect on orexigenic peptides as exposing the zebrafish to ethanol treated water.[34] In our study, brine shrimp were treated with either saline, carboplatin, or 5-FU such that the approximate amount of drug in the brine shrimp was 20 mg drug/g brine shrimp. Treated brine shrimp were then fed to each treatment group once every day for 3 min, then any remaining food was removed. The each group was treated for either 1, 4, or 7 days.

Representative data of dopamine release in zebrafish that is fed with treated either chemotherapy drugs or saline brine shrimp for 7 days are shown in Fig. 4. Electrically evoked dopamine release in zebrafish fed with carboplatin treated food, similar to water treatment method group, was diminished after 7 days of treatment. Interestingly, the amount of dopamine release in 5-FU treatment group after 7 days was also reduced, this result is different from the water treated 5-FU group and indicates that delivering the drug to zebrafish orally is the more efficient way to accurately provide chemotherapy treatment when compared to the habitat water treatment method.

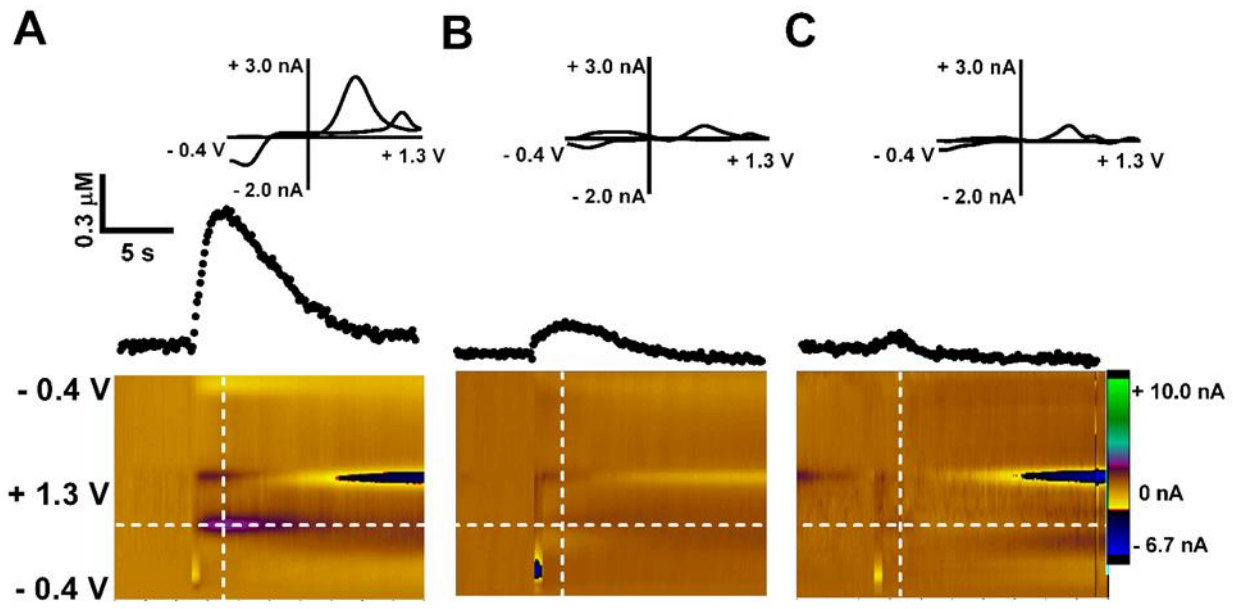

Figure 4. Representative data of evoked dopamine release in chemotherapy treated zebrafish by food treatment. (A) Representative data of dopamine release in control. The oxidation current response (top) of dopamine release was sampled at the horizontal trace of color plot (bottom). The background subtracted cyclic voltammogram (top, insert) was extracted from vertical white line of color plot. (B) Representative data of dopamine release in carboplatin treated zebrafish after 7 days of food treatment. Oxidation current response of dopamine release was reduced after the treatment. (C) Evoked dopamine release in 5-fluorouracil treated zebrafish after 7 days of food treatment. There is no changes in evoked dopamine release after zebrafish was treated with 5-fluorouracil for 7 days. Similar to carboplatin treated fish, the amount of dopamine release was reduced.

.

Dopamine release in zebrafish, fed with brine shrimp treated with either saline, carboplatin, or 5-FU, was measured and compared in Fig. 5. For the control treatment group, like the water control treatment group, the different treatment duration did not affect the amount of dopamine released (n=5, two way ANOVA, $p = 0.76$).

Carboplatin fed zebrafish shown significant impairment in dopamine released after one day of treatment (n=5, two way ANOVA, $p < 0.05$). Moreover, after 7 days of treatment, evoked dopamine release was further diminished (n=5, two way ANOVA, $p < 0.01$: day 1, 0.21 ± 0.05 µM; day 4, 0.23 ± 0.04 µM; day 7, 0.15 ± 0.04 µM). To elucidate the impact of chemotherapy intake method on dopamine release compared to water treatment method, zebrafish were fed 5-fluorouracil treated brine shrimp. As shown in Fig.5, the amount of dopamine release was diminished with 5-FU intake method not only after 7 days of treatment but also only after 1 day of treatment (n=5 for day 1 and day 4, n = 4 for day 7 treatment group, two way ANOVA, $p < 0.05$).

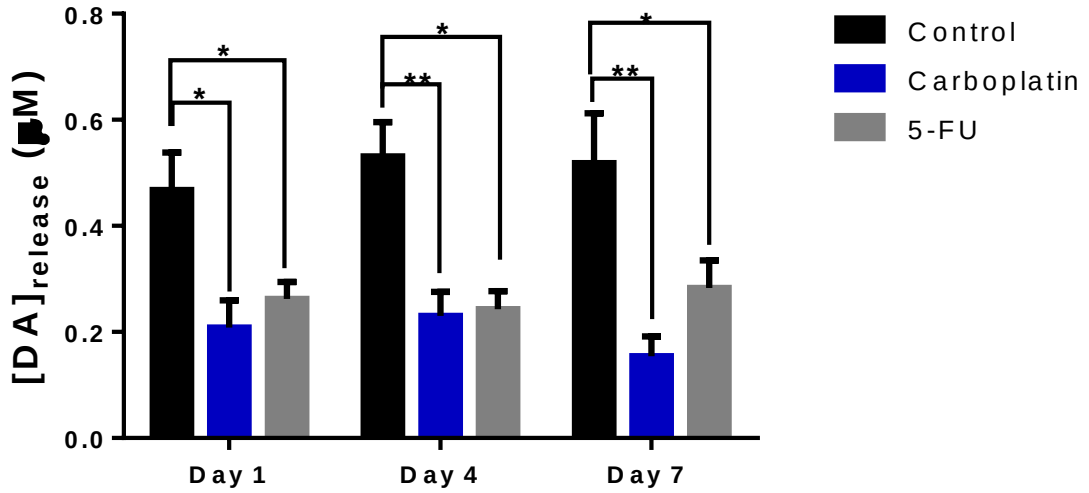

Figure 5. Evoked dopamine release in zebrafish measured after different periods of treatment with brine shrimp. The amount of dopamine release in both carboplatin and 5-flurouracil treated fish was significantly reduced after 1 day of treatment (n=5, two way ANOVA, * represents $p < 0.05$, ** represent $P < 0.01$).

These phenomenon suggests that the effect of carboplatin on dopamine release in zebrafish is similar to that of results in rodent animal models. However, when the chemotherapy drug was delivered orally, chemotherapy treatment was more efficient than when the drug was delivered by treating habitat water. This observed difference in release may be related to the amount of intact drug that reaches the animal. It is not clear how much 5-FU and carboplatin can cross the skin and enter the blood stream; as such, it is likely that the water treated fish are receiving less than a 100 μM dose. During food treatment, the fish are ingesting the drug instead of absorbing it through the skin or breathing through the gills. Additionally, carboplatin can cross the small intestine of rats[33], thus zebrafish are more likely to receive the entire intended dose that may lead to the observed increase in efficiency. This hypothesis is supported by the fact that in the water treated fish the

significant changes were not observed until after day 7, whereas, in the shrimp treated, fish the effect was immediate.

3.4 Modeling of the 1st Order Rate Constant for Dopamine Uptake

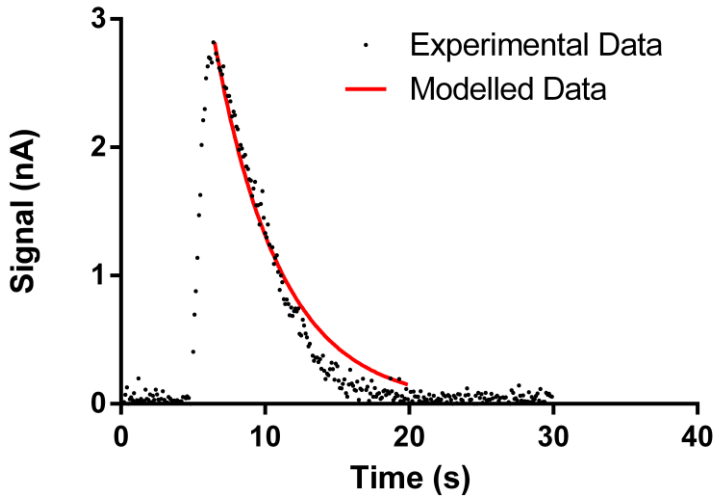

Figure 6: Representative figure showing the representative data of electrically evoked dopamine release with the modeled data overlaid.

In the preceding sections, it has been shown that chemotherapeutic treatment has an effect on the release of electrically evoked dopamine. With this result in mind we wanted to determine if uptake was also affected by modelling the 1st order rate constant of uptake (k). Understanding uptake is important because of the influence it has on both the length of time dopamine is available to activate signaling pathways as well as the peak extracellular dopamine achieved after, both of these phenomenon may play a role in the observed differences discussed above. The red line in Fig. 6 is a fit of the data using the equation $A_t = A_{max}\, e^{-kt}$ from the point maximum signal to 80% decay of the signal. A_{max} was held at the experimentally determined

maximum for release and k was allowed to float[23, 24]. The fit was determined to be valid if the modeled data had a Pearson coefficient greater than 0.8 when it was overlaid with the raw experimental data. The rate constant is a measure of the efficiency of the transporters as they uptake the released dopamine. The k can also be used to calculate a $t_{1/2}$which is the measure of how long it take half of the released dopamine to be up taken. The results of the modelling are shown in Fig. 7.

It was determined that there was no significant difference between any of the treatment groups, because of this all the control data was pooled and an average for k was determined to be $0.2418 \pm 0.018\ s^{-1}$ with an n of 25 fish. This value is much larger than the reported numbers for both rats (0.012 to $0.027\ s^{-1}$)[24] and fruit flies ($0.062 \pm 0.004\ s^{-1}$)[23]. This could indicate a fast reuptake in the zebrafish compared to both rats and fruit flies. The data presented here point to uptake not being involved in the differences observed in max dopamine released after treatment; however, more work needs to be done to both calculate the Michaelis-Menten kinetic parameters for zebrafish as well as to take into account diffusion which this current model assumes doesn't exist.

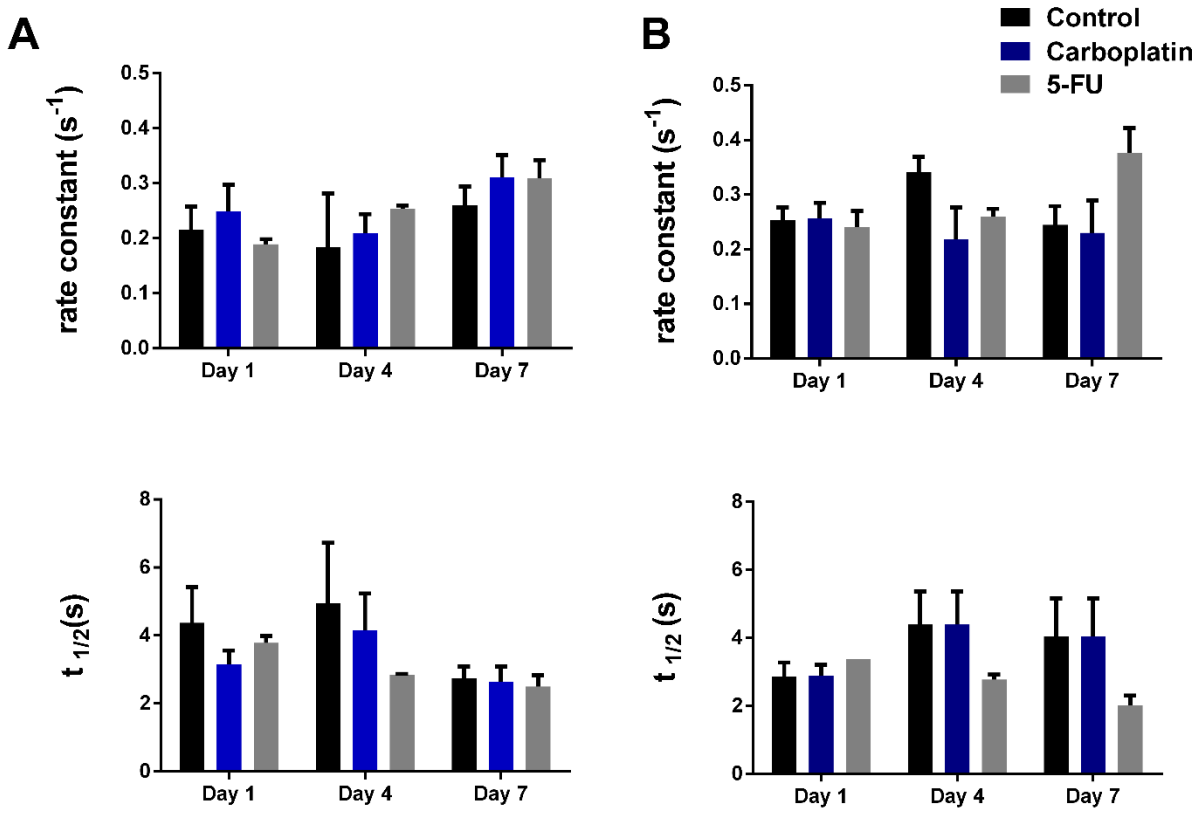

Figure 7. The averages of the 1st order rate constant and $t_{1/2}$ in chemotherapy drug treated zebrafish. (A). The average of 1st order rate constant (top) and $t_{1/2}$ (bottom) in zebrafish housed in treated system water with carboplatin or 5-FU over different treatment durations. (B). The average of 1st order rate constant (top) and t 1/2 (bottom) in zebrafish fed with carboplatin or 5-FU treated shrimp food over the treatment time. There was no significant difference observed in either treatment pathway or treatment time.

5.4 Conclusions

The electrochemical measurement of dopamine release in zebrafish was conducted using fast-scan cyclic voltammetry at carbon fiber microelectrodes, and stimulation parameters were optimized. Furthermore, in addition to quantifying dopamine release and stimulation optimization, we established zebrafish as a chemobrain animal model. We investigated the changes in dopamine release and uptake in zebrafish that were housed in chemotherapy treated habitat water for 1, 4, and 7 days. Additionally, to determine if different administration methods have any influence on the result in dopamine regulation, the chemotherapy drugs were administered to the zebrafish with their food. The data here suggest that the chemotherapy drugs have an effect on dopamine release and uptake in zebrafish similar to that observed in the rodent animal models. Moreover, it was observed that the treatment method had a significant effect on dopamine release with shrimp treatment showing the greater change.

3.6 Reference

[1] Youlden, D. R., Cramb, S. M., Dunn, N. A., Muller, J. M., Pyke, C. M., and Baade, P. D. (2012) The descriptive epidemiology of female breast cancer: an international comparison of screening, incidence, survival and mortality, *Cancer Epidemiol. Biomarkers Prev., 36*, 237-248.

[2] Raffa, R. B., Duong, P. V., Finney, J., Garber, D. A., Lam, L. M., Mathew, S. S., Patel, N. N., Plaskett, K. C., Shah, M., and Weng, H. F. J. (2006) Is 'chemo-fog'/'chemo-brain' caused by cancer chemotherapy, *J. Clin. Pharm. Ther., 31*, 129-138.

[3] Scheibel, R. S., Valentine, A. D., O'Brien, S., and Meyers, C. A. (2004) Cognitive dysfunction and depression during treatment with interferon-alpha and chemotherapy, *J. Neuropsychiatry Clin. Neurosci., 16*, 185-191.

[4] Meyers, C. A., Albitar, M., and Estey, E. (2005) Cognitive impairment, fatigue, and cytokine levels in patients with acute myelogenous leukemia or myelodysplastic syndrome, *Cancer, 104*, 788-793.

[5] Ahles, T. A., and Saykin, A. J. (2007) Candidate mechanisms for chemotherapy-induced cognitive changes, *Nat. Rev. Cancer, 7*, 192-201.

[6] Bäckman, L., Nyberg, L., Lindenberger, U., Li, S.-C., and Farde, L. (2006) The correlative triad among aging, dopamine, and cognition: current status and future prospects, *Neurosci. Biobehavio. Rev. 3,0*, 791-807.

[7] Schultz, W. (2002) Getting formal with dopamine and reward, *Neuron, 36*, 241-263.

[8] Cousins, M., and Salamone, J. (1996) Involvement of ventrolateral striatal dopamine in movement initiation and execution: a microdialysis and behavioral investigation, *Neuroscience, 70*, 849-859.

[9] Zhang, L., Le, W., Xie, W., and Dani, J. A. (2012) Age-related changes in dopamine signaling in Nurr1 deficient mice as a model of Parkinson's disease, *Neurobiol. Aging, 33*, 1001.e1007-1001.e1016.

[10] Ortiz, A. N., Kurth, B. J., Osterhaus, G. L., and Johnson, M. A. (2010) Dysregulation of intracellular dopamine stores revealed in the R6/2 mouse striatum, *J. Neurochem., 112*, 755-761.

[11] Ortiz, A. N., Kurth, B. J., Osterhaus, G. L., and Johnson, M. A. (2011) Impaired dopamine release and uptake in R6/1 Huntington's disease model mice, *Neurosci. Lett., 492*, 11-14.

[12] Ortiz, A. N., Osterhaus, G. L., Lauderdale, K., Mahoney, L., Fowler, S. C., von Hoersten, S., Riess, O., and Johnson, M. A. (2012) Motor function and dopamine release measurements in transgenic Huntington's disease model rats, *Brain Res., 1450*, 148-156.

[13] Zhang, L., Zhou, F.-M., and Dani, J. A. (2004) Cholinergic drugs for Alzheimer's disease enhance in vitro dopamine release, *Mol. Pharmacol., 66*, 538-544.

[14] Kaplan, S. V., Limbocker, R. A., Gehringer, R. C., Divis, J. L., Osterhaus, G. L., Newby, M. D., Sofis, M. J., Jarmolowicz, D. P., Newman, B. D., Mathews, T. A., and Johnson, M. A. (2016) Impaired Brain Dopamine and Serotonin Release and Uptake in Wistar Rats Following Treatment with Carboplatin, *ACS Chem. Neurosci., 7*, 689-699.

[15] Ortiz, A. N., Kurth, B. J., Osterhaus, G. L., and Johnson, M. A. (2010) Dysregulation of intracellular dopamine stores revealed in the R6/2 mouse striatum, *J. Neurochem., 112*, 755-761.

[16] Blesa, J., and Przedborski, S. (2014) Parkinson's disease: animal models and dopaminergic cell vulnerability, *Front. Neuroanat., 8*, 155.

[17] Sengupta, P. (2013) The Laboratory Rat: Relating Its Age With Human's, *Int. J. Prev. Med., 4*, 624-630.

[18] Simmons, D. (2008) The Use of Animal Models in Studying Genetic Disease: Transgenesis and Induced Mutation, *Nature, 1*, 70.

[19] Fetcho, J. R., and Liu, K. S. (1998) Zebrafish as a Model System for Studying Neuronal Circuits and Behaviora, *Ann. N. Y. Acad. Sci., 860*, 333-345.

[20] Xi, Y., Noble, S., and Ekker, M. (2011) Modeling neurodegeneration in zebrafish, *Curr. Neorology Neurosci. Rep., 11*, 274-282.

[21] Tamaru, Y., Ishikawa, H., Avsar-Ban, E., Nakatani, H., Miyake, H., and Akiyama, S.-i. (2011) Research and development of biotechnologies using zebrafish and its application on drug discovery, *Analysis and Modeling to Technology Applications*, pp 243-256,

[22] Kraft, J., Osterhaus, G., Ortiz, A., Garris, P., and Johnson, M. (2009) In vivo dopamine release and uptake impairments in rats treated with 3-nitropropionic acid, *Neuroscience, 161*, 940-949.

[23] Vickrey, T. L., Xiao, N., and Venton, B. J. (2013) Kinetics of the dopamine transporter in Drosophila larva, *ACS Chem. Neurosci., 4*, 832-837.

[24] Sabeti, J., Adams, C. E., Burmeister, J., Gerhardt, G. A., and Zahniser, N. R. (2002) Kinetic analysis of striatal clearance of exogenous dopamine recorded by chronoamperometry in freely-moving rats, *J. Neurosci. Metho., 121*, 41-52.

[25] Barros, T. P., Alderton, W. K., Reynolds, H. M., Roach, A. G., and Berghmans, S. (2008) Zebrafish: an emerging technology for in vivo pharmacological assessment to identify potential safety liabilities in early drug discovery, *Br. J. Pharmacol., 154*, 1400-1413.

[26] Longley, D. B., Harkin, D. P., and Johnston, P. G. (2003) 5-fluorouracil: mechanisms of action and clinical strategies, *Nature Rev. Cancer, 3*, 330-338.

[27] Han, R., Yang, Y. M., Dietrich, J., Luebke, A., Mayer-Pröschel, M., and Noble, M. (2008) Systemic 5-fluorouracil treatment causes a syndrome of delayed myelin destruction in the central nervous system, *J. Bio., 7*, 1.

[28] Fassas, A. B.-T., Gattani, A. M., and Morgello, S. (1994) Cerebral demyelination with 5-fluorouracil and levamisole, *Cancer invest., 12*, 379-383.

[29] de Souza, A. (2013) Movement disorders and the osmotic demyelination syndrome, *Parkinsonism Relat. Disord., 19*, 709-716.

[30] Pavelka, M., Lucas, M. F. A., and Russo, N. (2007) On the Hydrolysis Mechanism of the Second-Generation Anticancer Drug Carboplatin, *Chem. Euro. J., 13*, 10108-10116.

[31] Fuertes, M. A., Alonso, C., and Pérez, J. M. (2003) Biochemical modulation of cisplatin mechanisms of action: enhancement of antitumor activity and circumvention of drug resistance, *Chem. Rev., 103*, 645-662.

[32] Weng, Q., Tan, B., Wang, J., Wang, J., Zhou, H., Shi, J., He, Q., and Yang, B. (2014) 5-Fluorouracil causes severe CNS demyelination by disruption of TCF7L2/HDAC1/HDAC2 complex in adolescent mice, *Toxicology, 325*, 144-150.

[33] Binks, S. P., and Dobrota, M. (1990) Kinetics and mechanism of uptake of platinum-based pharmaceuticals by the rat small intestine, *Biochem. Pharma., 40*, 1329-1336.

[34] Sterling, M., Karatayev, O., Chang, G.-Q., Algava, D., and Leibowitz, S. (2015) Model of voluntary ethanol intake in zebrafish: Effect on behavior and hypothalamic orexigenic peptides, *Behav. Brain. Rev., 278*, 29-39.

Chapter 4. Electrochemical Measurements of 4-hydroxyphenylacetic acid and Dopamine with Fast-scan cyclic voltammetry

In this chapter, we describe the electrochemical properties of 4-hydroxyphenylacetic acid, an electroactive by-product formed during the photoactivation of p-hydroxyphenacyl-based caged compounds, such as p-hydroxyphenylglutamaate. We also have optimized fast-scan cyclic voltammetry waveform parameters, such as holding and switching potential and scan rates, so that both 4HPAA and dopamine can be detected in a single voltammogram and quantified simultaneously. The results presented in this chapter are from "Simultaeous Measurement and Quantitation of 4-hydroxyphenylacetic acid and dopamine with fast-scan cyclic voltammetry" published in *The Analyst*, 2015,140, 3039-3047.

4.1 Introduction

The small molecule, 4-hydroxyphenylacetic acid (4HPAA), is a naturally occurring, electroactive phenolic compound formed in humans by the metabolism of aromatic amino acids.[1] Recent interest in phenolic compounds has centered on its propensity to become nitrated; thus, 4HPAA has been proposed to be a biomarker for certain disease conditions that result in an increase of nitrosative stress.[2] In addition, 4HPAA is used as a nutrient substrate in microorganisms that metabolize it to pyruvate and succinate during the aerobic respiration.[3] More recently, 4HPAA has gained interest as an attenuator of DNA binding by Neisserial adhesin regulator (NadR) protein, a gene suppressor protein found in most hypervirulent strains of meningococcal bacteria [4, 5].

In addition to its biological functions, 4HPAA is a degradation product of the photoreaction of phenacyl-based caged compounds.[6, 7] A caged compound possesses a photoactive

trigger that inhibits the activity of its biological ligand; photoactivation, induced by exposure to light of the proper wavelength, results in the near-instantaneous release of the photocage and subsequent activation of the ligand. Caged compounds have frequently been employed in the study of brain function, both ex vivo and in vivo. [8-11]

The phenacyl-based photoreaction (Scheme 1) involves a Favorskii rearrangement, resulting in the formation of the activated biological molecule and 4HPAA. This reaction occurs, in some cases, within microseconds.[12] The quantitation of 4HPAA, therefore, provides an opportunity to indirectly quantify that amount of biologically active molecule formed by this reaction. Neurotransmitter molecules similar in structure to 4HPAA, such as tyramine and octopamine, have been shown to be electroactive and are readily detectable by fast-scan cyclic voltammetry (FSCV) at carbon-fiber microelectrodes. FSCV is a well-established electrochemical method that provides sub-second temporal resolution and good chemical selectivity when used for the detection of biogenic amine neurotransmitters.[13] Similarly, in this study, we have found that 4HPAA is also easily detectable by FSCV.

We have recently focused our efforts towards the sub-second quantitation of 4HPAA with the goal of quantitatively measuring the impact of caged compound photoactivation on dopamine release in brain tissue slices and in vivo. An important step in this process is the electrochemical characterization and optimization of 4HPAA with FSCV. Our results suggest that 4HPAA undergoes an irreversible, two-electron oxidation that involves the formation of the conjugated species. Moreover, we have optimized the voltammetric waveform to enhance sensitivity to 4HPAA while also detecting dopamine simultaneously within the same scan. Using the optimized waveform, a limit of detection of 100 nM and a linear response up to 500 μm was found, indicating

that FSCV could be used to detect 4HPAA in physiological fluid as well as quantify how much caged compound was photoreleased in the brain, both *in vivo* and *ex vivo*.

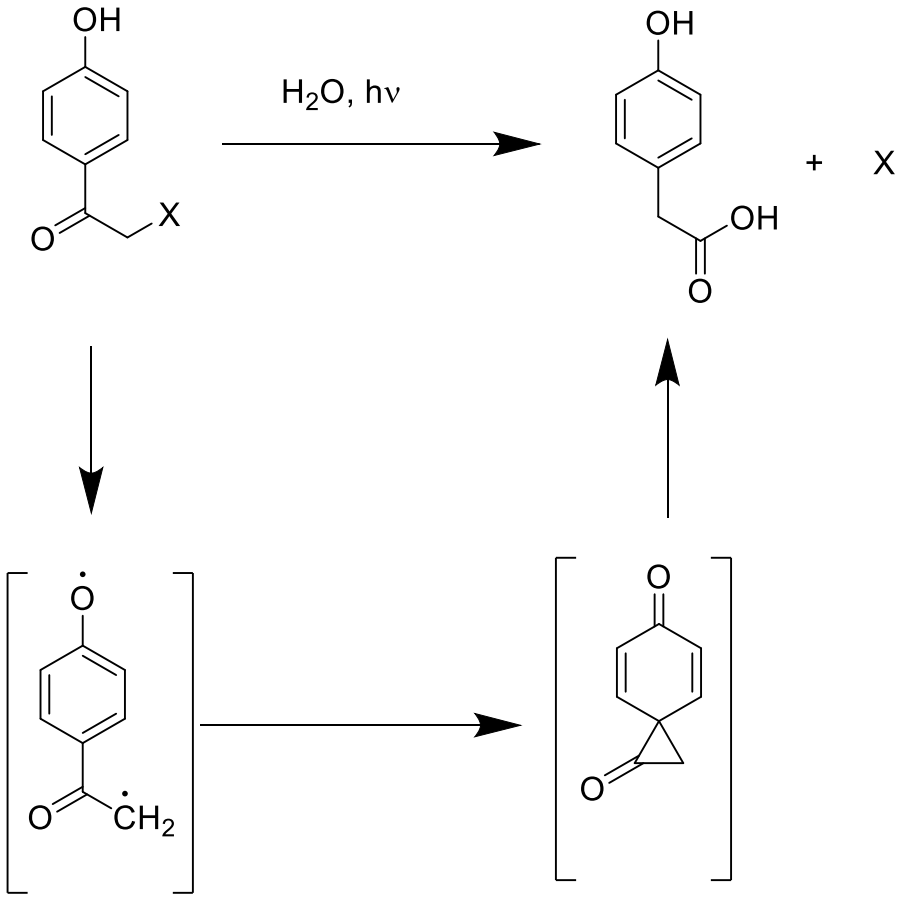

Scheme 1. The mechanism of Favorskii rearrangement.

4.2 Materials and Methods.

4.2.1 Chemicals and Solutions.

Dopamine (DA), 4-hydroxyphenylacetic acid (4HPAA), and 4-methoxyphenylacetic acid (4MPAA) were purchased from Sigma-Aldrich (St. Louis, MO, USA). Methyl-4-hydroxyphenyl acetate (M4HPA) was acquired from Alfa Aesar (Ward Hill, MA). All aqueous solutions were made with purified (18.2 MΩ) water. Flow cell injection experiments were carried out in artificial cerebrospinal fluid (aCSF) or phosphate buffer as specified. The aCSF consisted of 126 mM NaCl, 2.5 mM KCl, 1.2 mM NaH_2PO_4, 2.4 mM $CaCl_2$, 1.2 mM $MgCl_2$, 25 mM $NaHCO_3$, and 20 mM HEPES, and the pH was adjusted to 7.4. The phosphate buffer consisted of 3.3 mM KH_2PO_4 and 5.8 mM $NaH_2PO_4 \cdot {}_2H_2O$, and the pH was adjusted to 2.71, 6.71, and 10.71. Concentrated stock solutions were prepared in 0.2 M perchloric acid and were diluted with appropriate buffer for each experiment to desired concentrations on the beginning day of each experiment.

4.2.2 Carbon-fiber microelectrode fabrication

Cylindrical carbon-fiber microelectrodes were fabricated as previously described.[14] Briefly, a 7 μm diameter carbon-fiber (Goodfellow Cambridge LTD, Huntingdon, UK) was loaded into a glass capillary tube (1.2 mm O.D and 0.68 mm I.D, 4 in long; A-M system Inc, Carlsborg, WA, USA), which was then pulled using a PE-22 heated coil puller (Narishige Int. USA, East Meadow, NY). Next, the carbon fiber was trimmed to about 30 μm from the pulled glass tip, which was sealed with epoxy resin (EPON resin 815C, EPIKURE 3234 curing agent, Miller-Stephenson, Danbury, CT, USA) and cured at 100°C for 1 hour. The electrodes were backfilled with 0.5 M potassium acetate to obtain an electrical connection between the carbon-fiber and electrode holder. Prior to the experiment, all electrodes were soaked in isopropanol for 10 minutes,

and then electrochemically pretreated by scanning with the appropriate waveform, used for each experiment, at a frequency of 60 Hz for 15 min and 10 Hz for 10 min. A Ag/AgCl wire, locally fabricated, was used as the reference electrode.

4.2.3 Electrochemical experiments

FSCV data were collected with a custom-modified ChemClamp potentiostat (Dagan, Minneapolis, MN, USA) and TarHeel CV software provided by R.M. Wightman and M.L.A.V. Heien (University of North Carolina, Chapel Hill, NC, USA). Measurements were acquired using a two-electrode electrochemical cell. For flow cell injection analysis, a six-port sample injector valve with 2 mL sample loop was mounted on a 2-position electric actuator (Valco Inc. Houston, TX, USA). As the actuator was triggered by the software, it rotated the valve to inject the sample for five seconds into a locally-constructed flow cell where the carbon-fiber working electrode and reference electrode were located. Cyclic voltammograms were collected every 100 ms. The scan rate and waveform potentials were varied as needed.

Conventional scan cyclic voltammetry was carried out using a 730E biopotentiostat (CH Instruments, Austin, TX) with a standard three-electrode system. A 3 mm glassy carbon electrode was used as the working electrode, a platinum wire was used as the counter electrode, and a Ag/AgCl electrode was used as the reference electrode (CH Instruments, Austin, TX). Prior to collecting measurements, the glassy carbon electrode was polished with an electrode polishing kit (CH Instruments, Austin, TX). For cyclic voltammetry experiments, 2 mM 4HPAA was prepared in aCSF (pH 7.4) and then loaded into a locally constructed electrochemical cell. The potential was scanned from −0.4 V to either +1.0 V or +1.3 V, and the back to −0.4 V, at a scan rate of 10 mV s^{-1}. The glassy carbon electrode was re-polished between experiments, and the reference

electrode was stored in 1 M KCl while not in use. For data analysis, Electrochemical Analyzer software (CH Instruments, Austin, TX) was used.

4.2.4 Statistics

All numerical values were represented as mean ± standard error of the mean (SEM). For all analyses, n is equal to the number of electrodes. GraphPad Prism 6 (GraphPad Software Inc, La Jolla, CA, USA) was used to conduct statistical calculations and to present data.

4.3. Results and discussion

4.3.1 Fast-scan cyclic voltammetry of 4HPAA at Standard Waveform

The chemical structure of 4HPAA features a phenol group with an acetic acid group attached at the para position (Scheme 2A). For our initial detection of 4HPAA with FSCV, a standard triangular waveform, similar to that used to previously detect DA, [15] was applied to a carbon-fiber microelectrode by linearly scanning the electrode potential from −0.4 V to +1.0 V and back to −0.4 V at a scan rate of 400 V s−1 and an update rate of 10 CVs s−1. The non-faradaic charging current was removed by subtraction of a set of averaged background scans collected from the same file. A representative CV is shown in Fig. 1A.

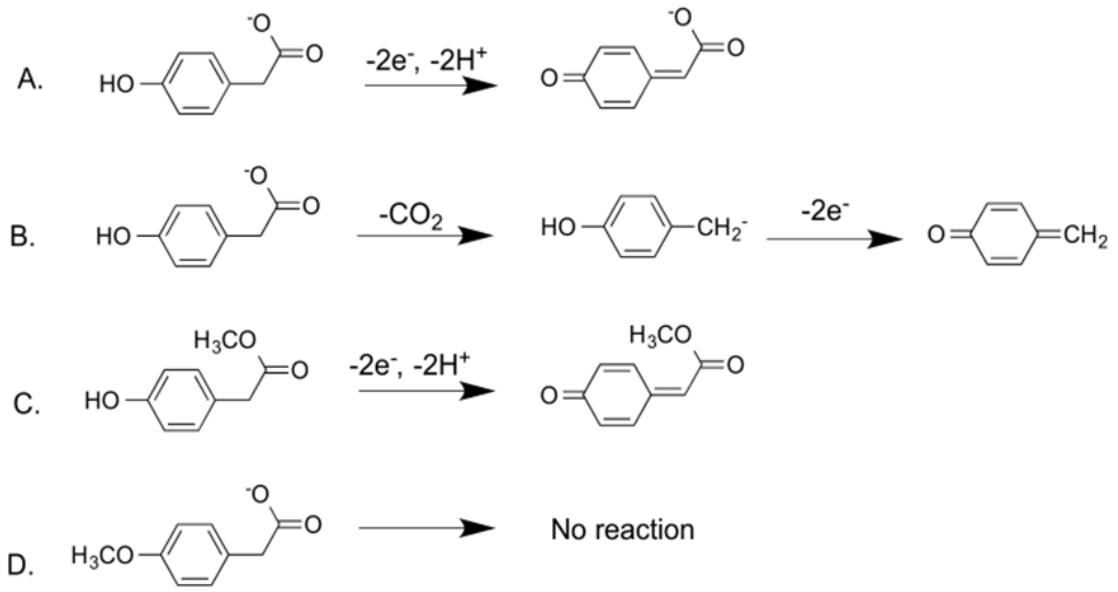

Scheme 2. Proposed oxidation reactions of 4HPAA, M4HPA, and 4MPAA. (A) Oxidation of 4HPAA to form a conjugated species and (B) the decarboxylation of 4HPAA. (C) Oxidation of methyl-4-hydroxyphenyl acetate (M4HPA) and (D) 4-methoxyphenylacetic acid (4MPAA).

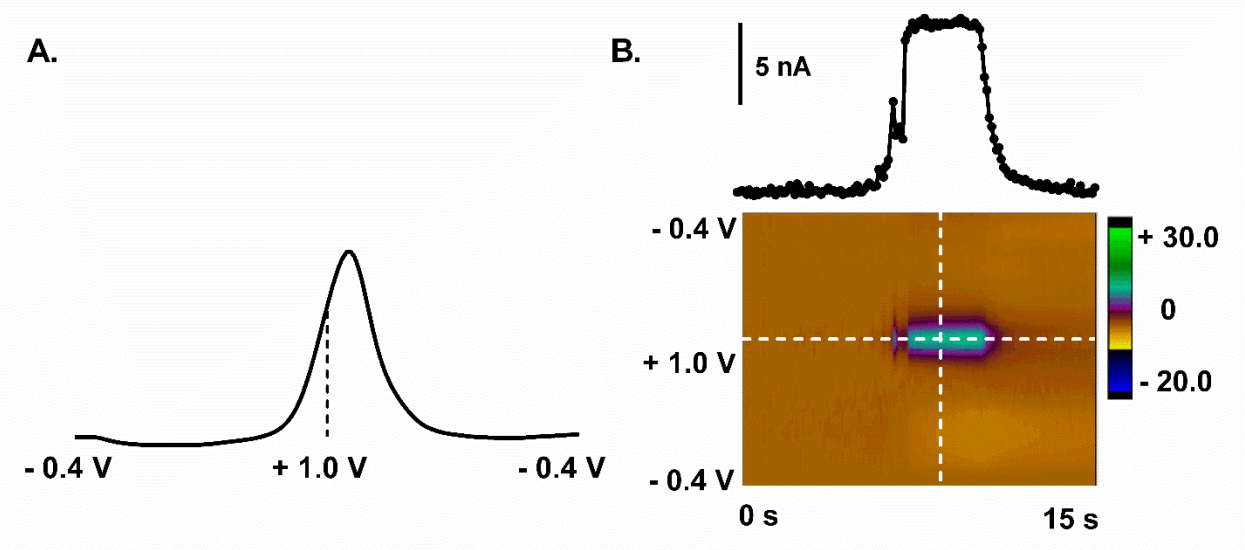

Figure. 1 Background subtracted cyclic voltammetry of 4HPAA. (A) Unfolded cyclic voltammogram of 100 μM 4HPAA in aCSF, physiological pH 7.4, obtained using the waveform −0.4 V to +1.0 V to −0.4 V at 400 V s^{-1} every 100 ms. The oxidation peak of 4HPAA was detected around +0.9 V on the reverse scan. (B) The color plot (bottom) and oxidation current response (top), taken at the oxidation peak of 4HPAA, were acquired as the carbon-fiber electrode was exposed to 4HPAA bolus for 5 s during the flow injection analysis.

The CVs obtained by FSCV were plotted in an unfolded manner, in which the switching potential is located at the center of the plot, in order to clarify the location of the oxidation peaks. The color plot and corresponding CV revealed that a large, faradaic current peak, due to the oxidation of 4HPAA, occurs at approximately +0.9 V as the potential was being scanned from +1.0 V to −0.4 V. The occurrence of this peak on the reverse scan is atypical. For example, current due to the oxidation of many electroactive neurotransmitters, such as DA and serotonin (5-HT), occur on the front, forward scan. On the other hand, the oxidation peak of hydrogen peroxide also occurs on the reverse scan under similar scan parameters.[16] Additionally, histamine and adenosine

have oxidation peaks detected on the reverse scan, exhibiting similar electrochemical behavior to that of 4HPAA and hydrogen peroxide.[17, 18] These studies suggested that this phenomenon could have been caused by the time required for electron transfer. It should also be noted that the oxidation peak of 4HPAA occurred on the reverse scan even before filtering the file.

A broad, shallow negative current (less than 10% of the oxidation current) also occurred on the forward scan. The cause of this peak is unclear; however, this particular peak does not appear on the first CV collected, but does appear on CVs collected 2 seconds after the electrode was exposed to a 4HPAA bolus (data not shown). Therefore, it is possible that the peak is caused by the formation and adsorption of a species as a result of the initial 4HPAA oxidation.[19] However, it is not clear if this current is faradaic or if it occurs as a result of an alteration in the electrode background.

The current response at the oxidation potential of 4HPAA is shown in Fig. 1B. This current trace (top) has a square response to a 4HPAA bolus during the sample injection analysis. Overall, the features of this CV, namely, the disparity in magnitude and the absence of a faradaic reduction peak on the reverse scan, suggest that 4HPAA undergoes an irreversible electrochemical reaction under these conditions.

4.3.2 Mechanisms of Oxidation of 4HPAA

4.3.2.1 The Effect of pH on Oxidation Current of 4HPAA

Two potential mechanisms that could be responsible for the oxidation current in Fig. 1 include the oxidation of 4HPAA to form a conjugated species (Scheme 2A) and/or the decarboxylation of 4HPAA (Scheme 2B). The conjugated species is formed by a two-electron oxidation reaction in which the phenolic proton and one of the protons located on the β-carbon are

removed. On the other hand, the decarboxylation reaction occurs when one of the protons located on the negatively-charged carboxylic acid group is removed, forming a radical that results in the release of a carbon dioxide molecule.

To examine these potential mechanisms, we obtained CVs of 4HPAA and the related compounds, methyl-4-hydroxyphenyl acetate (M4HPA) and 4-methoxyphenylacetic acid (4MPAA) (Schemes 1C and D, respectively) at pH values of 2.71, 6.71, and 10.71 (Fig. 2). The same electrochemical parameters employed in Fig. 1 were used for these pH studies. At all pH values, 4HPAA and M4HPA showed substantial faradaic oxidation currents that occurred on the reverse scan at about +0.9 V and +0.8 V, respectively, while 4MPAA showed no appreciable current at any pH. The pH value significantly impacted the oxidative current; responses progressively decreased for 4HPAA and M4HPA, with the highest current observed at pH 2.71 and the lowest current observed at pH 10.71 ($p < 0.0001$, $n = 4$, two-way ANOVA, $F(2.90) = 56.94$).

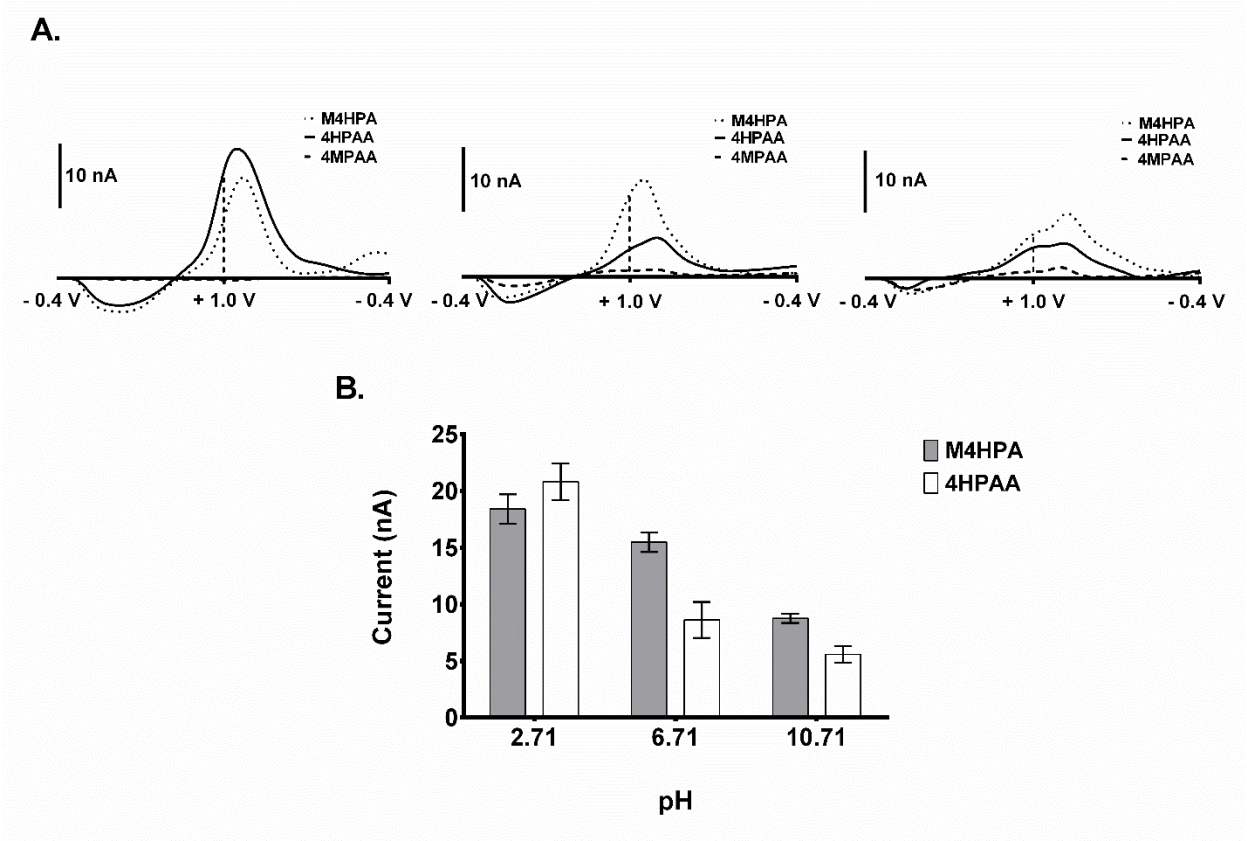

Figure. 2 Changes in oxidation signal of 4HPAA and M4HPA in response to pH. (A) Unfolded CVs of 4HPAA and M4HPA at pH values of 2.71 (left), 6.71 (center), and 10.71 (right). Oxidation peaks of both species were detected on the reverse scan. (B) The effect of pH on oxidation current of 4HPAA and M4HPA. Both species showed similar overall current trends in response to changes in pH. There was a significant pH-driven effect on oxidation current ($p = 0.0007$, $n = 4$, two-way ANOVA, $F(2,90) = 56.94$).

The evidence presented here suggests that the oxidation of 4HPAA proceeds through the formation of conjugated species. The para-methoxy derivative form of 4HPAA, 4MPAA, showed only a negligible oxidation current compared to 4HPAA. This is not surprising, given that the methoxy group on the ring would be expected to make the formation of the conjugated species

energetically unfavorable. On the other hand, M4HPA showed an oxidation current similar to 4HPAA at all pH values. Given that both M4HPA and 4HPAA possess an oxidizable phenol group, both compounds can readily form the conjugated species (Schemes 2A and C).

The idea that M4HPA and 4HPAA undergo similar oxidation mechanisms is supported by other reports in which the redox behavior of parabens and other analogues was investigated.[21] Gil *et al.* have employed an electrochemical method to investigate the association between the inductive effect of different types of parabens and their redox behavior.[20] This study suggests that the phenolic hydroxyl group affects the oxidation state of parabens; thus, changes in pH influence redox reactions, especially those involving H^+.

This overall trend of decreasing oxidation current with decreasing pH seems to be influenced by pH-induced charged states of 4HPAA and M4HPA. The pKa values of the phenolic carboxylic acid and hydroxyl group of 4HPAA are 4.48 and 9.67, respectively; thus, 4HPAA is neutral under highly acidic conditions and negatively charged under neutral and basic conditions.[21] However, the pKa value of M4HPA is 8.4, making M4HPA neutral under both acidic and neutral conditions and negatively charged under highly basic conditions. When the waveform in Fig. 1 is employed, the surface of the carbon-fiber microelectrode is held at a potential of −0.4 V during the 93 ms that elapses in between 7 ms-duration voltage sweeps. This electron-rich state would be expected to promote adsorption of positively-charged species while repelling negatively-charged species. Our observations in Fig. 2 are consistent with this logic. The oxidation currents for both 4HPAA and M4HPA are lowest at a pH of 10.71, conditions under which both species are negatively charged, and are greatest at a pH of 2.71, at which both species are neutral in charge.

The currents arising from the oxidation of M4HPA are greater than those arising from 4HPAA oxidation at pH values of 6.71 and 10.71. This difference likely occurs because 4HPAA

possesses a single negative charge compared to the neutral charge state of M4HPA at a pH of 6.71. Similarly, 4HPAA has a double negative charge while M4HPA has a single negative charge at a pH of 10.71. The increased negative character of 4HPAA would be expected to decrease its association with the negatively-charged electrode surface to a greater extent than M4HPA, thereby decreasing the measured oxidation currents of 4HPAA at neutral and basic pH.

In addition to altering the charge state of the molecules of interest, pH can also influence the carbon-fiber microelectrode surface. Oxide groups on the surface can undergo protonation and deprotonation as environmental pH changes, thereby affecting electrochemical responses.[19 22, 23] Moreover, the changes in pH tend to influence redox reactions, especially those involving a loss or gain of H+, as is commonly observed in phenolic compounds.[24] It is not clear if these modifications would differentially influence oxidation currents obtained from 4HPAA and M4HPA.

4.3.2.2 The Effect of Scan Rates on Oxidation Current at the Standard Waveform.

Currents measured at the electrode may be controlled in two fundamental ways: (1) the electron transfer reaction of 4HPAA adsorbed onto the electrode surface cannot keep up with the high scan rates employed when using FSCV (electron transfer-limited current) and (2) the oxidation currents are limited by the ability of 4HPAA to diffuse to the electrode due to the high scan rates employed (diffusion-limited current). To determine if the current is adsorption- or diffusion-limited, we obtained CVs at scan rates ranging from 100 to 800 V s^{-1} (Fig. 3). When the current response was plotted against various scan rates, shown in Fig. 3A, linear responses were observed up to 500 V s^{-1} (R^2 = 0.9882), suggesting that the electrochemical reaction is adsorption dependent up to this scan rate.[25] At scan rates greater than 500 V s^{-1}, linearity is lost; however,

when these current responses were plotted versus square root of scan rate, as shown in Fig. 3B, the plot yielded a linear trace ($R^2 = 0.9822$), suggesting diffusion control.[15, 26] Therefore, we conclude that electron transfer kinetics for 4HPAA oxidation are influenced mostly by adsorption at scan rates below 500 V s^{-1}, and diffusion at scan rates greater than 500 V s^{-1}.[17] These factors likely contribute to the movement of the peak from higher to lower potentials (Fig. 3C), that is, the electron transfer reaction shifts farther to the right of the switching potential of +1.0 V.

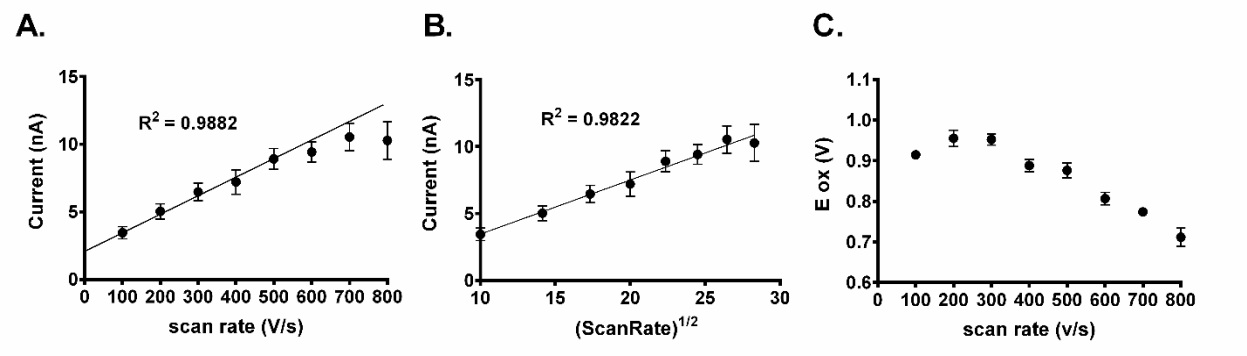

Figure. 3 The effect of scan rate on currents generated from the oxidation of 4HPAA. (A) Plot of current versus scan rate. The R^2 value applies to measurements obtained from 100 to 500 V s^{-1}. (B) Plot of current versus the square root of the scan rate. CVs were obtained using the waveform −0.4 V to +1.0 V to −0.4 V at selected scan rates. The currents were obtained from the oxidation peaks. (C) Plot of oxidation potential (E_{ox}) versus scan rate.

4.3.2.3 Fast-Scan Cyclic Voltammetry of 4HPAA at Extended Waveform

To determine if additional oxidation processes can be induced at higher potentials, the waveform was modified so that the potential was scanned up to +1.3 V, while the holding potential was still maintained at −0.4 V at 400 V s^{-1} (Fig. 4). The resulting CV revealed the formation of

two individual oxidation peaks, indicating the occurrence of two distinct electrochemical processes (Fig. 4A). The first and second peaks were observed at +1.2 V on the forward scan ('peak 1') and at +1.0 V on the reverse scan ('peak 2'), respectively. To understand the possible mechanism of these two oxidation peaks' formation, the current traces were analyzed. The current for peak 1 increased more rapidly upon 4HPAA injection compared to peak 2 (Fig. 4B, top) and reached a steady state almost before the second oxidation peak had begun to form. These traces are consistent with a mechanism in which the primary oxidation reaction, resulting in peak 1, is followed by a secondary oxidation reaction, resulting in peak 2.

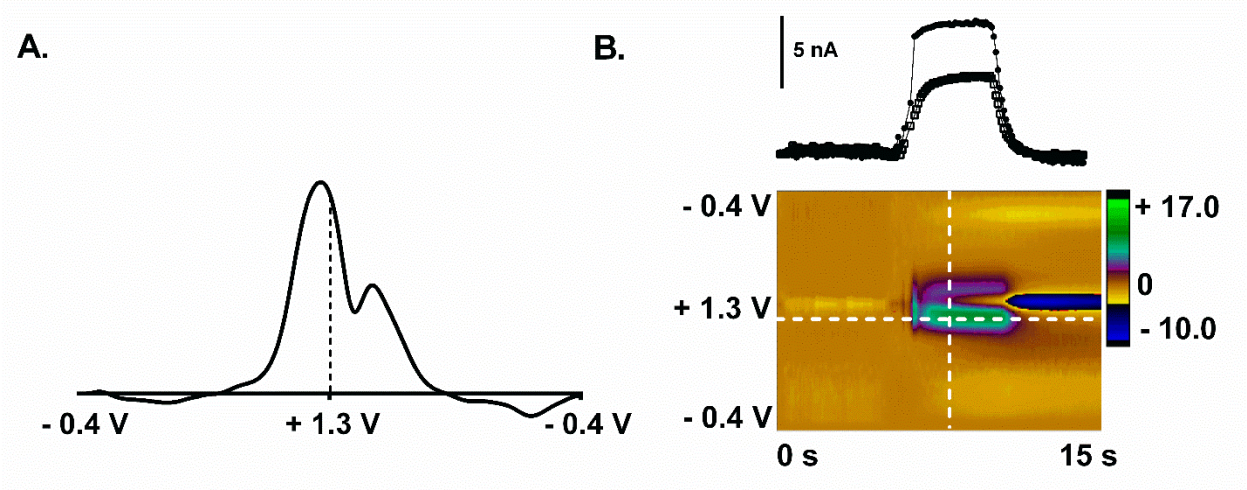

Figure. 4 Fast-scan cyclic voltammetry of 4HPAA. (A) Unfolded cyclic voltammogram of 100 µM 4HPAA in aCSF (pH 7.4) obtained using the waveform −0.4 V to +1.3 V to −0.4 V at 400 V s^{-1} repeated every 100 ms. Two oxidation peaks were observed, one around +1.2 V on the forward scan and the other one around +1.0 V on the reverse scan. (B) Color plot (bottom) and current traces taken at the first oxidation peak, observed on the forward scan.

4.3.2.4. Conventional Cyclic Voltammetry of 4HPAA

Further analysis of 4HPAA with conventional cyclic voltammetry was conducted for comparison. For this experiment, a three electrode system was used. The potential at a glassy carbon electrode, immersed in a solution of 2 mM 4HPAA in aCSF, was scanned from −0.4 V up to +1.0 V and back to −0.4 V at a scan rate of 10 mV s^{-1} (Fig. 5A). In contrast to the measurements obtained with FSCV, the oxidation peak was detected at +0.65 V on the forward scan. Moreover, when the electrode was scanned up to the higher switching potential of +1.3 V, the two oxidation peaks were observed on forward sweep, at +0.65 V and +1.06 V, as expected (Fig. 5B).

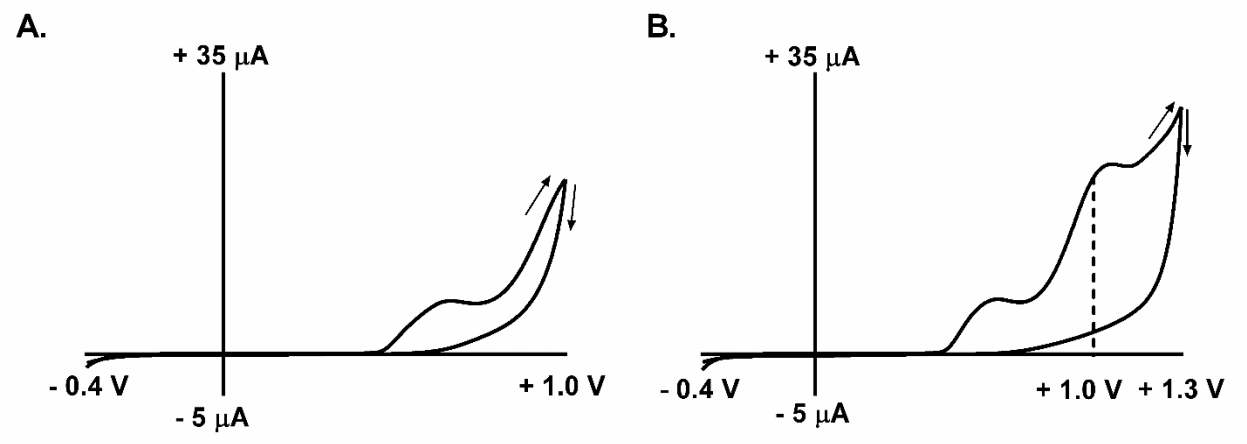

igure. 5 Conventional cyclic voltammetry of 4HPAA prepared in aCSF (pH 7.4). (A) CV obtained using the waveform −0.4 V to +1.0 V to −0.4 V showing a single faradaic peak. (B) CV obtained using the waveform −0.4 V to +1.3 V to −0.4 V showing the appearance of an additional peak at +1.06 V. The dashed line denotes the location of the +1.0 V potential. The concentration of 4HPAA was 2 mM and the scan rate was 10 mV s−1.

Although the electrochemical mechanism underlying the formation of this second peak is not clear, it is possible that a dimerization occurs. The phenol group of the 4HPAA molecule is reactive since the proton from the hydroxyl group is acidic. Therefore, as the oxidation potential is applied to the electrode, the first electron is transferred from the phenol to the electrode, forming a phenoxy radical that further couples with another 4HPAA molecule to electrochemically generate a dimer, similar to that occurring with other phenolic compounds.[20, 21, 27-29] As the dimer forms, the second electron transfer takes place, which would be responsible for the second oxidation peak.[21]

During the collection of multiple CVs, the oxidation current of 4HPAA dropped substantially after the first scan, necessitating that the electrode must be polished between each scan (data not shown). With this in mind, it should be mentioned that poly-4HPAA can passivate the electrode surface, resulting in electrode fouling and slower electron transfer. Nevertheless, electrode fouling appeared not to substantially impact current from the FSCV experiments. One explanation for this is that the electrode was scanned at such a high rate that there is not enough time for electrodeposition to occur.[21]

4.3.3 Optimization of FSCV scanning parameters

To minimize the effect of the secondary product (peak 2) while enhancing the response of the main peak (peak 1), oxidation current responses of 4HPAA at different switching potentials, holding potentials, and scan rates were studied. First, we obtained CVs containing both main and secondary peaks at selected switching potentials ranging from +1.0 V to +1.4 V at the constant holding potential of −0.4 V and a scan rate of 400 V s^{-1}. Overall, the current response of peak 1 increased as the switching potential was changed from +1.0 V to +1.4 V (Fig. 6A). A slight drop

in current was found at +1.4 V. As higher switching potentials are applied, the hydrophobicity of the carbon-fiber electrode surface changes by increasing the number of oxide groups, which improves the electron transfer kinetics at the electrode surface and enhances sensitivity.[30, 31] Such an improvement could also arise from an increase in the microscopic area of the electrode surface [32, 33] and enhancement of hydrogen atom transfer, resulting in changing the charge at the electrode surface.[34, 35]

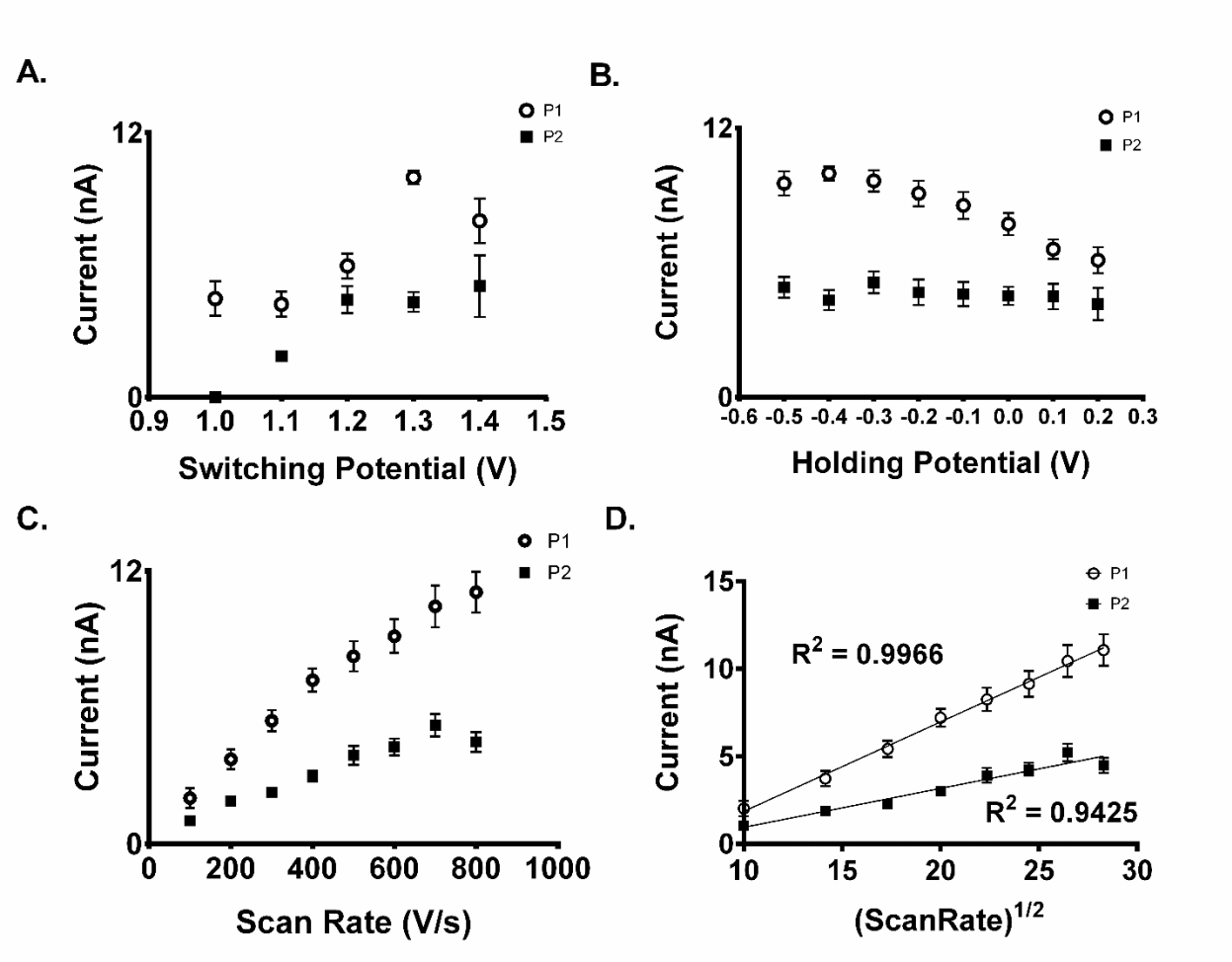

Figure 6. Optimization of FSCV scanning parameters. (A) Effect of switching potential on oxidation current for the primary peak (circles) and secondary peak (squares) was studied. Switching potential was varied between +1.0 V and +1.4 V while holding potential was held constant at −0.4 V using a scan rate of 400 V s^{-1}. (B) The holding potential was varied from −0.5 V to +0.2 V while the switching potential was held at +1.0 V with a scan rate of 400 V s^{-1}. Current responses of peak 1 (circle) and peak 2 (square) at each holding potential were plotted. (C) Dependence of oxidation current of peaks 1 and 2 on scan rate (C) and square root of scan rate (D). The waveform −0.4 V to +1.3 V to −0.4 V was used (for all figures $p < 0.001$, $n = 4$, peak one compared to peak two, two-way ANOVA).

The current response due to the secondary reaction also increased with greater switching potential in the fast-scan CV traces, but not as much as the main peak. In fact, the current response of peak 1 was more than double that of peak two at +1.3 V. A similar effect has been well-documented when measuring DA.[36, 37] Therefore, in order to optimize the ability of FSCV to measure DA, while also enhancing the 4HPAA signal, we selected +1.3 V as the switching potential.

Current response was measured at selected holding potentials (between −0.5 V and +0.2 V) while maintaining a switching potential at +1.3 V at a scan rate of 400 V s^{-1}. (Fig. 6B). 4HPAA is negatively charged at the physiological pH, so we expected to see lower current responses for both peak 1 and peak 2 due to the repulsive action between the negatively charged electrode and 4HPAA conjugate base. However, a higher current response for peak 1 was observed as more negative holding potentials were applied except at −0.5 V, due to the unreliable background current at lower holding potentials.[17] This enhancement of catecholamine signal at negative holding potentials had previously been suggested to occur as a result of the increased amount of adsorption at the electrode surface.[15] The adsorption of 4HPAA apparently plays a major role, thereby explaining the current response increases that occur as the holding potential becomes more negative.

Increasing scan rate has also been shown to enhance the current response of adsorbed species (see Fig. 3).[38] Fig. 6C shows a plot of oxidation current of 4HPAA versus scan rate. As expected, the current for both peak 1 and peak 2 increased with scan rate. As faster scan rates are applied, the time spent at the holding potential increases, which also increases the amount of time for adsorption as well. Even though the highest current is obtained at the scan rate of 800 V s−1, we decided to use 600 V s^{-1} as an optimized parameter. This choice represents a compromise. At

high scan rates, faradaic currents can be buried under the background current[36] which is proportional to the scan rate.[22] Moreover, DA, as well as other electroactive neurotransmitters, undergo hysteresis—the oxidation occurs at a more positive potential, the reduction occurs at a more negative potential—which may cause increased overlap with the 4HPAA peak.[15, 39]

4.3.4 Cyclic voltammetry of 4HPAA and DA

One of our goals is to be able to quantify how much 4HPAA has been photo-released from p-hydroxyphenacyl-based caged compounds.[6, 40] A specific application of this approach is the photorelease of glutamate, the most abundant excitatory neurotransmitter in the central nervous system,[41] in brain tissue and measuring subsequent alterations in the electrically evoked release of DA. This approach has the advantages of being able to apply glutamate within short timeframes and confined spatial dimensions. Both of these advantages are critical because glutamate is excitotoxicity, [42] making the bath application of brain slices impractical.

Unfortunately, determining with high precision the amount of glutamate, or any other caged compound that has been photoreleased, has historically relied upon experimental determination of the number of moles of photons per second supplied by the light source and multiplying this parameter by the quantum yield (moles of compound photoreleased/moles of photons supplied) of the caged compound of interest.[8] This method is inherently imprecise due to variations in the output of the light source as well inconsistencies in tissue density at various recording sites.

One goal in the electrochemical characterization of 4HPAA is to use this electrochemical signature to quantify glutamate photorelease within brain tissue slices more reliably than the existing method described, independent of the number of photons reaching the tissue. Therefore,

it is important to optimize our voltammetric parameters for the simultaneous detection of DA and 4HPAA.

To enhance the peak separation, voltammetric measurements were obtained from a mixture of 4HPAA (100 μM) and DA (1 μM) at selected switching potentials while the holding potential was kept at −0.4 V (Fig. 7A). As shown, the separation of peak oxidation potential (Eox) between 4HPAA (100 μM) and DA (1 μM) was greatest at a switching potential of +1.3 V. The use of higher switching potentials is not well-suited for the detection of dynamic changes of catecholamine release due to the increased response time.[37] Therefore, we decided to use +1.3 V in the optimized waveform. Holding potential and scan rate did not significantly affect peak separation, so a potential of −0.4 V and rate of 600 V s^{-1} (the optimized scan rate for 4HPAA) was used.

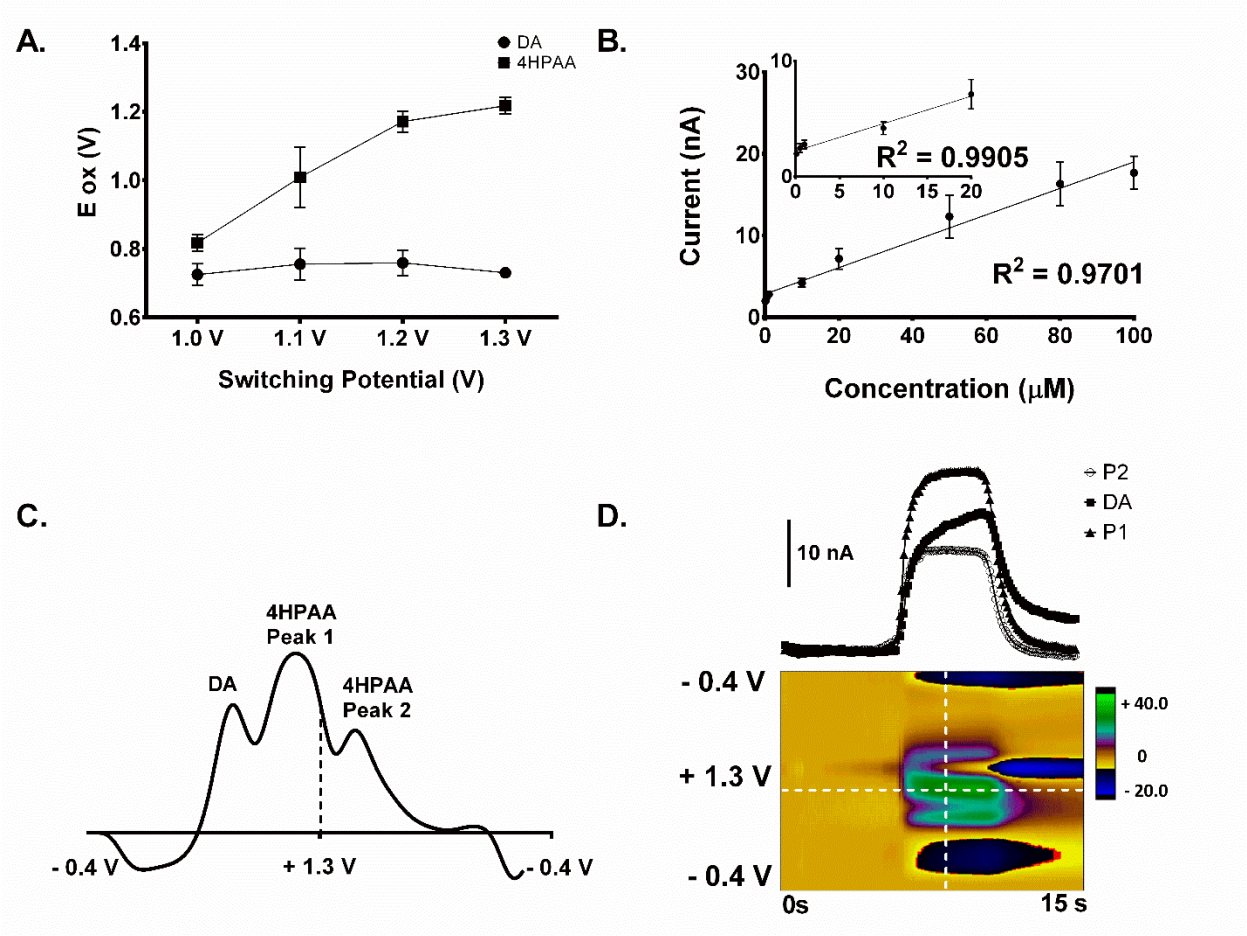

Figure. 7 Cyclic voltammetry of 4HPAA and DA at optimized waveform. (A) Study of oxidation peak potential of 100 μM 4HPAA and 1 μM DA. (n = 4, $p < 0.0001$, two-way ANOVA). (B). Concentration study of 4HPAA in the presence of DA. Current responses of the primary oxidation peak was plotted against 4HPAA concentration. (n = 3, $p = 0.0091$, t-test) (C) Unfolded CV of 4HPAA and DA. Three oxidation peaks were observed, oxidation peak of DA and 4HPAA (peak 1) were shown on forward sweep and 4HPAA (peak 2) on reverse sweep. (D) Color plot (bottom) and current traces of 4HPAA and DA was obtained from the flow injection analysis.

An example of the detection of 4HPAA and DA using this optimized waveform is shown in Fig. 7C and D. The oxidation peaks for both 4HPAA (peak 1) and DA rise rapidly after injection. Moreover, the peaks are clearly separated on the CV. The optimized waveform was used to measure the current signal of a mixture of 4HPAA and DA at selected concentrations (Fig. 7D).

The current traces of both peak 1 and 2 have square responses due to the sample injection compared to that of DA, which shows a slower response under the same conditions. A similar difference in current response has been shown between DA and ascorbate. This is likely due to DA being strongly adsorbed and desorbed at the electrode surface.[15] For the data analysis on the calibration curve, the current was taken at the main oxidation peak of 4HPAA. Fig. 7B shows the oxidation current responses of the main peak as a function of 4HPAA concentration which was varied from 0.1 μM to 100 μM in the presence of 1 μM DA in solution. The oxidation current of 4HPAA increases linearly with the concentration with correlation coefficient of 0.9905 up to 20 μM and 0.9701 up to 100 μM. The limit of detection of 4HPAA was found to be 100 nM based on the signal to noise ratio of 3.

4.4. Conclusions

The goal of this study was to develop a method to quantitatively and simultaneously measure sub-second changes in DA and 4HPAA levels. Our intent is to apply this method to examine neurotransmitter interactions in brain slices as well as in vivo. We found that the optimum waveform for the detection of 4HPAA was to scan linearly from a holding potential of −0.4 V to +1.3 V and back to −0.4 V at a scan rate of 600 V s^{-1}. This waveform provided good limits of detection and sensitivity for the measurement of 4HPAA. Moreover, this optimized waveform was effective for the simultaneous detection of 4HPAA and DA. Along with quantifying 4HPAA in

biological preparations, the results from this work will allow the electrochemical measurement of photoactivation reactions that generate 4HPAA as a by-product as well as provide a framework for measuring the photorelease of electroactive by-products from caged compounds that incorporate other chromophores.

4.5 Reference

[1] Umeo Takahama, , T. O., and , H. M. (2002) The presence of 4-hydroxyphenylacetic acid in human saliva and possibility of its nitration by salivary nitrite in the stomach, FEBS Lett., 518, 116-118

[2] Kalyanaraman, B., Darley-Usmar, V., Davies, K. J., Dennery, P. A., Forman, H. J., Grisham, M. B., Mann, G. E., Moore, K., Roberts, L. J., 2nd, and Ischiropoulos, H. (2012) Measuring reactive oxygen and nitrogen species with fluorescent probes: challenges and limitations, *Free rad. Bio. Med., 52*, 1-6.

[3] Hareland, W. A., Crawford, R. L., Chapman, P. J., and Dagley, S. (1975) Metabolic function and properties of 4-hydroxyphenylacetic acid 1-hydroxylase from Pseudomonas acidovorans, *J. Bacteriol., 121*, 272-285.

[4] Metruccio, M. M. E., Pigozzi, E., Roncarati, D., Scorza, F. B., Norais, N., Hill, S. A., Scarlato, V., and Delany, I. (2009) A novel phase variation mechanism in the meningococcus driven by a ligand-responsive repressor and differential spacing of distal promoter elements, *PLoS Pathog., 5*, No pp. given.

[5] Brier, S., Fagnocchi, L., Donnarumma, D., Scarselli, M., Rappuoli, R., Nissum, M., Delany, I., and Norais, N. (2012) Structural Insight into the Mechanism of DNA-Binding

Attenuation of the Neisserial Adhesin Repressor NadR by the Small Natural Ligand 4-Hydroxyphenylacetic Acid, *Biochemistry, 51*, 6738-6752.

[6] Givens, R. S., and Lee, J.-I. (2003) The p-hydroxyphenacyl photoremovable protecting group, *J. Photosci., 10*, 37-48.

[7] Givens, R. S., Heger, D., Hellrung, B., Kamdzhilov, Y., Mac, M., Conrad, P. G., II, Cope, E., Lee, J. I., Mata-Segreda, J. F., Schowen, R. L., and Wirz, J. (2008) The Photo-Favorskii Reaction of p-Hydroxyphenacyl Compounds Is Initiated by Water-Assisted, Adiabatic Extrusion of a Triplet Biradical, *J. Am. Chem. Soc., 130*, 3307-3309.

[8] Ellis-Davies, G. C. R. (2007) Caged compounds: photorelease technology for control of cellular chemistry and physiology, *Nat. Meth., 4*, 619-628.

[9] Callaway, E. M., and Katz, L. C. (1993) Photostimulation using caged glutamate reveals functional circuitry in living brain slices, *Proc. Natl. Acad. Sci., 90*, 7661-7665.

[10] Wang, S. S. H., and Augustine, G. J. (1995) Confocal imaging and local photolysis of caged compounds: dual probes of synaptic function, *Neuron, 15*, 755-760.

[11] Nerbonne, J. M. (1996) Caged compounds: tools for illuminating neuronal responses and connections, *Curr. Opin. Neurobiol., 6*, 379-386.

[12] Givens, R. S., and Yousef, A. L. (2005) Photoremovable protecting groups used for the caging of biomolecules. p-hydroxyphenacyl: a photoremovable protecting group for caging bioactive substrates, pp 55-75, Wiley-VCH Verlag GmbH & Co. KGaA.

[13] Cooper, S. E., and Venton, B. J. (2009) Fast-scan cyclic voltammetry for the detection of tyramine and octopamine, *Ana. Bio. Chem., 394*, 329-336.

[14] Johnson, M. A., Rajan, V., Miller, C. E., and Wightman, R. M. (2006) Dopamine release is severely compromised in the R6/2 mouse model of Huntington's disease, *J. Neurochem., 97*, 737-746.

[15] Bath BD, M. D., Trafton BJ, Joseph JD, Runnels PL. Wightman RM. (2000) subsecond adsorption and desorption of dopamine at carbon-fiber microelectrode, *Anal. Chem., 72*, 5994-6002.

[16] Sanford, A. L., Morton, S. W., Whitehouse, K. L., Oara, H. M., Lugo-Morales, L. Z., Roberts, J. G., and Sombers, L. A. (2010) Voltammetric Detection of Hydrogen Peroxide at Carbon Fiber Microelectrodes, *Anal. Chem., 82*, 5205-5210.

[17] B. E. Kurama Swamy, a. B. J. V. (2007) subsecon detection of physiological adenosine concentration using fast scan cyclic voltammetry, *Anal. Chem., 79*.

[18] Chang, S. Y., Jay, T., Munoz, J., Kim, I., and Lee, K. H. (2012) Wireless fast-scan cyclic voltammetry measurement of histamine using WINCS--a proof-of-principle study, *The Analyst, 137*, 2158-2165.

[19] Takmakov, P., Zachek, M. K., Keithley, R. B., Bucher, E. S., McCarty, G. S., and Wightman, R. M. (2010) Characterization of Local pH Changes in Brain Using Fast-Scan Cyclic Voltammetry with Carbon Microelectrodes, *Anal. Chem., 82*, 9892-9900.

[20] Eric de S. Gil, a Carolina H. Andrade,a Núsia L. Barbosa,a Rodolpho C. Bragaa and, and Serranob, S. H. P. (2012) A Cyclic Voltammetry and Computational Chemistry Studies on the Evaluation of the Redox Behavior of Parabens and other Analogues, *J. Braz. Chem. Soc., 23*, 565-572.

[21] Rodrigues, L. P., Ferreira, D. C., Sonoda, M. T., Madurro, A. G. B., Abrahão, O., and Madurro, J. M. (2014) Electropolymerization mechanisms of hydroxyphenylacetic acid isomers, *J. Mol. Structure., 1072*, 298-306.

[22] Takmakov, P., Zachek, M. K., Keithley, R. B., Walsh, P. L., Donley, C., McCarty, G. S., and Wightman, R. M. (2010) Carbon Microelectrodes with a Renewable Surface, *Anal. Chem., 82*, 2020-2028.

[23] Petrise L. Runnels, J. D. J., Michael J. Logman, and R. Mark Wightman. (1999) Effect of pH and surface functionalities on the cyclic voltammetric responses of carbon-fiber microelectrodes, *Anal. Chem., 71*, 2782-2789.

[24] Arslan, G., Yazici, B., and Erbil, M. (2005) The effect of pH, temperature and concentration on electrooxidation of phenol, *J. Hazar. Mat., 124*, 37-43.

[25] Allen J. Bard, L. R. F. (2001) Introduction and overview of electrode processes, *Electrochemical methods: Fundermentals and applications*, 2nd ed., pp 1-43, John Wiley and Sons, Inc.: New York.

[26] Chandra, U., Kumara Swamy, B. E., Gilbert, O., Sharath Shankar, S., Mahanthesha, K. R., and Sherigara, B. S. (2010) Electrocatalytic oxidation of dopamine at chemically modified carbon paste electrode with 2,4-Dinitrophenyl hydrazine, *Int. J. Electrochem. Sci., 5*, 1-9.

[27] Castro, C. M., Vieira, S. N., Goncalves, R. A., Brito-Madurro, A. G., and Madurro, J. M. (2008) Electrochemical and morphologic studies of nickel incorporation on graphite electrodes modified with polytyramine, *J. Mater. Sci., 43*, 475-482.

[28] Tenreiro, A. M., Nabais, C., Correia, J. P., Fernandes, F. M. S. S., Romero, J. R., and Abrantes, L. M. (2007) Progress in the understanding of tyramine electropolymerisation mechanism, *J. Solid State. Chem., 11*, 1059-1069.

[29] Ferreira, M., Varela, H., Torresi, R. M., and Tremiliosi-Filho, G. (2006) Electrode passivation caused by polymerization of different phenolic compounds, *Electrochimica. Acta., 52*, 434-442.

[30] Deakin, M. R., Kovach, P. M., Stutts, K. J., and Wightman, R. M. (1986) Heterogeneous mechanisms of the oxidation of catechols and ascorbic acid at carbon electrodes, *Anal. Chem., 58*, 1474-1480.

[31] Yue, Z. R., Jiang, W., Wang, L., Gardner, S. D., and Pittman, C. U. (1999) Surface characterization of electrochemically oxidized carbon fibers, *Carbon, 37*, 1785-1796.

[32] Wightman, R. M., Deakin, M. R., Kovach, P. M., Kuhr, W. G., and Stutts, K. J. (1984) Methods to improve electrochemical reversibility at carbon electrodes, *J. Electrochem. Soc., 131*, 1578-1583.

[33] Stutts, K. J., Kovach, P. M., Kuhr, W. G., and Wightman, R. M. (1983) Enhanced electrochemical reversibility at heat-treated glassy carbon electrodes, *Anal. Chem., 55*, 1632-1634.

[34] Kamau, G. N., Willis, W. S., and Rusling, J. F. (1985) Electrochemical and electron spectroscopic studies of highly-polished glassy carbon electrodes, *Anal. Chem., 57*, 545-551.

[35] Deakin, M. R., Stutts, K. J., and Wightman, R. M. (1985) The effect of pH on some outer-sphere electrode reactions at carbon electrodes, *J. Electroanal. Chem. Interfacial Electrochem., 182*, 113-122.

[36] Richard B. Keithley, P. T., † Elizabeth S. Bucher,† Anna M. Belle,† Catarina A. Owesson-White,†, and Jinwoo Park, a. R. M. W. (2011) higher sensitivity dopamine measurement with fast scan cyclic voltammetry, *Anal. Chem., 9,* 3563–3571.

[37] Heien, M. L. A. V., Phillips, P. E. M., Stuber, G. D., Seipel, A. T., and Wightman, R. M. (2003) Overoxidation of carbon-fiber microelectrodes enhances dopamine adsorption and increases sensitivity, *Analyst, 128,* 1413-1419.

[38] Peter T. Kissinger, W. R. H. (1996) *In Laboratory Techniques in Electroanalytical Chemistry*, 2nd ed., Marcel Dekker, Inc., New York.

[39] Hsueh, C., Bravo, R., Jaramillo, A. J., and Brajter-Toth, A. (1997) Surface and kinetic enhancement of selectivity and sensitivity in analysis with fast scan voltammetry at scan rates above 1000V/s, *Anal. Chim. Acta., 349,* 67-76.

[40] Givens, R. S., Rubina, M., and Wirz, J. (2012) Applications of p-hydroxyphenacyl (pHP) and coumarin-4-ylmethyl photoremovable protecting groups, *Photochem. Phtobio. Sci., 11*, 472-488.

[41] Cooper, J. R. (1997) Principles of Neuropsychopharmacology by R. S. Feldman, J. S. Meyer and L. F. Quenzer, *Trends Neurosci., 20,* 544.

[42] Mark, L. P., Prost, R. W., Ulmer, J. L., Smith, M. M., Daniels, D. L., Strottmann, J. M., Brown, W. D., and Hacein-Bey, L. (2001) Pictorial review of glutamate excitotoxicity: fundamental concepts for neuroimaging, *AJNR Am. J. Neuroradiol., 22,* 1813-1824.

Chapter 5. Conclusions and Future Directions.

5.1 Electrochemical Measurements of Evoked dopamine Release in Zebrafish

For the first time, we were able to measure evoked dopamine release and uptake in a harvested zebrafish whole brain with fast-scan cyclic voltammetry at a carbon-fiber. microelectrode. Conducting several pharmacological manipulations provided strong evidence that the electrochemical species released due to the stimulation is dopamine. One of the unique benefits we discovered while using the harvested whole zebrafish brain is that the brain is small enough to stay viable for more than 6 hours which allows us to conduct any pharmacological studies needed. Moreover, using the intact whole brain allow us to preserve the entire neuronal circuitry and leads to the possibility of studying that circuitry, especially the dopaminergic neuronal pathway. Besides, the use of the whole brain could allow us to understand how the dopaminergic neuronal pathway is associated with neurological disorders or neurotoxicity events.

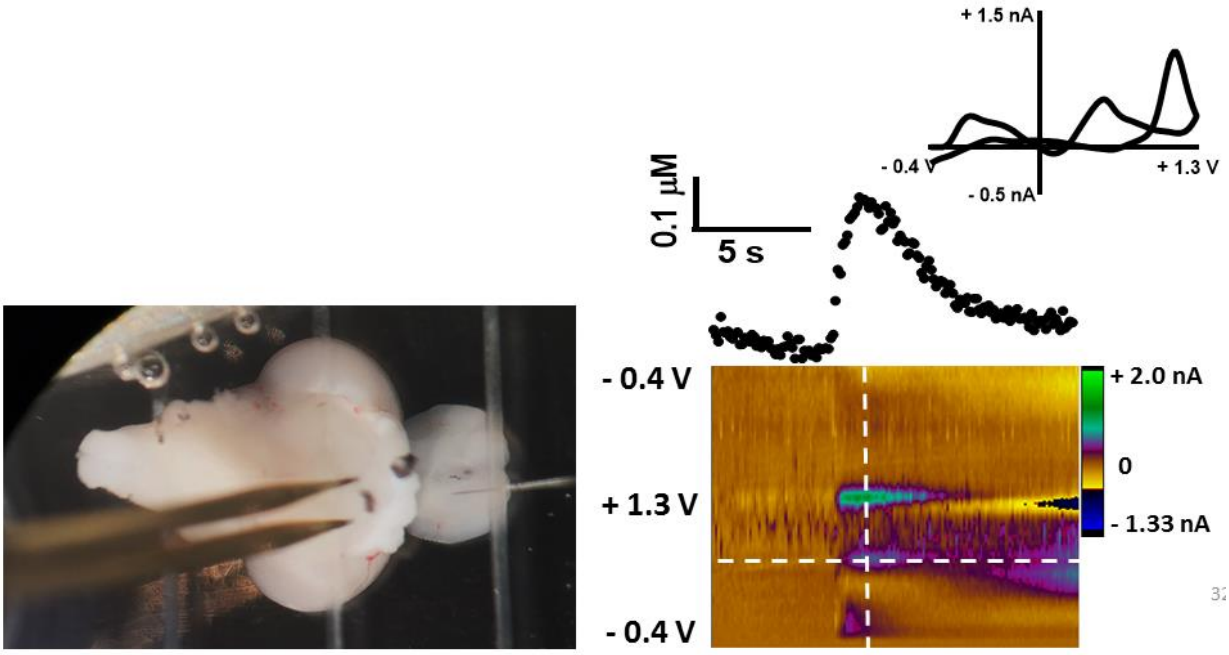

Figure 1. Representative data of evoked dopamine release due to remote stimulation. Image of the harvested whole brain with stimulation electrodes positioned at ventral diencephalon as the carbon-fiber microelectrode is positioned at the ventral telencephalon to measure dopamine release after remote stimulation (left). The concentration versus time plot (right, top) was sampled from the horizontal dashed white line of the color plot (right, bottom) and the cyclic voltammogram (right, top insert), sampled from the vertical dashed white line of the color plot, indicates that the electrochemical change observed in the color plot is indeed dopamine released due to the remote stimulation.

Many histochemical and imaging studies have suggested that the zebrafish's dopamine neurons send an ascending projection from the ventral diencephalon to the ventral telencephalon. [1] To expand the use of zebrafish as a model to study these projections, we have tried to evoke dopamine release remotely. As shown in Fig. 1, dopamine release at the ventral telencephalon was observed while applying stimulation at the ventral diencephalon. Stimulation parameters of

350 µA, 35 pulses, 4ms per pulse, at 60 Hz were used in order to evoke dopamine release. This very promising preliminary data points towards our group having the ability to stimulate the dopamine pathway, thus allowing us to study dopamine's circuitry in zebrafish without having to use *in vivo* methods

Once we establish a robust protocol to measure remotely stimulated dopamine release, we can conduct experiments to determine if pharmacological agents show the same affect during both local and remote stimulation. Moreover, we can determine how the dopaminergic pathway is involved in different neurotoxicity events, such as chemobrain.

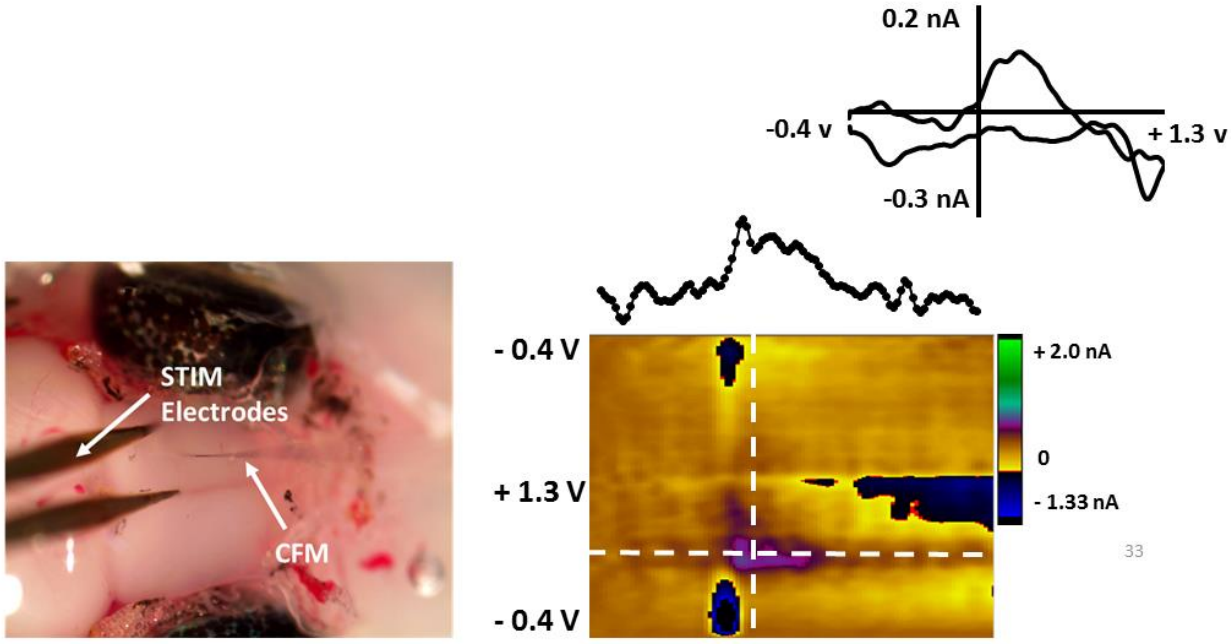

Figure 2. Representative data of locally stimulated dopamine release in an ex vivo whole brain mount. The image of the whole intact brain in a euthanized and decapitated zebrafish head is shown with both the working and stimulation electrodes inserted dorsally rather than ventrally (left). The concentration versus time plot (right, top) due to dopamine release and the cyclic voltammogram (right, top insert) suggest that dopamine can be released while brain is still intact in the zebrafish's head.

The ultimate research goal for the zebrafish study will be the development of methods to measure dopamine release *in vivo*. We were able to measure evoked dopamine release in a euthanized zebrafish. After the zebrafish was euthanized, the head was decapitated and part of the skull was removed exposing the dorsal portion of the entire zebrafish brain. Then, as shown in Fig. 2, we inserted stimulation electrodes and a carbon-fiber microelectrode dorsally rather than ventrally. Dopamine was released after the application of 120 pulses, 100 μA, and frequency of 60 Hz. It is important to mention that we were able to access the ventral side of zebrafish brain while electrodes are introduced from the dorsal side and successfully measure dopamine release. The data presented in Fig. 2 is promising because it demonstrates this was possible, an important first step towards developing in vivo methods in zebrafish. These methods, once fully developed, will allow other researchers to use the zebrafish as a model for neurotoxicity that that can lead to potential therapeutic interventions.

5.2 Dopamine release in chemotherapy treated zebrafish.

In this study, we treated zebrafish with two different chemotherapy drugs, carboplatin and 5-fluorouracil, that are used to treat many cancers. We also have treated the zebrafish in two different pathways; habitat water treatment and food treatment. Dopamine release in zebrafish treated with carboplatin through both habitat water treatment and food treatment was diminished; the same result was shown in chemotherapy treated rats. Moreover, zebrafish were treated with 5-fluorouracil and dopamine release was measured. The data acquired suggested that dopamine release in zebrafish that were fed with 5-flurouracil treated food was reduced; however, there

was no significant changes in dopamine release from zebrafish that were housed in treated habitat water.

To determine if dopamine release impairment in chemotherapy treated zebrafish is due to dopamine synthesis disruption or alteration of dopamine receptors function, we will need to study the total content of dopamine available in zebrafish brain. To carry out this experiment, we are currently developing quantification method using mass spectrometry. This study will provide information relating to how the total content of dopamine differs in control and chemotherapy treated zebrafish. Furthermore, we will study dopamine release and uptake kinetics using modeling software written by R.M Wightman (University of North Carolina, Chapel Hills, NC, USA).

This modeling software will allow us to determine dopamine per pulse, which is the amount of dopamine released per stimulation, and V max, which is the maximum rate of released dopamine uptake. [2, 3] This is valuable information that can be used to study the kinetics of dopamine release and uptake. However, to model the data, the software requires a Km value that will be held constant, this value describes how the dopamine transporter functions. The Km value in rats and mice is known to be about 0.2 µM [4]; however, there is no known Km value available for zebrafish. Therefore, our group, in the future, plans to determine the Km value in zebrafish by introducing known amounts of dopamine into the ventral telencephalon and measure how fast dopamine is uptaken. Once the Km value is determined, we can use this Km value to figure out dopamine per pulse and Vmax.

5.3 Measurement of 4HPAA and dopamine in cage compounds study.

In this study, electrochemical characterization and mechanism of 4HPAA was studied with fast-scan cyclic voltammetry at a carbon fiber microelectrode. An optimized waveform was developed and found to be effective for the simultaneous detection of both 4HPAA and dopamine in a single measurement. The goal of these studies was to develop a method to quantify the amount of biologically active compound photo-released after photoactivation of p-hydroxyphenacyl (pHP) based caged compounds, especially pHP glutamate. This study is innovative because glutamate cannot be quantified using electrochemical method due to it being non-electroactive.

In addition to optimizing the detection of 4HPAA, our research group has been interested in incorporating fast-scan cyclic voltammetry detection within a microfluidic device. Moreover, our group wants to study how different concentrations of glutamate influence dopamine regulation in the zebrafish brain using caged compounds. To conduct caged compound experiments in mice brain slices, we use a mercury lamp as a light source that is modulated with a computer controlled shutter. The light is delivered by 100 μm diameter fiber optic cable which is positioned by a micromanipulator. However, there are a couple of challenges during the electrochemical detection of 4HPAA and dopamine upon the photo-release of pHP-glutamate on brain slices. To perform the experiment, the stimulation electrodes, carbon fiber electrode, and the fiber optic cable need to be positioned in the same spot with a specific geometry over the brain slice. This is challenging since there is limited space to position all the electrodes between recording chamber and microscope objective lenses. Moreover, a large amount of pHP-glutamate, which must be custom synthesized and is available in limited quantities, is required to perfuse the compound over the brain slice. To perform our experiments in a more cost effective

and efficient manner, our group was interested incorporating the caged compound experiment with microfluidic systems, which requires the use of small volume of solvent.

Microfluidics has emerged as a powerful technology in bioengineering, bioanalytical, and pharmacological research over the past decade. [5-7] The miniaturization of a system offers several advantages, for example, fast analysis time, high throughput, and the ability to incorporate numerous detection techniques. [8, 9] Mass spectrometry, laser induced fluorescence, and optical measurements are the most common detection systems incorporated with microfluidics. However, these detection systems are typically employed in a "off-chip" format since these system are significantly large. Therefore, electrochemical detection can be ideal for use in a microfluidic system since different shapes and types of microelectrodes can be easily fabricated on chips. Constant potential amperometry has been widely used as an electrochemical detection method in microfluidics due to its simplicity, but suffers from poor chemical selectivity compared to fast-scan cyclic voltammetry. Since fast scan cyclic voltammetry in a "on-chip" format has not been demonstrated, we need to prove that it is feasible to use with a microfluidic system.

The microfluidic chip is made of polydimethylsiloxane (PDMS), which is a silicon-based polymer widely used for microfluidic chip fabrication. The top layer consists of a 50 μm wide single flow channel with two reservoirs and the bottom layer contains a 30 μm carbon fiber (Specialty Materials, INC. Lowell, MA, USA) positioned perpendicular to the flow channel. To bond the top and bottom layers and embed carbon-fiber electrode onto the PDMS chip, we modified a spin coating fabrication method. Schematic diagram of the chip fabrication process can be found in Appendix 1. A sequential injection using gravity feed as the main driving force

was applied to introduce sample to the microfluidic channel, shown in Appendix 2. Using this injection method, 32 nL of sample was injected each time at the flow rate of 1.8 µL/min.

Using this device, we were able to detect dopamine and serotonin. In the future, to test the feasibility of the chip, we will measure neurotransmitters in physiological samples such as microdialysates and urine. These collected data suggests that fast scan cyclic voltammetry can be employed on microfluidic chip requiring only about 32 nL of sample. In addition, we will also further develop a microfluidic device that consists of a micro-vessel to deliver caged compound and a recording chamber to contain neural tissues to keep the tissue viable.

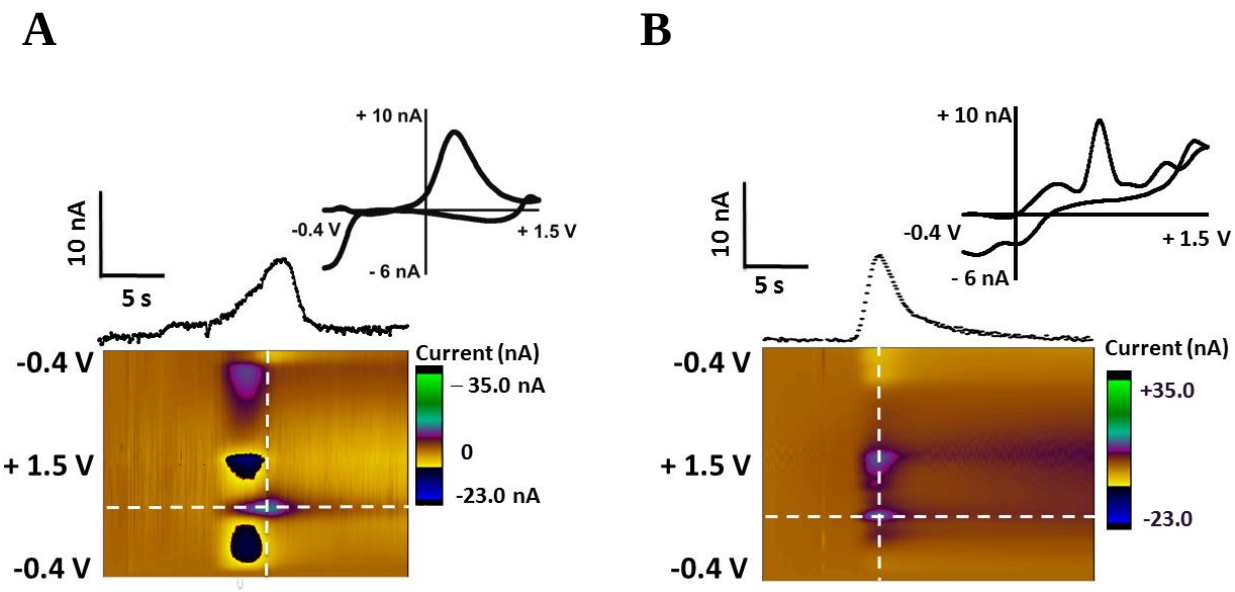

Figure 3. Representative data of the dopamine and serotonin detection using on-chip fast scan cyclic voltammetry the flow cell microfluidic chip. Cyclic voltammograms of 5nM dopamine (A) and 100 nM serotonin (B) were taken with a triangular waveform of -0.4V to +1.5V at 400 V/s every 100 ms. The oxidation peak dopamine can be observed at around 0.6 V and reduction peak at around -0.4 V. In addition, serotonin exhibited two oxidation peaks and one reduction peak at around 1.2 V, 1.4 V, and – 0.3 V respectively.

5.4 References

[1] Rink, E., and Wullimann, M. F. (2001) The teleostean (zebrafish) dopaminergic system ascending to the subpallium (striatum) is located in the basal diencephalon (posterior tuberculum), *Brain Res., 889*, 316-330.

[2] Joseph, J. D., and Wightman, R. M. (2002) Mechanisms and kinetics of neurotransmission measured in brain slices with cyclic voltammetry, pp 255-278, Marcel Dekker, Inc.

[3] Wightman, j. d. J. a. R. M. (2002) Mechanisms amd kinetics of neurotransmission measured in brain slices with cyclic voltammetry, In *electroanalytical methods for biological materials* (Chambers, A. B.-T. a. J. Q., Ed.), Marcel Dekker, Inc.

[4] Wu, Q., Reith, M. E. A., Wightman, R. M., Kawagoe, K. T., and Garris, P. A. (2001) Determination of release and uptake parameters from electrically evoked dopamine dynamics measured by real-time voltammetry, *J. Neurosci. Meth., 112*, 119-133.

[5] Mark, D., Haeberle, S., Roth, G., von Stetten, F., and Zengerle, R. (2010) Microfluidic lab-on-a-chip platforms: requirements, characteristics and applications, *Chem. Soc. Rev., 39*, 1153-1182.

[6] Weigl, B. H., Bardell, R. L., and Cabrera, C. (2007) Introduction to microfluidic techniques, pp 691-709, John Wiley & Sons Ltd.

[7] Ducree, J. (2009) Next-generation microfluidic lab-on-a-chip platforms for point-of-care diagnostics and systems biology, *Procedia. Chem., 1*, 517-520.

[8] Gunasekara, D. B., Hulvey, M. K., and Lunte, S. M. (2011) In-channel amperometric detection for microchip electrophoresis using a wireless isolated potentiostat, *Electrophoresis, 32*, 832-837.

[9] Choudhury, D., van Noort, D., Iliescu, C., Zheng, B., Poon, K. L., Korzh, S., Korzh, V., and Yu, H. (2012) Fish and Chips: a microfluidic perfusion platform for monitoring zebrafish development, *Lab. Chip.*, *12*, 892-900.

Appendices

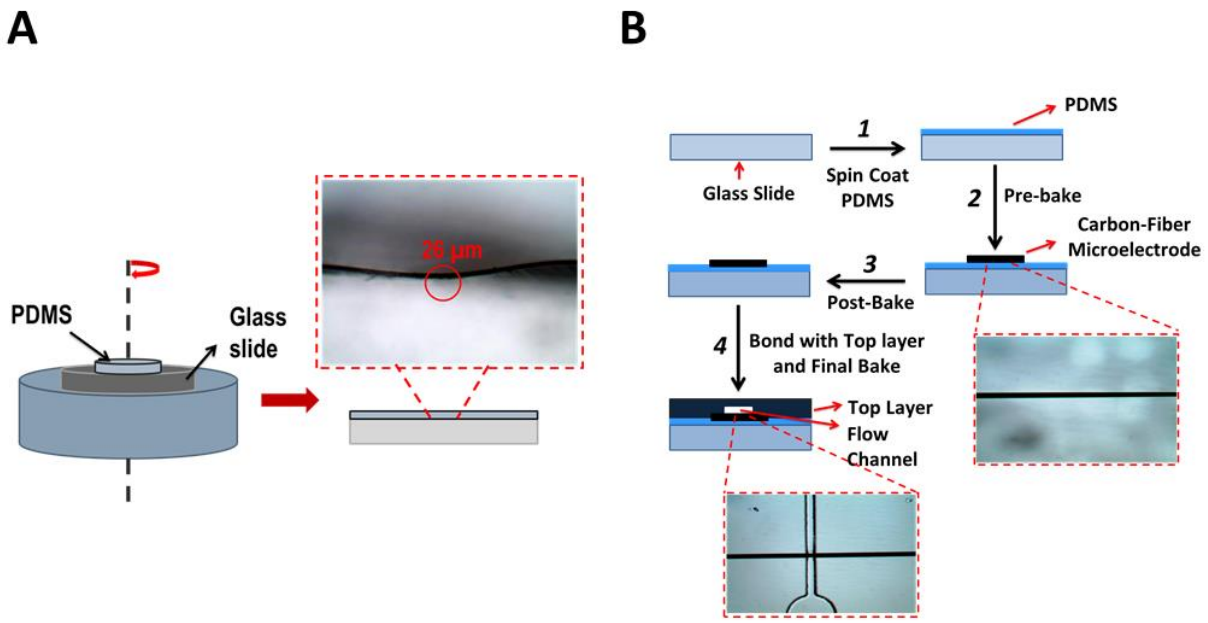

Appendix 1. Diagram of the modified spin coating chip fabrication. (A) Basic diagram of the spin coating method that creates a 26 µm thin film of PDMS on the glass slide (insert). (B) Schematic of the chip fabrication process shown step by step. 1. A pre-prepared mixture of 10:1 ratio PDMS and curing agent was poured at the center of the glass slide. The PDMS was deposited on top of the glass slide using spin parameters of 4000 rpm for 45 s with acceleration of 300 rpm/s. 2. Spin coated PDMS was pre-baked at 70 ºC and a trimmed 30 µm carbon-fiber was placed on the partially cured PDMS. 3. Post-baked the chip for 10 minutes at 70 ºC to seal the carbon fiber with the PDMS. 4. The fully cured top layer was bonded with post-baked bottom layer and the completely constructed chip was finally baked for three hours.

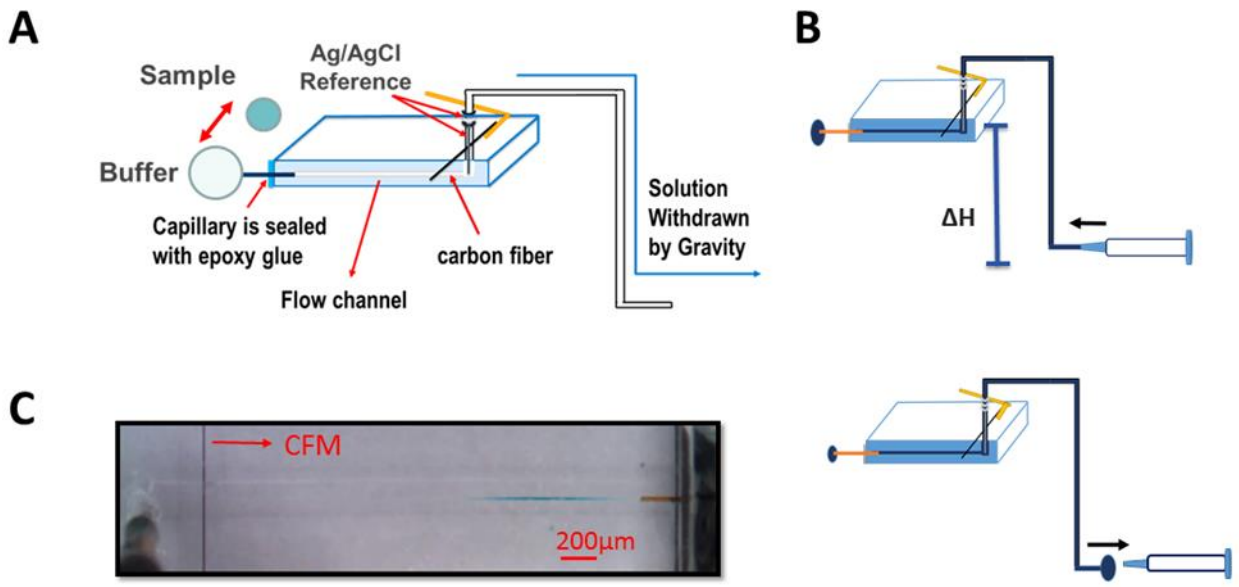

Appendix 2. The diagram of the sequential injection method. (A). Experimental set up for the sequential injection method. A fused silica capillary (1cm long and 50 um in diameter) was inserted into a flow channel and sealed with epoxy glue. An Ag/AgCl reference was positioned inside of the tubing which was connected to the outlet of the flow cell, achieving a closed system for gravity feed. (B). Diagram of gravity sample injection. Connection tubing (30 cm), flow channel, and capillary were filled with buffer solution using a 5 mL gastight glass syringe (top). As the syringe is disconnected, the buffer is withdrawn from the capillary into the flow channel (bottom). Once the flow was achieved as described above, the position of the buffer droplet was switched with the sample droplet C. micrograph of sample injection through the microfluidic flow cell.